AN ABSTRACT OF THE THESIS OF

Peter M. Anthoni for the degree of Doctor of Philosophy in Atmospheric Sciences presented on October 20th 1999. Title: Carbon and Energy Exchange of Semi-arid Ecosystems with Heterogeneous Canopy Structure

Abstract approved:

Redacted for Privacy

Carbon and energy fluxes were measured with the eddy covariance technique above two semi-arid ecosystems, ponderosa pine and juniper/sagebrush, located in central Oregon. The two ecosystems have low LAI and a very open canopy structure. The energy closure was ~70-80% at both ecosystems, equivalent to an imbalance of 150-250 W m^{-2} on cloudless summer days, when net radiation (R_n) was ~600-700 W m^{-2}. The lack of closure cannot be explained by the uncertainty of an estimate of available energy due to a single R_n sensor location. At the more open juniper/sagebrush ecosystem, a numerical model showed that spatial variation in R_n, even for large differences in surface radiation temperature and reflection coefficient between ecosystem components (soil and vegetation), is less than 10% of measured

R_n. The uncertainty in R_n at the two-layered ponderosa pine ecosystem with patches of young and old-growth trees is expected to be smaller than at the juniper ecosystem.

Net carbon exchange (NEE) at the pine site strongly depends on environmental factors effecting carbon assimilation (A_c) and ecosystem respiration (R_e). A more detailed analysis of the carbon budget showed a strong negative response of carbon uptake to large vapor pressure deficits (VPD), whereas water vapor exchange (LE) was less affected. At large VPD the vegetation maintains a sustainable water flow through the soil-plant system by stomatal control of transpiration. The stomatal closure leads to limitation in A_c, but LE is subject to a positive feedback from higher evaporative demand.

Annual NEE of the ponderosa pine forest (200-300 gC m^{-2}) was in the mid-range of reported NEE of temperate forest ecosystems, though, unusually, much of the annual carbon gain occurred during the fall through spring, because the relatively mild winters allowed carbon assimilation to occur and R_e rates were low.

The information gathered at our ponderosa pine site during two years with contrasting climate suggests that the carbon uptake of the ponderosa pine ecosystem will be more sensitive to global climate change than the water vapor exchange.

Carbon and Energy Exchange of Semi-arid Ecosystems with Heterogeneous Canopy Structure

by

Peter M. Anthoni

A Thesis Submitted

to

Oregon State University

In Partial Fulfillment of

the requirements for the

degree of

Doctor of Philosophy

Presented October 20th 1999

Commencement June 2000

Doctor of Philosophy thesis of Peter M. Anthoni presented on October 20th 1999

Approved:

Redacted for Privacy

Major Professor, representing Atmospheric Science

Redacted for Privacy

Dean of College of Oceanic and Atmospheric Sciences

Redacted for Privacy

Dean of Graduate School

I understand that my thesis will become part of the permanent collection of Oregon State University libraries. My signature below authorizes release of my thesis to any reader upon request.

Redacted for privacy

Peter M. Anthoni, Author

Acknowledgements

I am indebted to many people who were very involved in the progress of my dissertation. I greatly appreciate the help from professors, staff and fellow students at the College of Oceanic and Atmospheric Science at Oregon State University.

I want to thank my family in Germany, my parents Fritz and Hildegard Anthoni, my sisters Anette and Gabrielle Anthoni, my sister-in-law Doris Anthoni, and my little nephew Patrick. I hope to be able to make up for the many years we have not been in close contact. I like to especially thank my brother Klaus Anthoni, who has left us too early and hopefully is looking down on us from heaven. I hope to see you again.

I am very grateful to my advisor, Dr. Michael H. Unsworth. His experience and commitment all through the long process of my dissertation have been a great support. He has given me invaluable advice in every step of my studies and research.

I am also grateful to Drs. Beverly E. Law and Richard Waring, who helped me invaluably in linking atmospheric observation to the one thing that is ultimately responsible for most of our findings, the underlying vegetation.

I like to express my gratitude to many colleagues, to name a few: Drs. Dennis Baldocchi, Larry Mahrt, Mathew Williams, Richard Vong, and many more, who continually provided valuable comments on various aspects of data acquisition, analysis and presentation.

Thanks go to NASA, who provided funding for this project (grants #NAGW-4436 and #NAG5-7551).

Contribution of Authors

Drs. Beverly E. Law and Michael H. Unsworth were involved in the design, analysis, and writing of each manuscript. Dr. Richard J. Vong assisted in data collection, analysis, and writing of the first manuscript.

Table of Contents

List of Figures

Figure Page

List of Figures (continued)

List of Figures (continued)

Figure | Page

List of Tables

List of Appendix Figures

Figure Page

List of Appendix Tables

This work is dedicated to the loving memory

of my brother,

Klaus Anthoni.

Carbon and Energy Exchange of Semi-arid Ecosystems with Heterogeneous Canopy Structure

1 Introduction

There is much debate about potential global climate change induced by human activities. One of the most striking and well documented occurrences of global change is the increase in atmospheric CO_2 concentration from pre-industrial levels of about 280 ppm to current levels of about 360 ppm mainly caused by burning of fossil fuels and to a lesser extent by land use change (Keeling et al., 1989; Vitousek, 1994).

To balance the global carbon cycle (years 1980-1989) with emissions from fossil fuel (~5.5 ± 0.5 Gt yr^{-1}; 1Gt=10^{15}grams) and land use change (1.6 ± 1.0 Gt yr^{-1}), the observed increase in atmospheric CO_2 (3.3 ± 0.2 Gt yr^{-1}), an ocean sink of about 2.0 ± 0.8 Gt yr^{-1}, and uptake by the Northern Hemisphere forest regrowth of 0.5 ± 0.5 Gt yr^{-1}, an additional sink in the order of 1.3 ± 1.5 Gt yr^{-1} is needed (Houghton et al., 1996). The mechanism of the additional sink is poorly understood, but interpretation of the latitudinal gradient of CO_2 indicates that a significant portion of the net uptake of CO_2 occurs at mid-latitudes of the Northern Hemisphere, and leads to the hypothesis that the northern temperate terrestrial ecosystems act as a large sink for carbon dioxide (Tans et al., 1990; Denning et al., 1995).

Fan et al. (1998) indicated that North America might have been a sink for CO_2 in the order of 1.7 ± 0.5 Gt-C yr^{-1} in the late 1980s, which would be comparable in magnitude to U.S. emissions of 1.6 Gt-C yr^{-1} from burning of fossil fuels. But

considerable controversy exists about the findings of Fan et al. (1998). Holland and Brown (1999) estimated from direct forest C uptake based on inventory data of the U.S. Department of Agriculture, that in the late 1980s North America's net uptake of carbon was 0.17 Gt-C yr^{-1}. Potter and Klooster (1999) estimated from a model that the net C uptake for the years 1987 and 1988 was ~0.22 Gt-C yr^{-1} for North America and Canada combined.

Provisions defined in the Kyoto Protocol, an agreement to reduce CO_2 emissions among nations of the United Nations Framework Convention on Climate Change, include the possibility of taking into account net carbon uptake by terrestrial ecosystems in achieving emission reductions. This clearly points towards the need for better understanding the interactions between vegetation and the atmosphere.

In 1995 at a meeting in La Thuile, Italy, strategies for monitoring the long-term exchange of CO_2 and water vapor between terrestrial ecosystem and the atmosphere were developed. A concept for a network of long-term monitoring flux sites emerged from the meeting, summarized by Baldocchi et al. (1996):

> There is strong scientific need for long-term measurements of carbon dioxide and water vapor fluxes between terrestrial ecosystems and the atmosphere. Data compiled from a network of long-term measurements of canopy CO_2 exchange can be used to: (1) quantify the seasonal variations of carbon dioxide fluxes due to annual changes in insolation, temperature and canopy structure; (2) understand the biological and climatic processes that control canopy scale CO_2 exchange; (3) test carbon balance models; and improve the ability of models to simulate seasonal dynamics with fidelity (e.g., tune phenological switches that initiate budbreak, grow leaves and initiate leaf senescence); and (4) quantify the spatial and temporal (inter-annual and intra-annual) differences in carbon dioxide exchange rates that may be experienced within and among natural ecosystems.

About 80 sites measuring the carbon and energy exchange above terrestrial ecosystems have been organized in regional networks (AmeriFlux, EUROFLUX, OzNet, MEDEFLU, JapanNet) which are linked in a global network of flux sites (FLUXNET). These increased efforts will help to characterize the role of major terrestrial ecosystems (Table 1.1) in the global carbon cycle and improve the scientific knowledge of the importance and future potential of terrestrial ecosystem in terms of carbon cycling in a potentially altered global climate.

Table 1.1 Breakdown of 80 flux sites participating in FLUXNET by ecosystem functional type as of July, 1998.

FUNCTIONAL TYPE	Percent
Mixed Forest	3
Temperate Broad-leaved Forest	21
Temperate Conifer Forest	22
Boreal Broad-leaved Forest	1
Boreal Conifer	7
Semi-Arid Woodland	16
Alpine	6
Arctic	4
Grassland	7
Crop	6
Tropical Forest	3
Wetland	1

At each site, a suite of similar micrometeorological, physiological, and phenological data is gathered. At most of the flux sites the eddy covariance technique

is employed to measure the carbon, water and energy exchange on the ecosystem level (Baldocchi et al., 1988). Eddy-covariance gives an area integrated flux estimate of the exchange rates between the land and the atmosphere. Methods used for calculation of fluxes are described in more detail in Appendix B.

In 1996, in an effort to study the carbon and energy cycles of semi-arid Western ecosystem, the COSPECTRA (COoperative Spatial Energy and Carbon TRAnsfer) group (a collaboration of scientists at Oregon State University, Corvallis, OR and the Atmospheric Turbulence Diffusion Division at the National Labs, Oak Ridge,TN) initiated flux measurements in a ponderosa pine ecosystem (*Pinus ponderosa*). A short term study in summer of 1997 was performed in a juniper/sagebrush ecosystem. Both ecosystems have a very open canopy structure and are located in the semiarid region of Central Oregon. Ponderosa Pine and Juniper woodland are widespread in Central Oregon, and ponderosa pine are the most common pine in western North America (Whitney, 1985). These extensive forest types are subject to large seasonal variations in weather, with most of annual precipitation falling in winter. Summers are generally hot and very dry. Determining how the carbon and water use of these ecosystems respond to seasonal and interannual changes in environmental conditions (i.e., solar radiation, temperature, and water availability) will help to predict their response to possible climate change.

In semiarid ecosystems water becomes a major limiting factor in the dry season. Precipitation in semiarid systems ranges from about 250 to 510mm annually. In the vicinity of our two ecosystems, less than 10% of the annual rainfall occurs in July through August (~350mm annual normal precipitation in 1961-1990 in Sisters, OR;

Oregon Climate Service, pers. comm., http://www.ocs.orst.edu). The seasonal dynamics of carbon assimilation (A_c) and ecosystem respiration (R_e) determine the seasonal net carbon uptake of the ecosystem. The limited supply of water in the summer months is expected to have a substantial influence on the daily net carbon balance of the ecosystem. Increased partitioning of available energy into sensible heat leads to high ecosystem temperatures and to high vapor pressure deficits. Consequently, ecosystem respiration, R_e, rates are large and high VPD enforces a negative feedback on stomatal opening. As a direct result of the stomatal constraints on carbon assimilation (A_c) and the increased respiration, low net ecosystem exchange (NEE), possibly even net carbon loss, is expected to occur on summer days with high evaporative demand. Conditions for net carbon uptake may be more favorable during the wetter seasons, when temperatures and VPD are lower, and consequently respiration rates are small and carbon assimilation is less constrained by stomatal response to VPD.

A general approach to confirming the applicability of the eddy covariance technique for measuring ecosystem exchange rates is by determining the achievement of energy closure (Goulden et al., 1996). The major source of energy for the atmosphere-surface layer is solar radiation, where the net input of radiative-energy is determined by the difference in downwelling (subscript "d") and upwelling (subscript "u") short and long wave radiation,

$$R_n = (R_{sd} - R_{su}) + (R_{ld} - R_{lu}) \qquad (1.1)$$

where R_n denotes net radiation, R_s and R_l are short and long wave radiation.

Usually a one-dimensional energy budget is applied (thereby neglecting advection effects), where the available energy (F_a), calculated as net radiation (R_n) minus soil heat flux (G) and change in energy stored in the biomass (S), should be balanced by the sum of sensible heat (H) and latent heat exchange (LE),

$$F_a = R_n\text{-}G\text{-}S = H + LE \qquad (1.2)$$

Problems in energy closure can occur because of various factors: uncertainties in the measurements of eddy flux, soil heat flux, storage terms, and radiation, neglect of advection effects, and mismatch of source areas of sensors (Schmid, 1997; Schmid and Lloyd, 1999).

In heterogeneous, sparse vegetated ecosystems the radiation exchange is spatially variable compared with more homogeneous closed-canopy ecosystems (Paw U, 1992). A major uncertainty in the energy closure might result from assuming that the area average net radiation is the same as the value measured by a single sensor placed at one location above the canopy. Logistic problems generally do not allow an adequate sampling design with multiple instruments (excessive tower and sensor costs).

Interception of radiation by vegetation can influence estimates of R_n used in the calculation of available energy. Downwelling radiation is uniform during conditions of cloudless or completely overcast skies, but variability occurs in upwelling radiation. Large differences in surface radiation temperatures of vegetation and soil in sunlit and shaded areas can be expected in semiarid ecosystems on cloudless summer days. In

particular, dry soil can have a substantially higher surface radiation temperature than vegetation. Difference in shortwave reflection coefficients between the two main ecosystem components (soil and vegetation) can further increase the spatial variation in measured net radiation. Depending on the amount of soil "seen" by net radiometer the estimate of the net radiation will be different between measurement locations.

Chapter 2 is concerned with the uncertainty of estimating the mean net radiation from measurement at a single sensor location. This work was motivated by the observation that there was a considerable lack of closure of 20-30% at both the COSPECTRA sites. We used canopy structure and surface radiation properties in conjunction with geometrical models generated by rendering and ray tracing software to determine the spatial variation in the upwelling components of a net radiation measurement. The heterogeneous juniper/sagebrush ecosystem was chosen for a modeling exercise to determine the spatial variation in upwelling radiation components based on vegetation distribution around sensor locations. Even though large differences (~30K) in surface radiation temperatures between sunlit soil and vegetation were found at the juniper site during cloudless days, the uncertainty in estimating R_n from a single sensor, used in calculating energy closure, was found to be inadequate to explain the lack of energy closure encountered in these complex structured ecosystems. Because of the higher stand density and taller canopy structure at the pine site, it is expected that the spatial variability in R_n is comparable or less than the variability found at the juniper site. The lack of closure is currently unexplained at both sites and further investigation should be undertaken to explain the discrepancy.

Chapter 3 focuses on the seasonal and annual carbon and water vapor exchange of the ponderosa pine ecosystem where two years of data were available for detailed analysis. We explored ways in which environmental factors effected the two major components of net CO_2 exchange (carbon assimilation and ecosystem (autotrophic and heterotrophic) respiration). The difference between those two carbon fluxes is directly measured by eddy CO_2 flux. We found a strong response of the carbon assimilation to atmospheric vapor pressure deficit, whereas the water vapor exchange was fairly independent of varying conditions of evaporative demand, which suggests a strong stomatal control on the gas exchange at the pine ecosystem. Seasonal and intra-annual variation in environmental factors (temperature, vapor pressure deficit, and precipitation pattern) led to unexpected patterns in the seasonal and intra-annual net carbon exchange.

The seasonal dynamics of the net carbon exchange were dependent on environmental factors controlling the gross ecosystem production (CO_2 uptake by the ecosystem) and ecosystem respiration (CO_2 loss from the ecosystem). Fall through Spring ("dormant or off-season") net carbon gain was large: more commonly, ecosystem losses of carbon are reported in this season in higher latitude forests. The mild weather at the pine site led to favorable conditions for carbon assimilation but at the same time to small ecosystem respiration rates. Summer ("growing season") net carbon exchange was constrained by stomatal closure in response to large VPD and large respiration rates due to large ecosystem temperatures. Interannual variation in precipitation pattern, with more frequent precipitation in the summer of 1997 than in 1996, may have resulted in higher ecosystem respiration rates R_e in summer 1997 than

in 1996. The higher R_e offset the carbon gain in summer 1997 to the extent that the ecosystem was a source for CO_2 in the summer of 1997, but a sink for CO_2 in summer of 1996.

A summary of findings and concluding remarks will be presented in Chapter 4. The lack of energy closure at the pine and juniper sites was larger than reported for other research sites. Further investigation should focus on advection effects, specifically the role of a possible vertical transport of energy, which might be particularly important in this semi-arid ecosystem. Annual NEE of the ponderosa pine forest was mid-range of reported NEE of temperate forest ecosystems, though, unusually, much of the annual carbon gain occurred during the fall through spring. Water played a crucial role for the carbon uptake at the pine site. Summer water stress conditions inducing stomatal closure, constrained an otherwise high potential of carbon assimilation, but, due to the positive feedback, daily water use stayed fairly constant regardless of large variations in VPD.

2 Variation of Net Radiation over Heterogeneous Surfaces: Measurements and Simulation in a Juniper-Sagebrush Ecosystem

Peter M. Anthoni, Beverly E. Law,

Michael H. Unsworth and Richard J. Vong

Submitted to Agricultural and Forest Meteorology, In review.

College of Oceanic and Atmospheric Science, Oregon State University. 1999.

2.1 Abstract

Energy components in an open-canopied Juniper/Sagebrush ecosystem located in the semi-arid region of Eastern Oregon were measured with the eddy covariance technique. Daytime net radiation averaged 20-30% greater than the sum of sensible, latent and soil heat fluxes. On cloudless days several days after a rain event the imbalance was ~200-250 W m^{-2}, when measured net radiation was ~650-700 W m^{-2}.

A point measurement of net radiation above an open-canopied forest ecosystem is uncertain, because vegetation structure around the measurement location can be highly variable. Depending on location, various fractions of the upwelling radiation from the soil are intercepted by vegetation and do not reach the radiometer. To determine the magnitude of this uncertainty, we measured tree locations and dimensions, and surface radiation temperature (T_r) and shortwave reflection coefficients (α) of soils and vegetation in a 100 by 100 m area. Geometrical models generated by ray tracing and rendering software were used to calculate the upwelling radiation that would reach radiometers placed at random locations above the surface.

In summer, under cloudless skies the measured radiative surface temperatures of soil and vegetation varied considerably, from a mean of 56 °C for sunlit soil to 25 °C for shaded soil, and 27-29 °C for sunlit and shaded vegetation (trees and shrubs). The mean shortwave reflection coefficient varied little between components (with α_v = 0.10 for vegetation and α_s = 0.13 for soil).

Spatial variability in upwelling radiation (R_u) arises mainly from component variability at viewing angles from ~30 to ~60°, where contributions to R_u are large and variation in fractional cover between radiometer locations is large. Our measurements and modeling suggest that a radiometer deployed from a tower in a small clearing will only be affected slightly by the clearing since only about 10% of R_u arises from viewing angles less than 15° (directly below the radiometer).

The spatial variation in the upwelling radiation reaching a sensor above the canopy increases with increasing differences between the radiation temperatures and reflection coefficients of the various ecosystem components. For the radiative properties found at our site, where the radiative temperature of sunlit soil was ~30°C larger than the temperature of vegetation and shaded components, the spatial variability in the longwave upwelling radiation (R_{lu}) was less than 20 W m^{-2}. The spatial variation in the shortwave upwelling radiation (R_{su}) for the small differences in the reflection coefficient of the ecosystem components was less than 10 W m^{-2}. Consequently, the uncertainty associated with estimating the available energy from a single point measurement of net radiation is not enough to explain the lack of energy closure (200-250 W m^{-2}) in this complex open-canopy ecosystem.

2.2 Introduction

Net radiation is the driving term in the energy balance at the earth's surface, and is an essential component in widely used surface energy partitioning models (e.g. the

Penman-Monteith equation; Monteith and Unsworth, 1990). In open-canopy ecosystems, net radiation is difficult to measure accurately. The energy exchange of short sparse vegetation is often modeled as an one-dimensional system with fluxes from two components, soil and plant canopy (Shuttleworth and Wallace, 1985). However, over tall vegetation the three-dimensional structure of the canopy has an important impact on the radiation distribution (Paw U, 1992). For example, the overstory vegetation can intercept reflected shortwave and emitted longwave radiation from the soil surface, and the portion of the soil surface that is shaded from direct radiation varies with solar elevation, azimuth and overstory structure.

Many surface-atmosphere energy exchange studies have been undertaken over relatively homogeneous canopies, where micro-scale variations in canopy structure are small compared to the source area contributing to measured energy fluxes. In most flux studies, instrumentation is installed above the canopy at one location. Sensible and latent heat fluxes typically are measured with the eddy covariance technique, and a net radiometer measures the difference between upward and downward long- and shortwave radiation. Heat flux into or out of the soil is usually measured with heat flux plates buried underneath the soil surface. In addition, rates of temperature change in the canopy air layer and biomass of the ecosystem components (e.g. tree stems, leaves) are used to determine the energy storage below the measurement level.

Achievement of energy closure is generally used to test the validity of the eddy covariance technique in measuring atmosphere-surface exchange (Goulden et al., 1996). Usually a one-dimensional energy budget is applied, where available energy, calculated from net radiation (R_n) minus soil heat flux (G), should be balanced by the

algebraic sum of sensible heat (H), latent heat (LE), and change in energy storage in the ecosystem (S). Horizontal advection effects are usually assumed to be small by careful selection of a research site with uniform fetch in the prevailing wind directions. Lack of energy closure may occur because of neglect of advection effects, or errors in the measurements of eddy flux, energy storage, soil heat flux and net radiation terms.

In 1997 we made measurements of the energy exchange over an open-canopied juniper/sagebrush ecosystem using eddy covariance instrumentation. In this paper, we assess the magnitude of uncertainty in net radiation at our site, combining measurements and modeling to estimate spatial variability in the upwelling shortwave and longwave radiation. To determine the spatial variation in the surface and vegetation cover, we measured tree locations and dimensions, and surface radiation temperature (T_r), and solar reflection coefficients (α) of soils and plant species in a 100 by 100 m area. We then used geometrical models, generated by ray tracing and rendering software, to calculate the upwelling radiation reaching randomly selected radiometer locations above the surface.

2.3 Methods

2.3.1 Site description

Components of the energy exchange and associated microclimatic variables were measured above the canopy of a juniper/sagebrush ecosystem located about 15 km east of Sisters, Oregon (44°15′54″ N, 121°23′3″ W, elevation 945 m). The site is about 3 km southwest of a Juniper research site studied during the Oregon Transect Ecosystem Research (OTTER) project for which details of the ecosystem and its physiology were reported by Runyon et al. (1994) and Law and Waring (1994). The fetch is relatively flat and uniform for several kilometers in all wind directions. The overstory consists primarily of widely-dispersed juniper trees (*Juniperus occidentalis*) and has a spatial mean leaf area index (LAI) of less than 1. The understory consists of sagebrush (*Artemisia tridentata*), rabbit brush (*Chrysothamnus viscidiflorus*), bitterbrush (*Purshia tridentata*), and a small percentage of various grass species. The well drained sandy loam soils are classified as coarse-loamy, mixed, mesic aridic Haploxeroll (USDA, National Soil Survey Center - Soil Survey Laboratory).

2.3.2 Eddy covariance and microclimate measurements

Energy flux measurements were made using the eddy covariance technique (Baldocchi et al., 1988). Flux measurements were made on a tower at a height of 20 m, 13 m above the mean tree height. Wind speed and virtual temperature were measured with a three-dimensional sonic anemometer (model CSAT-3, Campbell Scientific Inc, Logan, UT). An open-path, infrared gas analyzer (IRGA) (Auble and Meyers, 1992) measured water vapor fluctuations. Half-hour eddy covariances and statistics were computed online from ~10 Hz raw data on a CR10X datalogger (Campbell Scientific Inc, Logan, UT). The means of three 10 minute sub-interval covariances, computed according to Reynolds averaging rules (Stull, 1988), were used to compute the half-hour eddy covariance flux estimates. Appropriate corrections for air density fluctuations (Webb et al., 1980) were applied. Fluxes were rotated to allow interpretation of the exchange rates normal to the streamlines following the local terrain. In the following sections, H and LE are reported as positive when directed away from the surface. A positive value for net radiation (R_n) indicates a net flux of energy to the surface. The flux measurements began on April 3rd, 1997, and the system was operational for ~50 days, until July 11th, 1997. Flux data acquisition was interrupted from May 3rd to June 2nd due to instrumentation problems.

Above-canopy meteorological measurements were recorded at the top of the tower (~20m above the surface), using a Campbell Scientific (CSI; Logan, UT) datalogger. Above-canopy net radiation (R_n) was measured with a net radiometer (model Q7 SN#Q96343, REBS, Seattle, WA) with factory calibration from December

12th 1996, deployed from the south side of the tower. Net radiation was corrected for the influence of wind speed, using an equation supplied by the manufacturer. Downward photosynthetically active radiation (PAR) was measured with quantum sensor (model LI-190SZ, LI-COR Inc, Lincoln, NE). Incoming total solar radiation (S_t) was estimated from measured PAR, using a conversion factor of 0.5 for cloudless skies determined from S_t and PAR data at a nearby ponderosa pine site (20 km West of the juniper site). Air temperature (T_a) and relative humidity (RH) were measured with a thermistor and capacitive RH sensor probe (model HMP35C, Vaisala, Helsinki, Finland).

Various other measurements were recorded at ground level using CSI dataloggers. Soil heat flux was measured at 0.02 m depth with two heat flux plates (model HFT-3, REBS, Seattle, WA), one at the north and the other at the south side of a Juniper tree. The heat fluxes at the two locations were equally weighted to estimate the soil heat flux for the ecosystem. Soil temperature was measured next to the heat flux plates with thermocouples at depths of 2, 16, and 32 cm. Rainfall was measured with a tipping-bucket rain gauge (model TE525MM, Campbell Scientific, Inc., Logan, UT), placed at least 5 m from surrounding trees.

2.3.3 Intensive mensuration plot

A 100 x 100 m area in the typical upwind fetch of the eddy covariance system was divided into 10 x 10 m cells. In each cell the x-y locations of trees with a

diameter at breast height > 7 cm were recorded. The total height of each tree and height to the base of live crown was measured with an inclinometer, and maximum crown radius was also recorded. Percentage cover estimates of the major ecosystem components (soil, juniper trees, shrubs, and grasses) were determined by the line intercept method on two 100 m long transects located within the 100 x 100 m area.

Leaf area index measurements were made with a LAI-2000 plant canopy analyzer (LICOR, Lincoln, NE) in July after full needle expansion. Measurements were made under uniform diffuse light conditions at 10 m grid points (n = 121 sample points). We used a 90° view restrictor to block the view of the operator, and to account for canopy gaps. The LAI-2000 was held at the soil level at each measurement point. A second LAI-2000 was located as a reference on top of the flux tower above the canopy. The instruments were synchronized and calibrated to one another prior to the measurements.

2.3.4 Measurements of surface properties of ecosystem components

During two cloudless days in summer 1997, measurements of longwave radiation emitted from individual surface components inside the 100 x 100 m plot were made with a handheld infrared radiation (IR) thermometer (model 43, Telatemp, Fullerton, CA). The instrument was calibrated prior to the field measurements over a well stirred water bath at several water temperatures.

The total upwelling longwave radiation (R_{lu}) originating from a surface is given by (Huband and Monteith, 1986)

$$R_{lu} = \varepsilon_s \sigma T_r^4 + (1- \varepsilon_s) R_{ld} \quad (2.1)$$

where ε_s is the surface emissivity, σ is the Stefan-Boltzman constant (5.67E-8 W m^{-2} K^{-4}) and T_r is the surface radiation temperature, R_{ld} is the downwelling longwave radiation. An IR thermometer will observe the total upwelling radiation and report an apparent surface radiation temperature (T_{ar}), determined by

$$R_{lu} = \sigma T_{ar}^4 \quad (2.2)$$

Hence the surface radiation temperature T_r of the surface component can be calculated by

$$T_r = \left[\frac{1}{\varepsilon_s \sigma} \left(\sigma T_{ar}^4 - (1 - \varepsilon_s) R_{ld} \right) \right]^{1/4} \quad (2.3)$$

For our modeling purposes we were interested in the total upwelling radiation originating from the main surface components (sunlit and shaded soil and vegetation). Apparent surface radiation temperatures were measured for surface components at several locations during the day (9:00 - 16:00 local time). Surface radiation temperatures for sunlit soil ($T_{r,s,su}$), shaded soil ($T_{r,s,sh}$), sunlit vegetation ($T_{r,v,su}$), and

shaded vegetation ($T_{r,v,sh}$) were calculated from measured T_{ar} using equation 2.3; R_{ld} was modeled from measured air temperature (T_a) at 20 m, according to $R_{ld} = -119 + 1.06\ \sigma\ T_a^4$ (Unsworth and Monteith, 1975) and emissivities were taken to be 0.93 for soil and 0.97 for vegetation (Hipps, 1989; Humes et al., 1994).

Shortwave reflection coefficients were measured with an Eppley pyranometer (model PSP, Eppley laboratory, Newport, Rhode Island). The pyranometer was held above the various ecosystem components at a height of ~1 m facing downward to measure the reflected shortwave radiation, and was then reversed and leveled to measure the incoming shortwave radiation. Reflection coefficients were measured for soil (α_s) and vegetation (shrubs and juniper trees; α_v) at several locations during the day (9:00 - 16:00 local time).

2.3.5 Modeling of the radiometer field of view

We used the 100 x 100 m plot information and ray tracing software (Blue Moon Rendering Tools; Gritz and Hahn, 1996) to generate scenes that would be viewed by a radiometer located 20m above the surface and facing downward. The measured tree pattern of the 100 x 100 m area was repeated outward in the model to generate a larger scene that allowed a viewing angle (ϕ) of at least 85° in all directions. Trees were modeled as paraboloids. Because shrub locations were not measured explicitly in the 100 x 100 m plot, we accounted for the shrub cover by randomly locating half-spheres with a radius of 1 m into the modeled scenes until the area covered was equal to the

percent cover for shrubs determined from line intercept method. We did not include the small percentage of grasses in the modeling, as they had senesced by the time we made the radiation measurements.

For each of 100 random instrument locations within the plot, scenes with a pixel size of 1x1 m were generated. Vegetation and soil were assigned different pixel colors. Figure 2.1 shows an orthogonal view of the 100 x 100 m area and a perspective view of the same area as seen from a radiometer placed at 20 m above the surface in the center of the area. The views were generated with BMRT ray tracing software; trees were modeled as paraboloids, shrubs were modeled as half-spheres, and the sun was at an elevation of 65° around solar noon. For image clarity, trees and shrubs were modeled without casting a shadow onto the soil in these scenes (Figure 2.1). The solar elevation and azimuth were held constant for the simulations, corresponding to solar noon in mid-summer (elevation ~65°). Sunlit and shaded areas were distinguished by different pixel shades (e.g. bright pixels were sunlit and dark pixels shaded).

a)

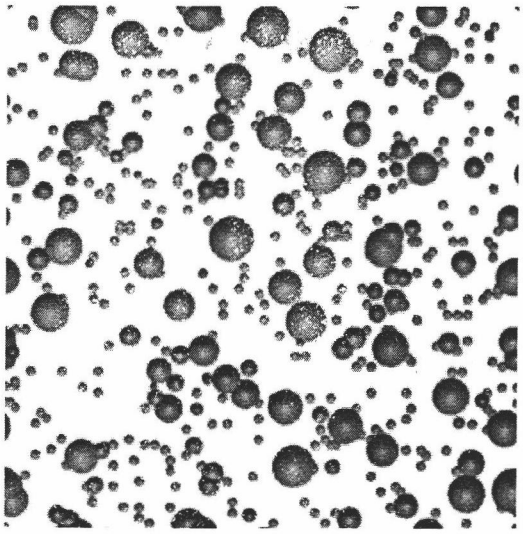

b)

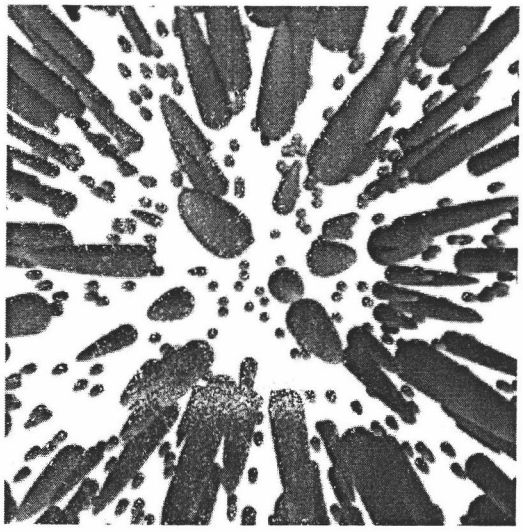

Figure 2.1 a) Orthogonal view of the 100x100 m^2 plot with known tree location and dimensions. b) View of the same area as seen from the perspective of a radiometer located at a height of 20m above the surface.

2.3.6 Calculation of upwelling longwave and shortwave radiation

In each scene, the fractions of sunlit ($f_{s\,su}$) and shaded soil ($f_{s.sh}$) and sunlit ($f_{v.su}$) and shaded ($f_{v.sh}$) vegetation were determined from pixel colors and shades in

concentric rings centered on the radiometer location. Taking into account the interception of radiation by the overstory, the upwelling longwave radiation ($R_{lu.3D}$) received by the radiometer can be calculated from fractional surface cover and the component specific upwelling radiation calculated from the measured surface radiation temperature of the sunlit and shaded soil and vegetation (Schwerdtfeger, 1976),

$$R_{lu.3D} = 2 \Sigma_m \Sigma_i \sin(\phi_i) \cdot \cos(\phi_i) \cdot \delta\phi_i \cdot R_{lu,m} \cdot f_{m,i} \quad (2.4)$$

where ϕ_i is the mean viewing angle of the i^{th} concentric ring (n=150), $\delta\phi_i$ is the width of the concentric ring in radians (see Figure 2.2), σ is the Stefan-Boltzman constant (5.67E-8 W m^{-2} K^{-4}) and $R_{lu,m}$ ($= \sigma T_{ar,m}^4 = \varepsilon_s \sigma T_{r,m}^4 + (1 - \varepsilon_s) R_{ld}$) is the total upwelling longwave radiation of the m^{th} surface component (e.g., sunlit soil, shaded soil, sunlit vegetation, and shaded vegetation) with fractional viewing cover of $f_{m,i}$ in the i^{th} concentric ring.

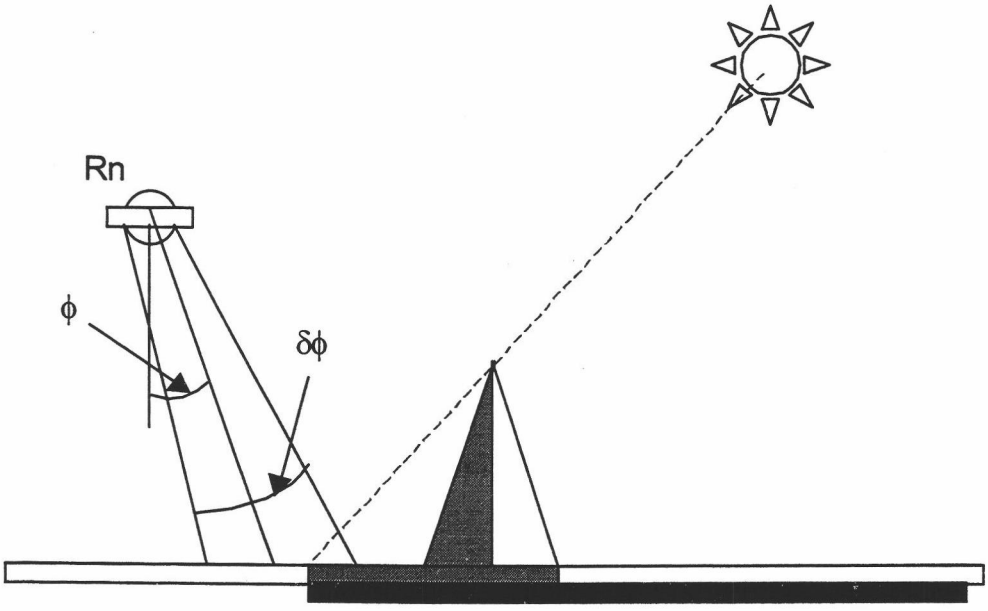

Figure 2.2 View schematic of radiometer over a surface with three dimensional structure. Shaded areas are shown in gray. The apparent area seen as shade by the radiometer is shown in black.

Similarly, the reflected solar radiation ($R_{su.3D}$) was determined using the measured reflection coefficients of the soil and vegetation. Total incoming solar radiation (S_t) was set at 900 W m^{-2}, a representative value measured around solar noon on cloudless summer days at this site. For reflection of diffuse radiation (S_d) by shaded areas, we estimated S_d to be 0.1 of S_t (Monteith and Unsworth, 1990). $R_{su.3D}$ received by the radiometer is then given by

$$R_{su.3D} = 2\,\Sigma_i\,(\sin(\phi_i)\cdot\cos(\phi_i)\cdot\delta\phi_i\cdot(\Sigma_{su}\ \alpha_{su}\cdot S_t\cdot f_{su,i} + \Sigma_{sh}\ S_d\cdot\alpha_{sh}\cdot f_{sh,i})) \qquad (2.5)$$

where ϕ_i is the mean viewing angle of the i^{th} concentric ring (n=150), $\delta\phi_i$ is the width of the concentric ring in radians, S_t is the total incoming radiation, S_d is the diffuse radiation, 'su' and 'sh' are the sunlit and shaded components of the ecosystem, respectively, α_{su} and α_{sh} are the reflection coefficients, and $f_{su,i}$ and $f_{sh,i}$ are the fraction covers of the scene components in the i^{th} concentric ring.

Taking into account the dependence of the vegetation fraction on viewing angle, the average vegetation fraction viewed by a radiometer as a function of viewing angle can be expressed as (Norman et al., 1995)

$$f_{v.av} = 1 - \exp(-k \cdot LAI / \cos(\phi)) \qquad (2.6)$$

where k is a light extinction coefficient, LAI is the leaf area index, and ϕ is the viewing angle. The average upwelling longwave ($R_{lu.av}$) and shortwave radiation ($R_{su.av}$) were then calculated using equations similar to (2.4) and (2.5) with vegetation cover fraction f_v calculated from $f_{v.av}(\phi_i)$ and soil cover fraction $f_s = 1 - f_{v.av}(\phi_i)$, together with an estimate of the shaded to sunlit fraction of the ecosystem. We estimated the shaded to sunlit fractions from the ratios of the orthogonal percentage cover fractions of the shaded and sunlit components (soil and vegetation).

Dolman (1993) suggested calculating the available energy for open-canopy ecosystem based on the fractional cover of understory and overstory. This two-dimensional approach neglects interception of upwelling radiation by three-dimensional structures. We calculated the longwave upwelling radiation ($R_{lu.2D}$) using this approach, according to

$$R_{lu.2D} = \Sigma_m R_{lu,m} \cdot f_m \quad (2.7)$$

where σ is the Stefan-Boltzman constant, and $R_{lu,m}$ ($= \sigma T_{ar,m}^4 = \varepsilon_s \sigma T_{r,m}^4 + (1-\varepsilon_s) R_{ld}$) is the total upwelling longwave radiation and f_m is the vertically projected fraction cover of the m^{th} surface component (e.g., sunlit soil, shaded soil, sunlit vegetation, and shaded vegetation).

Similarly, a two-dimensional estimate of upwelling shortwave radiation ($R_{su.2D}$) was calculated as,

$$R_{su.2D} = \Sigma_{su} \alpha_{su} \cdot S_t \cdot f_{su} + \Sigma_{sh} \alpha_{sh} \cdot S_d \cdot f_{sh} \quad (2.8)$$

where S_t is the total incoming radiation, S_d is the diffuse radiation, α_{su} and α_{sh} are the reflection coefficients, and f_{su} and f_{sh} are the vertically projected fractional cover of the 'su' (sunlit soil and vegetation) and 'sh' (shaded soil and vegetation) components of the ecosystem.

2.4 Results and discussions

2.4.1 Intensive mensuration measurements

There were 128 Juniper trees in the 100 x 100 m plot. The mean height of the trees was ~7 m, and mean spacing between the trees, calculated from the mean distance of the 5 closest neighbors of each tree in the plot, was about 9 m. Percent cover estimates from line intercept method were: 60% bare soil; 24% Juniper; 11% shrubs; and 5% grasses and other species. The vegetation percentage cover at our site is higher than at the nearby OTTER site, which had 7% juniper and 13% shrubs, estimated in the same way (Law and Waring, 1994). An analysis of the orthogonal view of the 100 x 100 m scene (Figure 2.1(a)) modeled with the sun at noon and elevation of 65°, showed that 58% of the area would be sunlit soil, 9% shaded soil, 21% sunlit vegetation, and 12% shaded vegetation. Some overlap of the randomly-placed shrubs with Juniper trees occurred in the modeled view scenes, which resulted in a tree and shrub percentage slightly lower than was found from the line intercept method.

2.4.2 Environmental conditions and energy closure

Skies were cloudless during the measurements of surface radiation temperatures and the reflection coefficients of the various ecosystem components in the 100 x 100

m plot. At the tower, midday solar radiation reached values of ~900 W m^{-2} and net radiation was about 650-700 W m^{-2}. Midday air temperature was ~23°C, and soil temperatures measured at 2 cm depth were ~40°C and ~20°C at the sunlit and shaded side of a tree, respectively. Measured surface radiation temperature varied considerable between soil and vegetation (Table 2.1).

Table 2.1 Mean surface radiation temperatures (T_r) and standard errors () for the major ecosystem components.

Type	**Mean T_r (SE) in °C**	**N [a]**
Soil (sunlit)	56 (0.7)	12
Soil (shade)	25 (1.1)	9
Juniper (sunlit)	29 (0.9)	15
Juniper (shade)	27 (1.2)	6
Shrubs (sunlit)	28 (0.5)	26
Grass (sunlit)	60 (1.3)	2
Grass (shade)	30 (3.2)	3

[a] Measurements were performed from 9:00 to 16:00 local time during two cloudless days in summer of 1997 (Day 203-204). T_r were calculated from measured T_{ar} using equation 2.3; N is the number of samples taken for each surface type.

The measured mean total upwelling longwave radiation was ~640 W m^{-2} for sunlit bare soil ($R_{lu,s,su}$), ~440 W m^{-2} for shaded soil ($R_{lu,s,sh}$) and ~460-470 W m^{-2} for the dominant vegetation ($R_{lu,v,su}$ and $R_{lu,v,sh}$). A similar pattern of surface radiation

temperature, with T_r of sunlit areas substantially higher than T_r of vegetation, has been reported at other research sites (Garratt, 1978; Blyth and Harding, 1995). Reflection coefficients differed little between vegetation and soil (Table 2.2).

Table 2.2 Measured mean reflection coefficient (α) and standard error () of the major ecosystem components.

Type	**Mean α (SE)**	**N [a]**
Soil	0.13 (0.013)	6
Juniper	0.10 (0.002)	30
Shrubs	0.11 (0.003)	52

[a] Measurements were performed from 9:00 to 16:00 local time during two cloudless days in summer of 1997 (Day 203-204). N is the number of samples taken for each surface type.

At a semi-arid site located in Idaho, Dirmhirn (1971) found higher reflectivity for shrubs (0.12-0.15) and soil (0.20) than at our site. The lower measured reflection coefficient of vegetation at our site may have been due to the influence of the underlying soil. Compared to reflection coefficients of dry soils ($\alpha = 0.19 \pm 0.06$) (Jones, 1992, pg. 31) our measured soil reflection coefficient was relatively low.

Neglecting the most likely small heat storage term in the low stand biomass at the juniper site, and using half-hour average data, 70 percent of the measured available energy (R_n-G) can be accounted for by the sum of measured sensible and latent heat fluxes ($H+LE = 0.70 (R_n - G) + 15$ W m^{-2}, $r^2 = 0.92$, N = 2310 half-hour records). To

account for uncertainties in G and the neglect of heat storage terms, we calculated the energy closure using daily total values. On a daily basis the energy closure improved slightly ($H+LE = 0.79 (R_n - G) + 0.36$ MJ $m^{-2} d^{-1}$, $r^2 = 0.90$, $N = 41$). Our energy closure was relatively low compared with values reported for denser forest ecosystems (~80-100%; Kelliher et al., 1992; Lee and Black, 1993; Laubach et al., 1994; Fan et al., 1995; Goulden et al., 1996; Blanken et al., 1997; Grelle, 1997; McCaughey et al., 1997).

Figure 2.3 shows the energy budget components and energy closure for several dry days following a period of rain in summer 1997. Energy closure degraded steadily from day 182 to day 185, then remained relatively constant (Figure 2.3(b)). Similarly, air and soil temperatures on the sunlit and shaded side of a tree increased then leveled off (Figure 2.3(c)). Several days after the rain, the closure was 60-70%, equivalent to an imbalance ($I=(R_n-G)-(H+LE)$) of ~200-250 W m^{-2}. The midday energy imbalance of all days with flux measurements was correlated with the difference between temperatures of sunlit ($T_{s,su}$) and shaded soil ($T_{s,sh}$), increasing by about 9 W m^{-2} per degree soil temperature difference ($I = -8.7$ W m^{-2} K^{-1} $(T_{s,su} - T_{s,sh}) - 34$ W m^{-2}, $N=48$, $r^2=0.66$, data not shown).

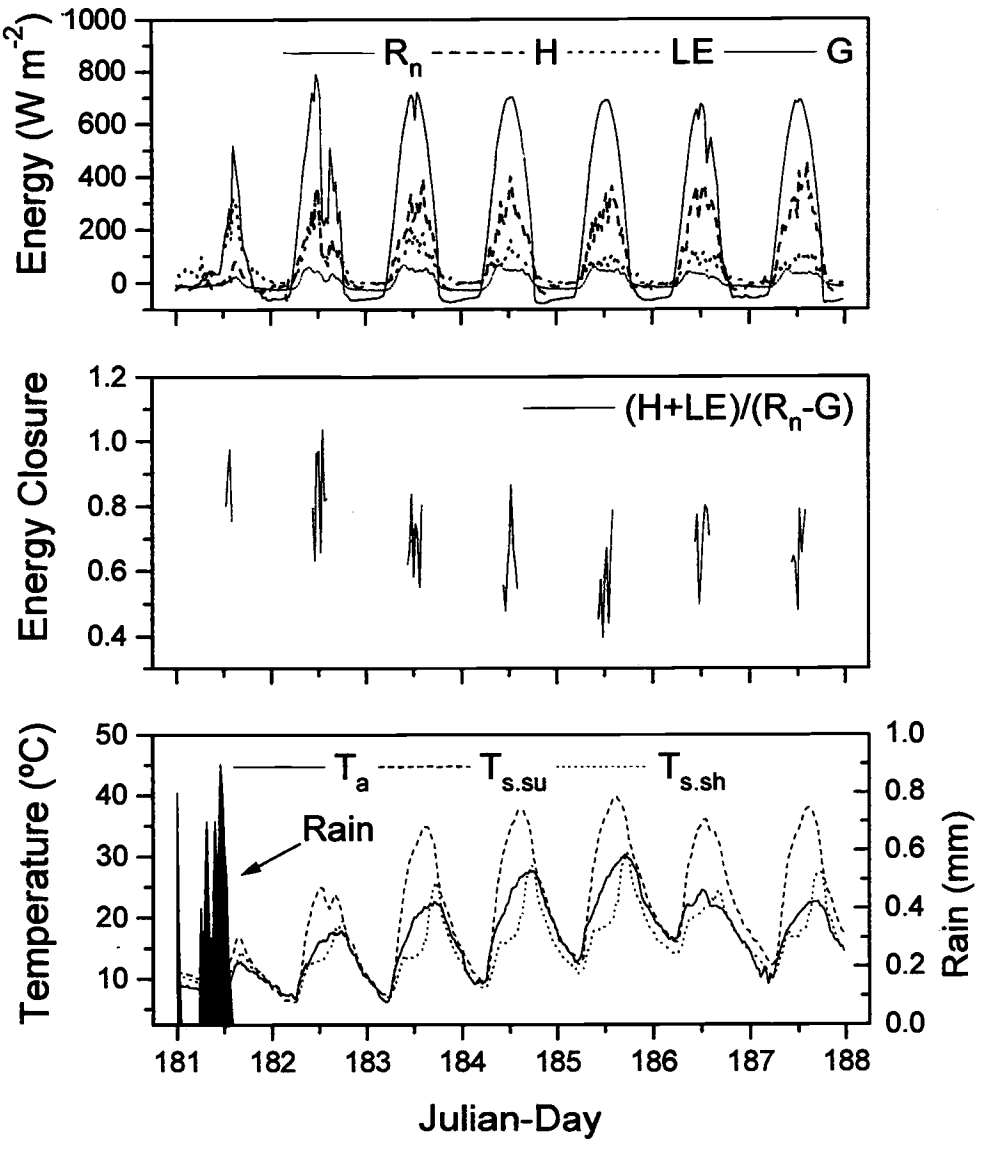

Figure 2.3 a) Energy budget components, b) midday (10:00-14:00) energy closure $(H+LE)/(R_n-G)$ and c) soil and air temperatures following a rain event (12 mm on day 181) in summer of 1997. H is sensible heat exchange, LE is latent heat exchange, R_n is net radiation, and T_a is air temperature, all measured at 20 m. G is soil heat flux, $T_{s,su}$ and $T_{s,sh}$ is soil temperature on the south (sunlit) and north (shaded) side of a tree, respectively, measured at 2 cm depth.

2.4.3 Modeled upwelling longwave and shortwave radiation

In the simulations, the variation in the vegetation fraction viewed by the randomly placed radiometers ($f_v = f_{v,su} + f_{v,sh}$; Figure 2.4) was large for viewing angles less than 15°, and decreased with increasing viewing angle. At all locations, f_v increased, and consequently f_s (=1 – f_v) decreased, for larger viewing angles until vegetation dominated the field of view. The relation between the vegetation fraction in the field of view of a radiometer and viewing angle (ϕ) is given by equation 2.6. Assuming a random leaf distribution with an extinction coefficient k = 0.5, the best fit of the equation 2.6 to the data in Figure 2.4 is for a LAI of 0.81 (r^2=0.91, Figure 2.4). This estimate agrees very well with our measured mean LAI of 0.77 (SE 0.06, n=121) in the 100x100 m plot.

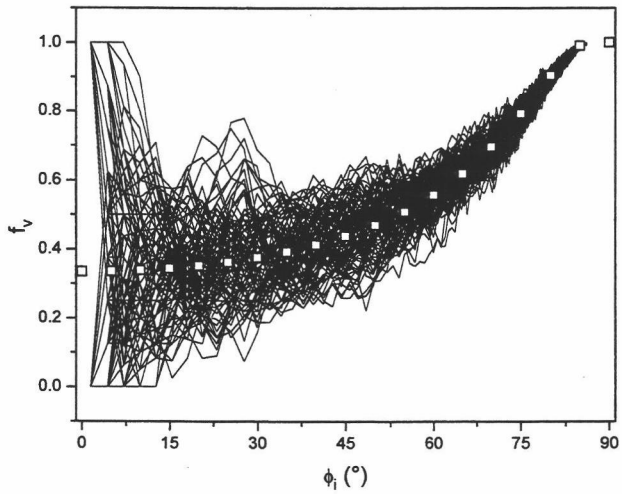

Figure 2.4 Vegetation fraction (f_v) versus viewing angle (ϕ) for all randomly-placed simulated radiometer locations. A fit of the average vegetation fraction viewed by a radiometer as a function of viewing angle (equation 2.6) is shown with open square symbols.

Figure 2.5 shows the contributions from different viewing angles to total (short + longwave) upwelling radiation ($R_{u.3D} = R_{su.3D}+R_{lu.3D}$) as a function of viewing angle for each of the 100 randomly-placed simulated radiometer locations. The highest contributions to $R_{u.3D}$ were from viewing angles around 45°. The variations in $R_{u.3D}$ were small for viewing angles less than 15° and greater than 70°. Areas with viewing angles of <15°, <42°, and <70° (corresponding to radial distances of 5, 18, and 55 m from the center) contributed 10%, 50%, and 90% of the upwelling radiation, respectively, which is in agreement with findings by Schmid (1997). The modeled scenes encompassed a viewing angle of up to 86°; contributions to R_u from larger angles than this are expected to be less than 0.5% of R_u, as can be estimated from Figure 2.5. Large variations in soil and vegetation fractions occurred close to the simulated radiometer locations but their contributions to the upward radiation are small since the area is small (sine weighting in equations 2.4 and 2.5). Variation in cover fraction decreases with higher viewing angles until the radiometer views mainly vegetation, and contributions from the soil become less important (Figure 2.4). The main cause of spatial variation in R_u arises from component variability at viewing angles from ~30 to ~60°, where contributions to R_u are high and variation in fractional cover between radiometer locations is large. Figure 2.4 and Figure 2.5 indicate that a radiometer deployed from a tower in a small clearing will only be affected slightly by the clearing, since only about 10% of R_u arises from viewing angles less than 15°.

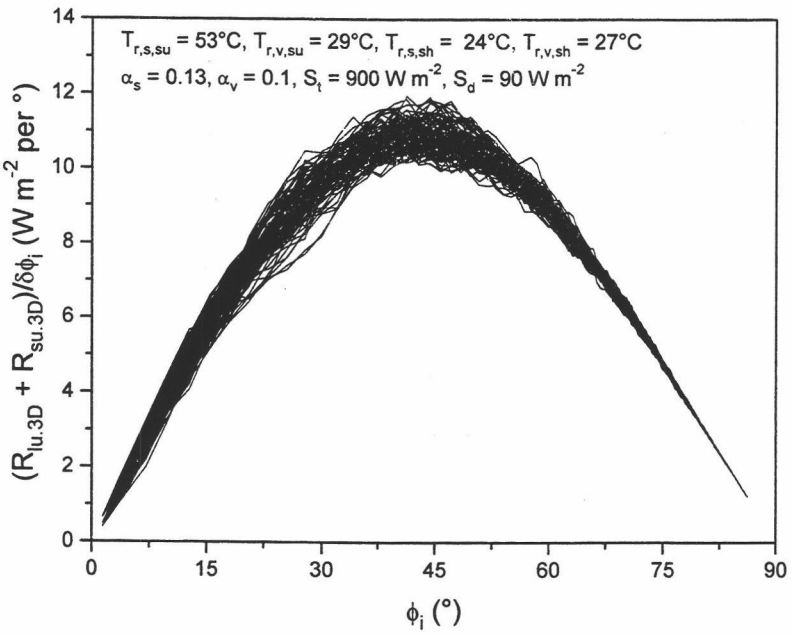

Figure 2.5 Contributions to the upwelling radiation ($R_u = R_{lu} + R_{su}$) versus originating viewing angle (ϕ) for all random radiometer locations.

The simple 2-D scaling of the upward radiation according to percent cover fraction (estimated from Figure 2.1(a)) (i.e. neglecting the three dimensional structure of the surface), and using representative values of T_r ($T_{r,s,su}$ = 56°C; $T_{r,s,sh}$ = 25°C; $T_{r,v,su}$ = 29°C; $T_{r,v,sh}$ = 27°C) for cloudless summer conditions and α_s = 0.13 for soil and α_v = 0.10 for vegetation resulted in $R_{lu.2D}$ = 566 W m^{-2} and $R_{su.2D}$ = 88 W m^{-2}. With the 3-D scaling, based on 100 randomly-placed simulated radiometers above the ecosystem, the mean values of $R_{lu.3D}$ and $R_{su.3D}$ were 534 W m^{-2} (SD 6.4) and 76 W m^{-2} (SD 2.7) respectively, both significantly lower (6 and 14%) than the 2-D scaling estimates. By taking into account the change in vegetation fraction with

viewing angle (Equation 2.3 with k = 0.5 and LAI = 0.81), $R_{lu.av}$ and $R_{su.av}$ would be 543 W m^{-2} and 82 W m^{-2}, respectively, slightly higher than the $R_{lu.3D}$ and $R_{su.3D}$.

We determined the sensitivity of R_{lu} to differences in T_r between the sunlit ecosystem components, by varying one T_r (i.e., that of sunlit soil or sunlit vegetation) while holding the other fixed at 29°C (Figure 2.6). For both cases, the shaded soil and shaded vegetation were assigned T_r values of 25°C and 27°C, respectively. The range of $R_{lu.3D}$ increased with increasing differences in the surface radiation temperatures of the ecosystem components (Figure 2.6). For temperature differences between $T_{r,s,su}$ and $T_{r,v,su}$ in excess of ~5 K, the range in $R_{lu.3D}$ was higher for the case of varying $T_{r,s,su}$ (Figure 2.6(a)) than for the case of varying $T_{r,v,su}$ (Figure 2.6(b)). Figure 2.6 shows that even for high temperature differences between soil and vegetation the uncertainty in R_{lu} due to a single point estimate is less than ~20 W m^{-2}. This uncertainty is small compared to the energy imbalance of ~200-250 W m^{-2} (Figure 2.3) on days when the difference between temperatures of sunlit soil and vegetation was large.

Figure 2.6 also show the 2-D estimates of $R_{lu.2D}$ for varying T_r. For our ecosystem, with larger soil percent cover than vegetation cover, the orthogonal percent cover fraction of sunlit soil was larger than the soil fraction seen by the 100 random radiometers. Therefore, $R_{lu.2D}$ increased with $T_{r,s,su}$ more than any of the $R_{lu.3D}$ values (Figure 2.6(a)), and increased less with $T_{r,v,su}$ than any of the $R_{lu.3D}$ values, but fell within the range of $R_{lu.3D}$ for $T_{r,v,su}$ > 35°C (Figure 2.6(b)). The 2-D and 3-D estimates of the upwelling longwave radiation are similar only for small differences between the soil and vegetation radiation temperatures or when $T_{r,v,su}$ is larger than $T_{r,s,su}$. When

$T_{r,s,su}$ is larger than $T_{r,v,su}$, the 2-D approach always results in an overestimate of the upwelling longwave radiation.

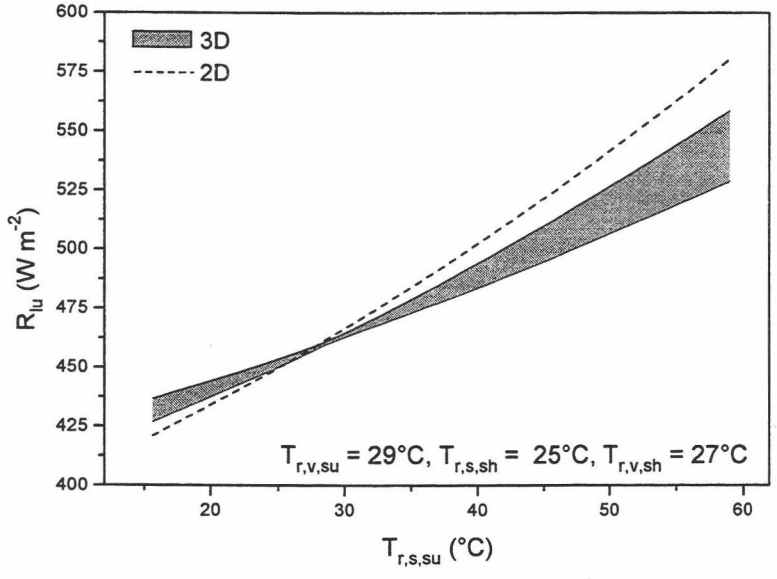

a)

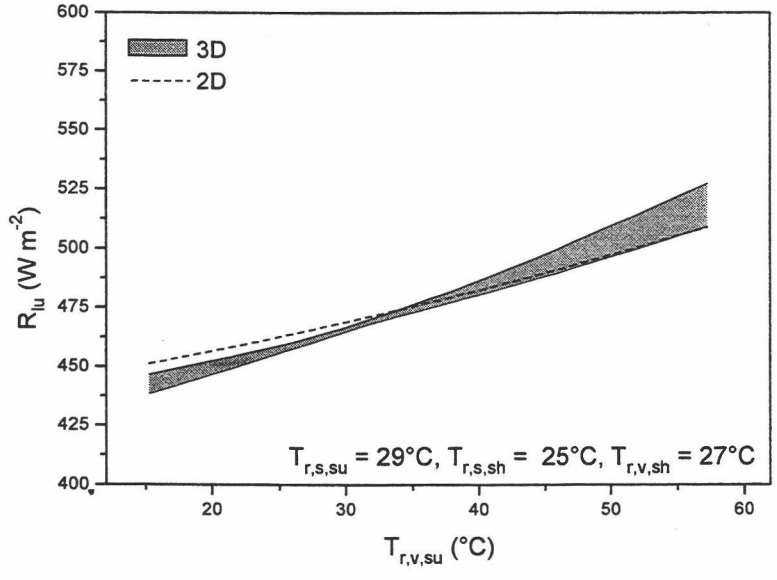

b)

Figure 2.6 Range in the modeled upwelling longwave radiation, $R_{lu.3D}$, of the 100 randomly-placed simulated radiometer locations versus varying surface radiation temperature of a) sunlit soil ($T_{r,s,su}$) and b) sunlit vegetation ($T_{r,v,su}$). The 2-D estimate of $R_{lu.2D}$ is shown as a dashed line.

Similarly, we determined the sensitivity of R_{su} to differences in the reflection coefficients between the soil and vegetation, by varying either α_s or α_v while holding the other fixed at 0.1 (Figure 2.7). S_t and S_d were specified as 900 W m^{-2} and 90 W m^{-2} respectively. The range in $R_{su.3D}$ increased with increasing difference between the ecosystem reflection coefficients, and was higher for the case of varying α_s (Figure 2.7(a)) than varying α_v (Figure 2.7(b)). Figure 2.7 shows that even for large differences in the reflection coefficients between soil and vegetation the uncertainty in R_{su} due to a single point estimate is less than ~25 W m^{-2}. As for $R_{lu.2D}$ and $R_{lu.3D}$, $R_{su.2D}$ increased with α_s more than any of the $R_{su.3D}$ values (Figure 2.7(a)) and increased less with α_v than any of the $R_{su.3D}$ values, but fell within the range of $R_{su.3D}$ for $\alpha_v > 0.15$ (Figure 2.7(b)). The 2-D and 3-D estimates of R_{su} will be similar for ecosystems with small differences between reflection coefficients or when α_v is larger than α_s, but a 2-D analysis will result in an overestimate of the upwelling shortwave radiation for the case when α_s is larger than α_v.

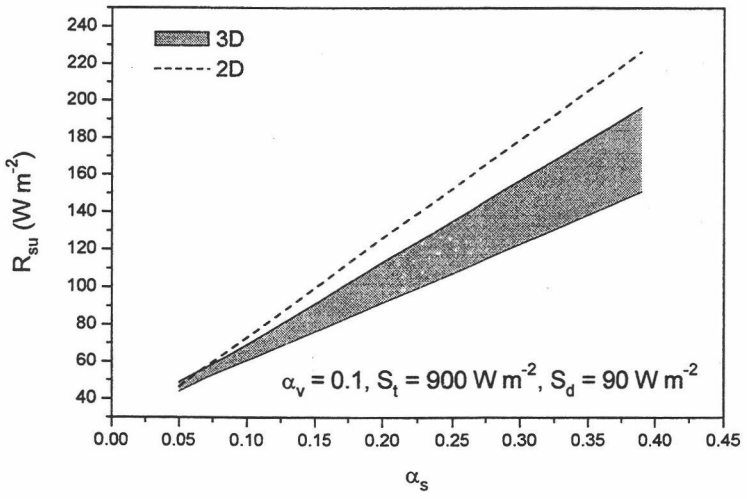

a)

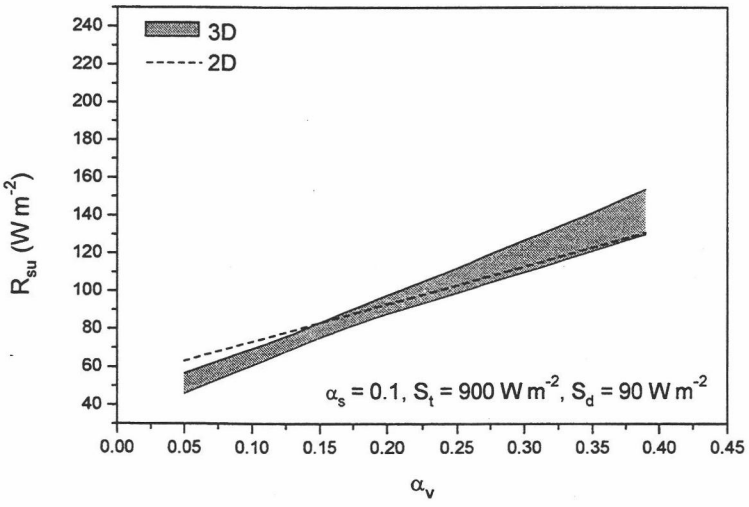

b)

Figure 2.7 Range in the modeled upwelling shortwave radiation, $R_{su.3D}$, of the 100 randomly-placed simulated radiometer locations versus varying reflection coefficient of a) soil (α_s) and b) vegetation (α_v). The 2-D estimate of $R_{su.2D}$ is shown as a dashed line.

Radiation emitted from the soil and blocked by vegetation becomes important for viewing angles higher than 45° (Figure 2.4). We found a difference of ~30 W m^{-2}

between the mean $R_{lu.3D}$ and $R_{lu.2D}$, for the case where the temperature difference between soil and vegetation was ~25-30 K. The difference between the mean $R_{su.3D}$ and $R_{su.2D}$ was ~15 W m^{-2} when the soil reflection coefficient (0.13) was slightly higher than the vegetation reflection coefficient (0.10). This indicates that ignoring the 3-D blocking effect may result in erroneous estimates of upwelling radiation.

The spatial variability of the upwelling radiation increased when soil radiative properties (i.e. radiative temperature, reflection coefficient) were larger then vegetation radiative properties, because radiation from the soil is blocked from reaching a radiometer by the surrounding vegetation. Vegetation contributions to upwelling radiation are also intercepted, but are replaced by contributions from foliage with similar radiative properties. For plants with a low height to distance ratio (e.g. lower canopy height with similar stand density), the amount of radiation blocked by the 3-D structure will usually be less than in our example, leading to smaller differences between the 2-D and 3-D estimates of R_u.

The uncertainty in an estimate of R_n from a single measurement location depends on the vegetation distribution around the measurement location. In our simulations, the uncertainty was less than ~10% of R_n even for conditions with large differences in the surface properties. For periods when there is significant shading (i.e., early morning hours, late afternoon, and seasons with low solar elevation), differences in radiative temperatures of the ecosystem components are probably small, and the uncertainty in the estimate of net radiation from one measurement location will also be small.

For vegetation with a closed-canopy, less variation in the upwelling components of R_n than we simulated here is expected, since vegetation structure is spatially more homogeneous and differences of surface radiation temperatures of the ecosystem components are most likely small. Nevertheless, Droppo and Hamilton (1973) detected up to 13% differences in midday net radiation above a deciduous forest when measured from three towers located only ~15 m apart. They surmised that the difference in R_n between locations was due to spatial variation in the vegetation structure around the measurement locations.

Smith et al. (1997) carefully intercalibrated net radiometers of different models and found a ~16% range of variation in measured R_n between sensors. Our measurements and modeling suggest that in open-canopy ecosystems, spatial variation in upwelling radiation components are comparable in magnitude to uncertainties in calibration coefficients. Consequently, the uncertainty in the estimation of net radiation for an open-canopy ecosystem makes it difficult to validate the accuracy of the eddy covariance method by determining the achievement of energy closure.

2.5 Conclusions

The three dimensionality of a forest canopy has a large impact on estimating upwelling longwave radiation from measured surface radiation temperature of ecosystem components. An estimate of upwelling radiation using simple cover fraction scaling (the 2-D approach) can be significantly different from the upwelling

radiation estimated by taking into account the three dimensional structure of the canopy. This difference occurs because part of the radiation emitted or reflected from the forest floor is intercepted by vegetation. Despite this radiative energy input to foliage, that supplements foliar interception of downwelling radiation, we found that radiative temperatures of juniper foliage were lower than radiative temperatures of soil on cloudless summer days. This is probably a consequence of the good coupling of the juniper leaves to the atmosphere and the ability of the plant to also lose energy as latent heat by transpiring water drawn from deep soil reserves.

Taking into account the change in vegetation fraction with viewing angle improves an estimate of the upwelling radiation at a radiometer location over the simple orthogonal cover fraction estimate. If vegetation parameters (k and LAI) are known accurately, it is possible to estimate the average upwelling radiation from radiation measurements made separately above the major ecosystem components (e.g., soil and vegetation). Adjustments for shade and sunlit fractions need to be made depending on sun position.

The upward radiation received by a single radiometer placed above an ecosystem depends on the distribution of the vegetation and soil around the instrument location and on the surface properties of the soil and vegetation that are in the field of view of the radiometer. The spatial variation is generally increased if surface properties (T_r and α) differ between the ecosystem components (i.e. soil and overstory). The variability is largest when the radiative flux from the ground is larger than the flux from the canopy, since it is the ground contributions that are intercepted by the canopy vegetation; radiation from the canopy that is intercepted is replaced by radiation from

foliage with similar properties. We conclude that at our site the measured upwelling component of the net radiation depends on measurement location but differs from the mean upwelling radiation by less than 10% even for large differences in T_r and α of the ecosystem components. This uncertainty is not enough to explain the lack of energy closure in this ecosystem. Further investigation should focus on quantifying loss of energy by advective processes, and determining the uncertainties and representativeness of measured turbulent fluxes of sensible and latent heat in the heterogeneous environment of this open canopy (Schmid and Lloyd, 1999).

2.6 Acknowledgments

This study was funded by NASA (grant #NAGW-4436 and #NAG5-7551). We are grateful to Will Hutchinson for his field assistance. We gratefully acknowledge the assistance of Teal Purrington from the Bureau of Land Management (BLM) in site selection. We thank Richard and Doris Waring for their help in establishing the study site. We thank Dr. Ronald Dobosy for his valuable comments on various aspects on aircraft-tower intercomparison of net radiation.

2.7 References

Auble, D.L. and Meyers, T.P., 1992. An open path, fast response infrared absorption gas analyzer for H_2O and CO_2. Boundary-Layer Meteorology, 59: 243-256.

Baldocchi, D.D., Hicks, B.B. and Meyers, T.P., 1988. Measuring biosphere-atmosphere exchanges of biologically related gases with micrometeorological methods. Ecology, 69(5): 1331-1340.

Blanken, P.D., Black, T.A., Yang, P.C., Neumann, H.H., Nesic, Z., Staebler, R., den Hartog, G., Novak, M.D. and Lee, X., 1997. Energy balance and canopy conductance of a boreal aspen forest: Partitioning overstory and understory components. Journal of Geophysical Research, 102: 28915-28927.

Blyth, E.M. and Harding, R.J., 1995. Application of aggregation models to surface heat flux from the Sahelian tiger bush. Agricultural and Forest Meteorology, 72: 213-235.

Dirmhirn, I. and Belt, G.H., 1971. Variation of albedo of selected sagebrush range in the intermountain region. Agricultural Meteorology, 9: 51-61.

Dolman, A.J., 1993. A multiple-source land surface energy balance model for use in general circulation models. Agricultural and Forest Meteorology, 65: 21-45.

Droppo, J.G. and Hamilton, H.L., 1973. Experimental variability in the determination of the energy balance in a deciduous forest. Journal of Applied Meteorology, 12: 781-791.

Fan, S.-M., Goulden, M.L., Munger, J.W., Daube, B.C., Bakwin, P.S., Wofsy, S.C., Amthor, J.S., Fitzjarrald, D.R., Moore, K.E. and Moore, T.R., 1995. Environmental controls on the photosynthesis and respiration of a boreal lichen woodland: a growing season of whole-ecosystem exchange measurements by eddy correlation. Oecologia, 102(4): 443-452.

Garratt, J.R., 1978. Transfer characteristics for a heterogeneous surface of large aerodynamic roughness. Quarterly Journal of the Royal Meteorological Society, 104: 491-502.

Goulden, M.L., Munger, J.W., Fan, S.-M., Daube, B.C. and Wofsy, S.C., 1996. Measurements of carbon sequestration by long-term eddy covariance: methods and critical evaluation of accuracy. Global Change Biology, 2: 169-182.

Grelle, A., 1997. Long-term water and carbon dioxide fluxes from a boreal forest. Ph.D. Thesis, Swedish University of Agricultural Sciences, Uppsala, Sweden.

Gritz, L. and Hahn, J.K., 1996. BMRT: A global illumination implementation of the RenderMan standard. Journal of Graphic Tools, 1(3): 29-47.

Hipps, L.E., 1989. The infrared emissivities of soil and *Artemisia tridentata* and subsequent temperature corrections in a shrub-steppe ecosystem. Remote Sensing of Environment, 27: 337-342.

Huband, N.D.S. and Monteith, J.L., 1986. Radiative surface temperature and energy balance of a wheat canopy. Boundary-Layer Meteorology, 36: 1-17.

Humes, K.S., Kustas, W.P., Moran, M.S., Nichols, W.D. and Weltz, M.A., 1994. Variability of emissivity and surface temperature over a sparsely vegetated surface. Water resources research, 30(5): 1299-1310.

Jones, H.G., 1992. Plants and microclimate: a quantitative approach to environmental plant physiology. Cambridge University Press, Great Britain.

Kelliher, F.M., Köstner, B.M.M., Hollinger, D.Y., Byers, J.N., Hunt, J.E., McSeveny, T.M., Mesert, R., Weir, P.L. and Schulze, E.-D., 1992. Evaporation, xylem sap flow, and tree transpiration in a New Zealand broad-leaved forest. Agricultural and Forest Meteorology, 62: 53-73.

Laubach, J., Raschendorfer, M., Kreilein, H. and Gravenhorst, G., 1994. Determination of heat and water vapour fluxes above a spruce forest by eddy correlation. Agricultural and Forest Meteorology, 71: 373-401.

Law, B.E. and Waring, R.H., 1994. Combining remote sensing and climatic data to estimate net primary production across Oregon. Ecological Applications, 4(4): 717-728.

Lee, X. and Black, T.A., 1993. Atmospheric turbulence within and above a Douglas-fir stand. Part II: Eddy fluxes of sensible heat and water vapour. Boundary-Layer Meteorology, 64: 369-389.

McCaughey, J.H., Laufleur, P.M., Joiner, D.J., Bartlett, P.A., M., C.A., Jelinski, D.E. and Ryan, M.G., 1997. Magnitudes and seasonal patterns or energy, water, and carbon exchanges at a boreal young jack pine forest in the BOREAS northern study area. Journal of Geophysical Research, 102(D24): 28997-29907.

Monteith, J.L. and Unsworth, M.H., 1990. Principles of Environmental Physics. Edward Arnold, Hodder Headline PLC, London.

Norman, J.M., Kustas, W.P. and Humes, K.S., 1995. Source approach for estimating soil and vegetation energy fluxes in observations of directional radiometric surface temperature. Agricultural and Forest Meteorology, 77: 263-293.

Paw U, K.T., 1992. Development of models for thermal infrared radiation above and within plant canopies. ISPRS. Journal of Photogrammetry and Remote Sensing, 47: 189-203.

Runyon, J., Waring, R.H., Goward, S.N. and Welles, J.M., 1994. Environmental limits on net primary production and light-use efficiency across the Oregon transect. Ecological Applications, 4: 226-237.

Schmid, H.P., 1997. Experimental design for flux measurements: matching scales of observations and fluxes. Agricultural and Forest Meteorology, 87: 179-200.

Schmid, H.P. and Lloyd, C.R., 1999. Spatial representativeness and the location bias of flux footprints over inhomogeneous areas. Agricultural and Forest Meteorology, 93: 195-209.

Schwerdtfeger, P., 1976. Physical principles of micro-meteorological measurements. Development in atmospheric science. Elsevier Scientific Publishing Company, Amsterdam.

Shuttleworth, W.J. and Wallace, J.S., 1985. Evaporation from sparse crops - an energy combination theory. Quarterly Journal of the Royal Meteorological Society, 111: 839-855.

Smith, E.A., Hodges, G.B., Bacrania, M., Cooper, H.J., Owens, M.A., Chappel, R. and Kincannon, W., 1997. BOREAS net radiometer engineering study. NASA Contractor Report (NASA Grant NAG5-2447), NASA-Goddard Space Flight Center, Greenbelt.

Stull, R.B., 1988. An Introduction to Boundary Layer Meteorology. Kluwer Academic, Dordrecht, The Netherlands.

Unsworth, M.H. and Monteith, J.L., 1975. Geometry of long-wave radiation at the ground. I. Angular distribution of incoming radiation. Quarterly Journal of the Royal Meteorological Society, 101: 13-24.

Webb, E.K., Pearman, G.I. and Leuning, R., 1980. Correction of flux measurements for density effects due to heat and water vapour transfer. Quarterly Journal of the Royal Meteorological Society, 106: 85-100.

3 Carbon and Water Vapor Exchange of an Open-canopied Ponderosa Pine Ecosystem

Peter M. Anthoni, Beverly E. Law, and Michael H. Unsworth

Anthoni, P.M., Law, B.E. and Unsworth, M.H., 1999. Carbon and water vapor exchange of an open-canopied ponderosa pine ecosystem. Agricultural and Forest Meteorology, 95(3): 151-168.

3.1 Abstract

Eddy covariance measurements of carbon dioxide and water vapor exchange were made above a ponderosa pine (*Pinus ponderosa* Dougl. ex P. & C. Laws.) forest located in a semiarid environment in central Oregon. The stand is a mixture of old-growth and young trees. Annual net carbon gain by the ecosystem (NEE) was 320 ± 170 gC m^{-2} yr^{-1} in 1996 and 270 ± 180 gC m^{-2} yr^{-1} in 1997. Compared to boreal evergreen forest at higher latitudes, the pine forest has a substantial net carbon gain (150 ± 80 gC m^{-2} yr^{-1} in 1996 and 180 ± 80 gC m^{-2} yr^{-1} in 1997) outside the traditionally defined growing season (from bud swell in early May (Day 125) to partial leaf-off in late September (Day 275)). Carbon assimilation continued to occur in the relatively mild winters, though at a slower rate (April, maximum leaf level assimilation (A_{max}) of 6-9.5 μmol m^{-2}-leaf s^{-1}), and ecosystem respiration was relatively low (~1.6 ± 0.1 gC m^{-2} d^{-1}). In the growing season, although photosynthetic capacity was large (July, A_{max} = 16-21 μmol m^{-2}-leaf s^{-1}), carbon assimilation was constrained by partial stomatal closure to maintain a sustainable water flow through the soil-plant system, and ecosystem respiration was large (3.5 ± 0.1 and 4.3 ± 0.1 gC m^{-2} d^{-1} in growing season of 1996 and 1997, respectively) because of high air and soil temperatures. Despite large changes in evaporative demand over just a few days (VPD changing from 0.5 kPa to 3.5 kPa), the ecosystem water use was remarkably constant in summer (~1.6-1.7 mm d^{-1}). Such homeostasis is most likely another result of stomatal control.

Interannual variations in climate had a large influence on the ecosystem carbon balance. In summer 1997, an El Niño year, precipitation was more frequent (17 days with 84 mm of rain) than in summer 1996 (5 days with 13 mm of rain), and the net ecosystem exchange was substantially lower in July-September 1997 (10 ± 60 gC m^{-2}) than during the equivalent period in 1996 (100 ± 60 gC m^{-2}). Although temperatures between years were similar, the carbon assimilation in 1997 was offset by increased respiration, probably because soils were more frequently wet, encouraging microbial respiration.

3.2 Introduction

As part of the NASA (National Aeronautics and Space Administration)-supported COSPECTRA (COoperative SPatial Energy and Carbon TRAnsfer) project, ecosystem carbon and water vapor flux and related biological and microclimate factors have been measured since March 1996 in a ponderosa pine (*Pinus ponderosa* Dougl. ex P. & C. Laws.) forest in central Oregon. Ponderosa pine is the most widely distributed and common pine in North America (Whitney, 1985). *P. ponderosa* ecosystems are generally open-canopied and have low leaf area index (LAI; m^2 half-surface leaf area per m^2 ground). The forest at our site has been managed by controlled understory burns, resulting in a sparse understory. For such open-canopied ecosystems, larger fractions of the whole ecosystem energy and carbon fluxes originate from the soil surface than in systems with high LAI (Baldocchi and Vogel,

1996). The processes controlling the energy and carbon exchange in open-canopied ecosystems must be understood, both to predict the influences of climate on hydrology and productivity, and to improve atmospheric models relating exchange to surface conditions (Huntingford et al., 1995; Sun and Mahrt, 1995).

Ponderosa pine forests in central Oregon experience wet, cold winters and dry, hot summers, so large seasonal differences in energy partitioning and water use are expected. Runyon et al. (1994) suggested that a *P. ponderosa* forest close to our site was potentially capable of gaining carbon throughout the year, but that net primary production was limited by periods of stomatal closure resulting from freezing, drought, or high vapor pressure deficits (VPD). Recently, Law et al. (1999b) reported that high temperatures in summer at our site resulted in large respiration rates from trees and soil. The combination of reduced carbon assimilation (because of stomatal closure) and increased respiration could lead to net ecosystem loss of carbon to the atmosphere in the dry season (July-September). Conditions for net carbon gain may be more favorable during the wetter spring and fall when soil temperatures and water stress are moderate.

P. ponderosa forests growing in semiarid environments are widely thought to use water efficiently. But in hot summer conditions, a delicate balance must be achieved between conserving water and avoiding damage from foliage overheating and xylem cavitation (Sperry, 1995; Mencuccini and Grace, 1996; Ryan and Yoder, 1997). Understanding how this balance is achieved at the ecosystem scale is important for improving models that link carbon and water relations.

The aims of this research were (1) to determine how net ecosystem exchange of CO_2 (NEE) and whole ecosystem water vapor exchange (LE) respond to environmental factors (e.g. radiation and VPD); (2) to compare the annual carbon balance derived from eddy covariance and associated measurements with values deduced from mensuration and respiration estimates; and (3) to improve understanding of factors controlling the long-term carbon and water vapor exchange of this semiarid ecosystem.

3.3 Methods

3.3.1 Site description

We made measurements above and below the canopy of an old-growth ponderosa pine forest located in a USDA Forest Service Research Natural Area (RNA) in the Metolius River basin, Oregon (44° 29' 56" N, 121° 37' 25" W, elevation 941 m). The fetch is uniform for several kilometers in the most common wind directions (south, west, and north). A forested north-south ridge lies about 1 km to the east of the site, with a rise in elevation of ~400 m. The forest has a very open canopy (LAI = 1.6; Law et al., 1999b), typical of this region. The stand includes areas with widely spaced old-growth trees (~250 years old and 33 m in height), patches of young trees (~45 years old and 9 m in height), and mixed-age stands (stand structural data are summarized in Table 3.1; Law et al., 1999b). The understory consists primarily of

bitterbrush (*Purshia tridentata*), strawberry (*Fragaria vesca*) and patches of bracken fern (*Pteridium aquilinum*). The understory LAI was 0.16 in summer 1996 (Law et al., 1999a). The sandy loam soils are classified as a dystric cryandept, a light-colored andic inceptisol that is low in nutrients.

Table 3.1 Mean characteristics of the dominant old trees and patches of young trees at the ponderosa pine site (standard errors in parentheses).

	Old trees	Young trees
Age of trees (yr)	250	45
Trees per hectare	70	550
Tree height (m)	33 (0.8)	9 (0.2)
Diameter at breast height (cm)	63 (2.7)	12 (0.2)
Sapwood volume (m^3 sapwood ha^{-1})	293 (3)	37 (0.1)

3.3.2 Eddy covariance measurements

Carbon and energy flux measurements were made with the eddy covariance technique (Baldocchi et al., 1988) from a tower at a height of 47 m, about 14 m above the dominant trees. The exchange rates of carbon dioxide (F_c), water vapor (LE) and sensible heat (H) were estimated following methods by Baldocchi and Vogel (1996).

Wind speed and virtual temperature were measured with a three-dimensional sonic anemometer (model 1012 R2, Gill Instruments, Lymington, England). An open-path, infrared gas analyzer (IRGA) (Auble and Meyers, 1992) measured CO_2 and water vapor fluctuations. Half-hour eddy covariances and statistics were computed online from ~10 Hz raw data, but these values were also stored for further analysis. Above-canopy fluxes were rotated to allow interpretation of the exchange rates normal to the streamlines following the local terrain. Appropriate corrections for cross-wind contamination of virtual temperature (Schotanus et al., 1983) and air density fluctuations (Webb et al., 1980) were applied. In the following sections, F_c, LE, and H are reported as positive if directed away from the surface. A positive value for net radiation (R_n) indicates a net flux of energy to the surface.

Flux measurements started on March 23, 1996. Data acquisition during winter was limited to two campaigns (Days 9-37 and 74-114) in 1997, because power supplied from solar panels was low. Data acquisition was generally continuous from April to November in both years, with a few data gaps caused by instrument problems.

3.3.3 Climate measurements

Figure 3.1 shows daily aggregated weather variables for 1996 and 1997. Above-canopy meteorological measurements were recorded at the top of the tower, using a Campbell Scientific Inc. (CSI) datalogger (model CR10X, CSI, Logan, UT). Above-canopy R_n was measured with a net radiometer (model Q7, REBS, Seattle, WA),

deployed from the south side of the tower. Downward global solar (S_r) and photosynthetically active radiation (PAR) were measured with radiation sensors (model LI-200SZ and LI-190SZ, respectively, LI-COR Inc, Lincoln, NE). Air temperature (T_a) and relative humidity (RH) were measured with a thermistor and capacitive RH sensor probe (model HMP35C, Vaisala, Helsinki, Finland). Wind speed and direction were monitored with a Wind Sentry set (model 03001, RM Young, Traverse City, MI).

Various other measurements were recorded below the canopy using CSI dataloggers (models CR10 and 21X, CSI, Logan, UT). T_a and RH were measured at 1 and 8 m with HMP35C sensors (Vaisala, Helsinki, Finland). Soil heat flux was measured at 0.02 m depth with four heat flux plates (model HFT-3, REBS, Seattle, WA). Spatial variation of soil temperature was measured at 18 locations with thermocouple probes at depths of 15 cm. Sapwood temperatures were measured in six trees with thermocouples placed about 2 cm into the sapwood at 1.5 m height. The rate of change in T_a, water vapor density, and sapwood temperature in the canopy layer was used to calculate change in energy storage (S).

Rainfall was measured with tipping-bucket rain gauges (model TE525I, CSI, Logan, UT), above and below the canopy. Soil water content (SWC) was monitored continuously in the upper 30 cm of soil with two soil water content sensors (model CS615, CSI, Logan, UT). The spatial variation of SWC was measured periodically (at 15 locations in 1996 and 3-5 locations in 1997) using time-domain reflectometry (TDR) (model 1502, Tektronix, Beaverton, OR). The TDR sampling rods were placed vertically in the soil to depths of 30 and 100 cm.

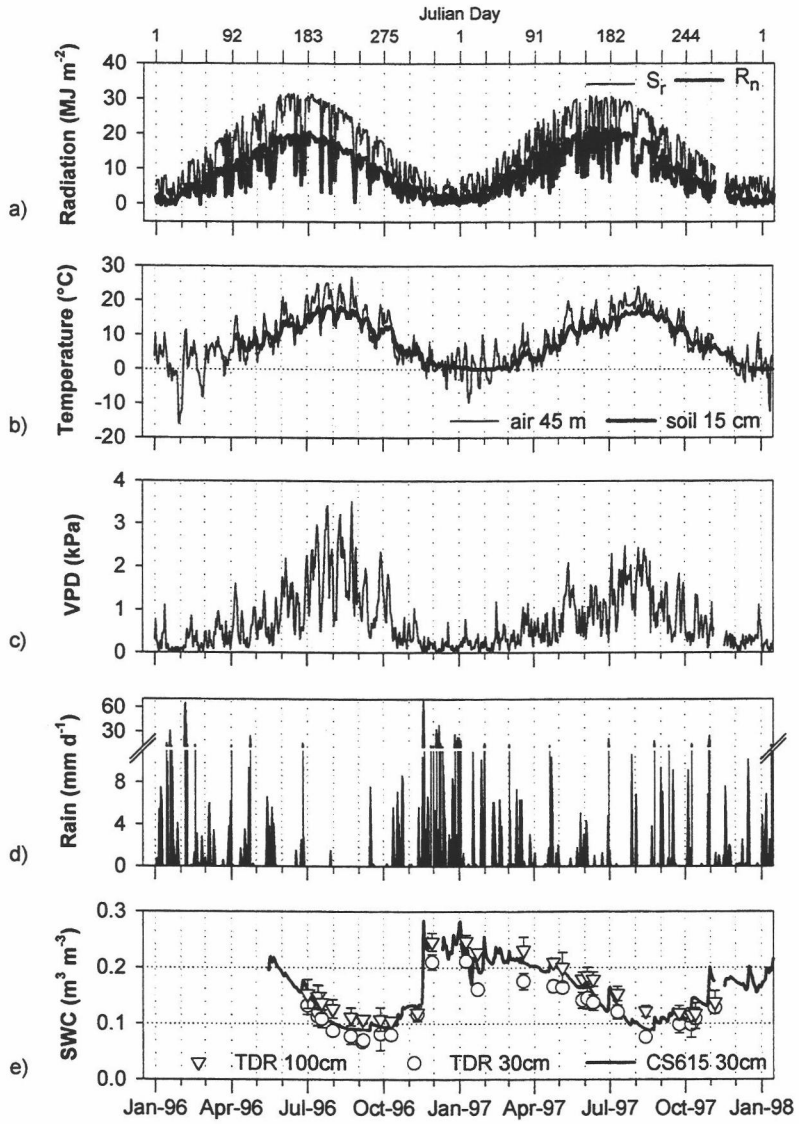

Figure 3.1 a) Daily above-canopy global solar (S_r) and net radiation (R_n), b) mean daily above-canopy air temperature and soil temperature at 15 cm, c) mean daylight above-canopy vapor pressure deficit (VPD), d) daily total rainfall, and e) mean soil water content (SWC) measured by TDR and CS615 sensor systems of the upper 30 and 100 cm soil layer for 1996 and 1997.

3.3.4 Carbon dioxide storage and vertical mass-flow term

The rate of change in carbon dioxide (F_{stor}) stored in the canopy air-layer was calculated from CO_2 profile measurements. Half-hour mean CO_2 concentrations at four heights (1, 8, 31, and 46 m) were measured with a IRGA (model LI-6262, LI-COR Inc, Lincoln, NE). The trend in the CO_2 concentration at each height over time was computed with a smoothing algorithm using running medians (S-PLUS, Mathsoft, Inc., Seattle, WA; Tukey, 1977). The value of F_{stor} below the eddy covariance system was then calculated by interpolating the CO_2 concentration trends in 1-m intervals and summing the change with time over all layers. During periods when the CO_2 profile system was not operational, the rate of change of the CO_2 signal of the eddy covariance IRGA, located above the canopy, was used to estimate F_{stor}.

The influence of vertical mass flow term (F_v) arising from horizontal flow divergence/convergence, resulting in a non-zero mean vertical velocity at the height of the flux observation was assessed following methods presented by Lee (1998). The mass-flow term was then added to the carbon dioxide flux, which was rotated to be normal to the plane defined by the horizontal velocity vector and the predicted mean vertical velocity.

3.3.5 Data screening

A data-screening procedure was used to remove possible eddy covariance instrumentation and sampling problems. The screening consisted of removal of periods with (1) kurtosis greater than 10 of wind speeds, IRGA CO_2 and H_2O signal, and virtual temperature; (2) excessive spikes in the sonic and IRGA data (due to precipitation, moisture or rime-frost on the sensors); (3) rainfall; (4) signals outside specified instrument limits; and (5) incomplete sampling over the entire half hour. Fluxes were also rejected when unreasonably large CO_2 fluxes ($|F_c| > 25$ μmol m^{-2} s^{-1}) were observed. After screening, about 75% of the above-canopy carbon flux and 85% of the energy fluxes remained available for further analysis.

3.3.6 Ecosystem respiration from scaled-up chamber measurements

Ecosystem respiration (R_e) of CO_2 was estimated from scaled-up chamber measurements of fluxes from the soil surface, tree stems and foliage. Temperature response equations were developed for soil surface CO_2 flux (F_s), wood (F_w), and foliage (F_f) respiration (Law et al., 1999b). We extended the analysis for 1997 by determining separate F_s equations for 1996 and 1997 from soil chamber measurements in each year, because F_s accounted for 75% of R_e, and different environmental conditions in the two years may have influenced root phenology and microbial activity. Good agreement was found between F_s and CO_2 flux measurement made

seasonally in 1996 and 1997 with an eddy covariance system setup above the forest floor (Law et al., 1999a). The temperature response equations for F_w and F_f from 1996 were used in 1997. Half-hourly respiration rates were calculated from continuously measured temperature data and R_e was calculated by summing the respiration rates from soil, wood, and foliage.

3.3.7 Net ecosystem exchange (NEE) from eddy covariance

Daytime (sunrise until sunset) NEE was calculated from eddy covariance measurements. At night, the sum of $F_c + F_{stor}$ did not compare well to independent R_e estimates from scaled-up chamber measurements for calm ($u_* \leq 0.25$ m s^{-1}) and more turbulent ($u_* > 0.25$ m s^{-1}) wind conditions (Law et al., 1999b). Under calm conditions, change in CO_2 storage alone compared well with R_e, probably because F_c is negligible (Law et al., 1999a). At sufficiently high wind speeds, the above-canopy F_c may be expected to give a good estimate of the nighttime CO_2 exchange (Grelle, 1997), but these conditions seldom occur at our site. As an alternative to $F_c + F_{stor}$, we used nighttime ecosystem respiration calculated from the scaled-up chamber measurements to estimate nighttime NEE. Apparently, our nighttime $F_c + F_{stor}$ would probably lead to an underestimation of nighttime NEE during more turbulent conditions. During calm conditions F_{stor} could be used as an estimator for R_e at our site, but the CO_2 profile system was operated only occasionally from fall through spring, because of its high power consumption. The NEE calculated by

micrometeorological methods and scaled-up chamber respiration will be referred to as NEE_m. An ecological sign convention is used for NEE, where positive NEE signifies a net gain of carbon by the ecosystem and negative NEE indicates that carbon is being lost to the atmosphere (Note: this is the reverse of the sign convention used for F_c).

For estimating annual NEE_m, missing days and screened-out data were filled in according to an empirical relationship, based on the light response of carbon assimilation (A_c), estimated by the difference between measured F_c and R_e from scaled-up chamber data, versus PAR of ~±20 surrounding days for times with low VPD. The reduction of A_c at high VPD was estimated by linear regression of the residual of A_c after accounting for the radiation dependence. Predicted net carbon flux (F_{cp}) was then calculated as

$$F_{cp} = \left(\frac{P_{max} \cdot PAR}{K_m + PAR}\right) + (a_0 + a_1 \cdot VPD) + R_e \qquad (3.1)$$

where P_{max} and K_m are empirically determined light-response parameters, and a_0 and a_1 are the VPD regression coefficients. The methods used to determine the model parameters are described in more detail in the Appendix. During the growing season, about 11% and 39% of missing NEE_m values were filled-in with F_{cp} in 1996 and 1997, respectively. About 65% and 60% of NEE_m values during the dormant season in 1996 and 1997, respectively, had to be filled-in using the empirical relationship.

3.3.8 Uncertainty assessment

Moncrieff et al. (1996) discussed random and systematic sources of errors in long term flux measurements. We evaluated possible systematic errors in our flux measurements. Uncertainties in the calibration of the gas analyzer due to calibration gases, which were compared to a NIST traceable calibration gas, were estimated to be about ±3%. Uncertainties from changes in the analyzer calibration due to dirt and residue build up on the IRGA optics was estimated as ~±5-10% by the relative change in the calibration coefficients from one calibration to the next. Instabilities in calibration coefficients due to diurnal variation in temperature and pressure are difficult to quantify, but are assumed to be less than 5%. Uncertainties in wind speed and virtual temperature measured by the sonic anemometer result in ~±2% uncertainty in scalar fluxes (Grelle, 1997). Combining all of the systematic errors geometrically, the overall uncertainty of the daytime carbon dioxide flux was ~±12%.

The systematic error in R_e estimated by the chamber method includes uncertainties in respiration measurements and in biomass estimates used for scaling respiration to the stand level. The uncertainty in R_e was estimated as ~±20% of the mean R_e (Law et al., 1999b) by recalculating respiration rates with the upper and lower confidence intervals (95%) for respiration rates, biomass and LAI.

3.3.9 Net ecosystem exchange from mensuration measurements

Net ecosystem exchange (NEE_p) can be calculated from net primary production (NPP) and heterotrophic respiration (R_h),

$$NEE_p = NPP + R_h \qquad (3.2)$$

with the sign convention that positive NPP indicates net production of carbon and negative R_h means a loss of carbon by the ecosystem. NPP was estimated from aboveground wood and foliage production, and belowground root production. Aboveground stemwood production was calculated as the mean annual wood increment estimated from the last 5 years growth rings in wood cores. Foliage production was calculated from the fraction of total foliage biomass that was newly expanded foliage. Details of methods and estimates are given by Law et al. (1999b).

Belowground root production was estimated as 50% of belowground carbon allocation (B) (Ryan, 1991a; Ryan, 1991b; Law et al., 1999b). According to Raich and Nadelhoffer (1989), B can be calculated from annual soil respiration minus annual litterfall, assuming that soil carbon storage is near steady state. Heterotrophic respiration (R_h) was estimated as 50% of B plus surface litter decomposition, calculate from the mean residence time of litter (~30 years) (Law et al., 1999c).

Uncertainty in NEE_p arises from uncertainties in: (1) estimates and scaling of production and respiration measurements to the stand level; (2) calculation of

belowground root production and R_h as a fraction of B; and (3) estimates of wood production for the current year as the mean wood increment of the last 5 years.

3.3.10 Water vapor exchange

Daily total ecosystem water vapor exchange (LE) was calculated from the measured above-canopy eddy covariance water vapor flux and the change in water vapor concentration in the canopy air-layer, which was estimated from half-hour changes in water vapor concentrations measured within the canopy. Screened-out data during the day were filled in by linear interpolation between neighboring data points.

For estimating an annual water budget, missing days were filled in according to an empirical relationship, based on the Penman-Monteith equation (Monteith and Unsworth, 1990), in which whole ecosystem bulk surface conductance was estimated seasonally (from 6-7 mm s^{-1} in the wet season down to 2-3 mm s^{-1} in the dry season) from measured LE. The IRGA was calibrated periodically with a dew-point generator (LI-610, LI-COR Inc., Lincoln, NE), and instrument performance was checked against measured water vapor density. The overall error in the latent heat exchange due to calibration uncertainties and systematic sonic anemometer errors was estimated to be ~±15%.

3.4 Results and Discussions

3.4.1 Energy closure and spectral analysis

Daily energy closure, evaluated as $(H+LE)/(R_n-G-S)$, was usually about 70% ($H + LE = 0.69 * (R_n-G-S) + 0.35$ MJ m^{-2} d^{-1}, $r^2 = 0.88$, n= 426), and was relatively independent of wind direction for winds from the most common directions. Closure was lower for winds from the south-east or north and it was generally lower than values reported for other forest ecosystems (~80-100%; Kelliher et al., 1992; Lee and Black, 1993; Laubach et al., 1994; Fan et al., 1995; Goulden et al., 1996; Blanken et al., 1997; Grelle, 1997; McCaughey et al., 1997). Possible causes of incomplete energy closure are errors and uncertainties in the spatial characterization of net radiation and soil heat flux, or in the detection and measurement of all turbulent and advective energy fluxes. All of these sources of error are likely to occur in open-canopied ecosystems. Large gaps in the canopy result in large spatial variations in soil heat flux and upwelling radiation. At a nearby juniper/sagebrush site with a more open-canopy structure, we estimated the uncertainty in the upwelling radiation due to net radiometer placement above the canopy (Anthoni et al., 1998). We found a spatial range of ~60 W m^{-2} in the upwelling radiation (unpublished data). Because of the differences in tree height and net radiometer placement the amount of soil or understory "seen" by the radiometer at the pine site is less than at the juniper site, but differences in the surface properties of the over- and understory cause uncertainty in measurements of net radiation from towers. Above a deciduous forest, Droppo and

Hamilton (1973) detected up to 13% difference in midday net radiation when measured simultaneously from towers just 15 m apart. There is also large uncertainty in the absolute calibration of net radiometers. Smith et al. (1997) found a ~16% range of variation in measured R_n from different net radiometer models.

Blanken et al. (1997) found low values of fractional energy closure over their boreal aspen forest at low wind speeds. Closure increased linearly with u_*, reaching within 20% of unity (perfect closure) when u_* exceeded 0.35 m s^{-1}. They suggested that lack of fully developed turbulence at low u_* was partly responsible for lack of closure. A similar problem may occur at our site, where energy closure was better at higher wind speeds (Mahrt, 1998). Horizontal advection of energy seems unlikely to be a significant source of lack of closure, because (a) closure was relatively independent of wind direction and (b) assuming a relatively large horizontal temperature gradient of 1 K km^{-1} and moisture gradient of 1 g kg^{-1} km^{-1} with a mean midday wind speed of 2 m s^{-1} would result in energy transport of less than 10 W m^{-2}.

Considering the possible large uncertainties in the estimation of the available energy, we conclude that it is very difficult to judge the validity of eddy covariance measurements in open-canopy ecosystems by testing the energy budget closure.

Spectral analyses of measured turbulent fluctuations were used to determine the reliability of our flux measurements. We generated power and co-spectra of measured fluctuations in vertical wind speed (w), CO_2, H_2O, and virtual temperature (T_v) by averaging the spectral coefficients from eight data segments, each with 4096 data points. The power spectra of w, T_v and H_2O exhibited an inertial subrange with the expected slope of -2/3 to about 5 Hz. The inertial subrange with a -2/3 slope of the

CO_2 power spectra reached about 1 Hz, with higher frequencies showing some random noise. The cospectra between vertical wind speed and T_v, CO_2, and H_2O were nearly identical, indicating similarity of the turbulent transport of these entities. Main contributions to the fluxes were from frequencies less then 1 Hz. Auble and Meyers (1992) used an open-path IRGA of the same design over a fully leafed deciduous forest and found very similar spectra. We conclude that the eddy covariance system recorded nearly all turbulent fluctuations, with only fluctuations of CO_2 and H_2O with frequencies higher than 1 Hz attenuated, most likely as a result of sensor separation between the IRGA and the sonic anemometer.

3.4.2 Storage and mass-flow corrections of daily NEE

It is common practice to assume horizontal homogeneity in the calculation of net ecosystem exchange by the eddy covariance method. Consequently NEE is the sum of measured eddy CO_2 flux (F_c) and the change in CO_2 concentration below the measurement level (F_{stor}). Lee (1998) pointed out that analysis should also usually include a vertical mass-flow term, F_v, that accounts for possible vertical advection due to a non-zero mean vertical wind component. The often-seen early-morning change in CO_2 concentration has to be accounted for by net plant uptake plus any exchange of CO_2 with the atmosphere, due to either a flush-out event (Grace et al., 1996), a vertical mass-flow F_v, or entrainment of CO_2 from above the boundary layer.

Figure 3.2 shows measured and modeled carbon flux components during late summer 1997 for groups of days when especially high or low CO_2 concentrations were encountered at night. For about 40% of the year, relatively turbulent conditions suppressed the build up of respired CO_2 at night (Figure 3.2(a)). The rest of the time, calm conditions at night led to a build up of CO_2, and concentrations exceeding 400 ppm were observed within and above the canopy air layer (Figure 3.2(b)). Concentrations decreased in the early morning hours, as was also observed with chamber measurements at the soil surface (425 ppm - 350 ppm between 7:30 and 10am). This decline led to large values of F_{stor} (Figure 3.2(d)).

To determine whether the estimation of NEE_m as $F_c + F_v + F_{stor}$ is reasonable at our site, we compared NEE_m estimates with potential net plant CO_2 uptake (F_{cp}). F_{cp} was calculated from an empirical model incorporating light and VPD responses (see equation 3.1), with model parameters determined from $F_c + F_v + F_{stor}$, using only periods when F_{stor} was small ($|F_{stor}| < 2$ μmol m^{-2} s^{-1}). At night, F_{cp} was assumed equal to the R_e value from the scaled up chamber measurements. On days following nights of a build up of CO_2 in the canopy air space, F_{cp} was substantially more positive than $F_c + F_v + F_{stor}$ for several hours in the morning (Figure 3.2(d)). Nighttime values of $F_c + F_v + F_{stor}$ underestimated the scaled-up chamber respiration estimate of R_e for more turbulent nights (Figure 3.2(c)), but there was agreement for calm nights (Figure 3.2(d)).

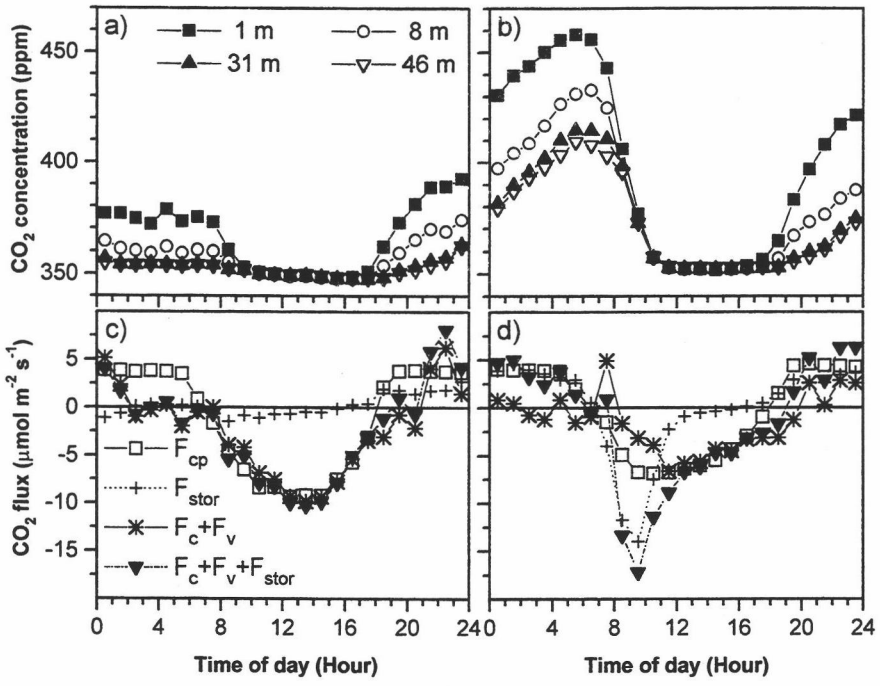

Figure 3.2 Mean diurnal CO_2 concentration within (1, 8, and 31 m) and above the canopy (46 m) and measured carbon flux components (F_c, F_v, F_{stor}) and potential net plant CO_2 uptake (F_{cp}; equation 3.1) during 38 days in late summer 1997. Shown are the average diurnal trends for (a, c) 10 days with more turbulent conditions at night ($u_* \geq 0.175$ m s^{-1}) and (b, d) 28 days with calm conditions at night ($u_* < 0.175$ m s^{-1}).

Daily total, daytime and nighttime sums of carbon flux components (F_c, F_v, F_{stor}) and potential net CO_2 uptake (F_{cp}) during days with and without nighttime build up of CO_2 in the canopy air layer are shown in Table 3.2. Using the nighttime $F_c + F_v + F_{stor}$ instead of R_e to estimate nighttime ecosystem respiration would lead to a substantial overestimation (~1 gC m^{-2} d^{-1}) of daily NEE_m on more turbulent nights. However, incorporating F_v improved the disagreement reported earlier between F_c+F_{stor} and the scaled-up ecosystem respiration estimate R_e at night (Law et al., 1999b). During

daytime, the mass-flow term F_v was small (less than 2% of daytime NEE_m) and continuous information for the vertical CO_2 gradient was not available. Therefore, we choose not to apply the mass-flow correction to the daytime eddy CO_2 flux in calculating daily NEE_m.

Table 3.2 Daytime, nighttime, and daily total of carbon flux components (F_c, F_v, F_{stor}) and potential net CO_2 uptake (F_{cp}; equation 3.1) during 38 days in late summer 1997 with and without nighttime build up of CO_2 in the canopy air layer. Positive values indicate a net carbon loss and negative values a net carbon gain by the ecosystem.

	$F_c + F_v + F_{stor}$ ($gC\ m^{-2}$)	F_{cp} ($gC\ m^{-2}$)	F_v ($gC\ m^{-2}$)	F_{stor} ($gC\ m^{-2}$)
a) 10 Days without buildup of nighttime CO_2 (nighttime $CO_2 < 400$ ppm, $u_* \geq 0.175\ m\ s^{-1}$)				
Day	-3.2	-3.1	-0.1	-0.3
Night	0.9	1.9	0.3	0.5
Daily total	-2.3	-1.2	0.2	0.2
b) 28 Days with buildup of nighttime CO_2 (nighttime $CO_2 \geq 400$ ppm, $u_* < 0.175\ m\ s^{-1}$)				
Day	-3.4	-2.1	-0.1	-1.6
Night	1.8	1.8	0.4	1.5
Daily total	-1.6	-0.3	0.3	-0.1

An unusual feature of our results is the high concentration of CO_2 that built up over substantial depth on calm nights (Figure 3.2). Most other sites observe less storage of CO_2. For an Amazonian rain forest Grace et al. (1995a; 1995b; 1996) reported high nighttime CO_2 concentrations similar to our observations. After calm

nights at their site, there was a consistent morning flush out in the eddy CO_2 flux, which accounted for part of the change in the CO_2 concentration in the canopy air-layer. Consequently the net effect of storage on daily NEE at their site was relatively small. After calm nights at our site, we seldom observed a consistent flush out in the eddy CO_2 flux (Figure 3.2(d)). This may be because the vertical CO_2 concentration became well mixed within and above the canopy (Figure 3.2(b)) shortly after sunrise. If we assume that the total amount of stored CO_2 is assimilated by the vegetation in the first few hours of the day, our daily estimates of NEE are implausibly large on calm days and disagree both with measured NEE on windier days and with the simple model (F_{cp}).

Other processes (e.g. horizontal advection or entrainment of air from above the boundary layer) could be responsible for the depletion of CO_2 during the early morning hours. In complex terrain, considerable differences in horizontal CO_2 concentrations can be expected. Large spatial variations in the nighttime CO_2 concentrations were observed in boreal forests (Baldocchi, pers. comm.), which can lead to horizontal advection effects (Sun et al., 1997). A north-south ridge to the east of our site shields the forest around the flux tower from direct radiation for 1-2 hours after sunrise, but areas farther west are sunlit earlier. This could lead to localized convective circulation as well as spatial variation in CO_2 exchange; these differences may result in a horizontal gradient in the CO_2 concentration in the early morning hours, but we do not yet have measurements to confirm this.

To avoid the uncertainties in daily NEE_m, when early morning periods included a large F_{stor} ($F_{stor} \leq -2$ μmol m^{-2} s^{-1}), we replaced $F_c + F_v + F_{stor}$ with the predicted F_{cp}.

Because model parameters for F_{cp} were determined mainly from periods with low F_{stor}, which are biased toward low CO_2 concentrations, the model may not account for increased assimilation as a consequence of CO_2 'fertilization'. However, a sensitivity analysis conducted using a process-based soil-plant-atmosphere model that incorporates Farquhar's equations (Williams et al., 1996) indicated that F_{cp} might underestimate the true net plant uptake by only about 0.5 μmol m^{-2} s^{-1} during conditions of high CO_2 concentrations (Williams, pers. comm.).

3.4.3 Environmental constraints on carbon and water vapor exchange

Figure 3.3 shows day-to-day variation in net ecosystem exchange, ecosystem respiration, whole ecosystem latent heat exchange, and environmental drivers over a period of 40 days in the summer of 1996. On several occasions during the summer (i.e., Day 201 and 220), weather systems moving over the region from the Pacific Ocean resulted in overcast conditions, cooler air temperatures and lower VPD (Figure 3.3(a, b, c)). During those conditions, ecosystem respiration (Figure 3.3(d)) decreased because of lower temperatures, and carbon assimilation was high due to less stomatal constraint, resulting in relatively large NEE_m (Figure 3.3(e)) by the ecosystem (up to 4 gC m^{-2} d^{-1}). After each weather system passed, T_a and VPD gradually increased, resulting in higher ecosystem respiration and lower carbon assimilation. In consequence, NEE_m declined steadily on successive days, particularly in the afternoon, and after a few days the ecosystem switched from gaining carbon to losing

carbon, until the next weather system moved in. During the whole period, LE remained relatively constant at 4-5 MJ m^{-2} d^{-1} (1.6-2.0 mm d^{-1}); only on days with variable radiation did LE show larger variations (Figure 3.3(f)).

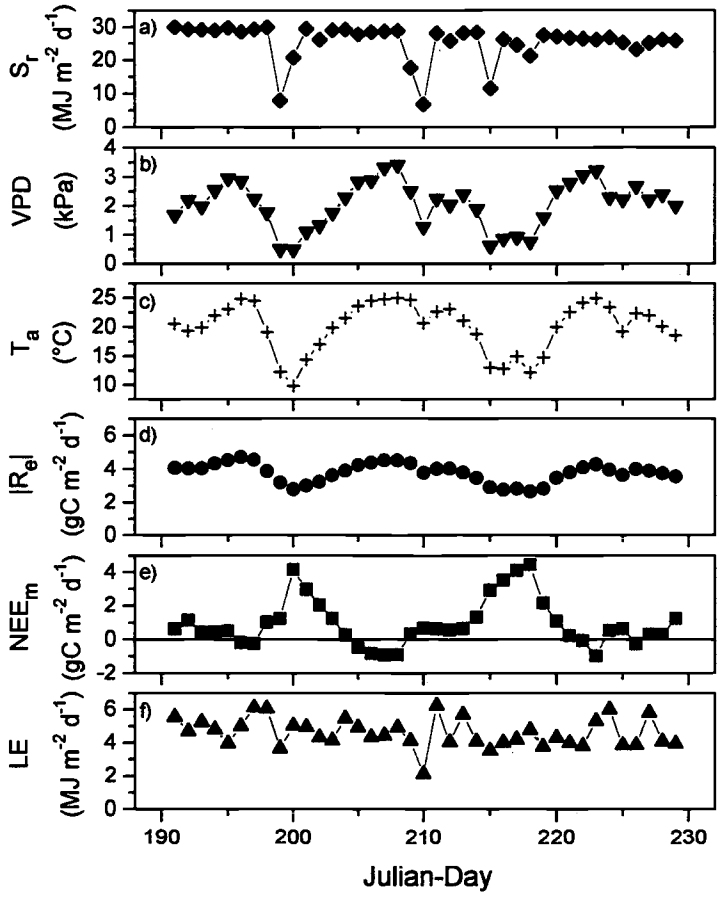

Figure 3.3 Day-to-day variations in a) daily total global solar radiation (S_r), b) mean daylight VPD, c) mean daily air temperature (T_a), and daily total d) ecosystem respiration (R_e; absolute value of R_e is shown), e) net ecosystem exchange (NEE_m), and f) whole ecosystem latent heat exchange (LE) during 40 days in summer 1996.

Figure 3.4(a) shows the variation of daily NEE_m with VPD for three classes of solar radiation levels. For days with high radiation (S_r > 20 MJ m^{-2} d^{-1}), daily NEE_m

declined at a rate of 1.5 gC m^{-2} d^{-1} per 1 kPa increase in VPD. Because VPD is positively correlated with temperature, Figure 3.4(a) confounds the effect of partial stomatal closure and increased respiration. For example, on high-radiation days, daily R_e (modeled as a function of temperature) increased by about -0.5 gC m^{-2} d^{-1} as VPD increased by 1 kPa, simply due to the accompanying higher temperatures. To remove this respiration response, Figure 3.4(b) shows the variation of daily gross ecosystem production GEP (= NEE_m - R_e) with VPD. On days with high radiation, there was a 1 gC m^{-2} d^{-1} decline in GEP per 1 kPa VPD increase. Thus the variation in NEE with increasing VPD was dominated by variation in gross carbon uptake rather than R_e, unlike findings of Jarvis et al. (1997).

Carbon assimilation did not halt at high VPD (>2 kPa), though NEE_m was occasionally negative (indicating that the system was a source of carbon to the atmosphere, Figure 3.3(e) and Figure 3.4(a)). Figure 3.4(b) suggests that on the sunniest days, daily gross carbon exchange was about twice as large when VPD was low (0.5-1 kPa) as it was when VPD was high (>2 kPa). As an exception, there were a few days with high radiation and low VPD (<1 kPa) when GEP was low. On most of those days, near-freezing nighttime temperatures followed by clear sky conditions may have led to photoinhibition, limiting carbon uptake.

In contrast to the reduction of carbon assimilation that occurred when VPD exceeded 1.0 kPa (Figure 3.4(b)), daily ecosystem latent heat exchange (LE) showed less response to high VPD (Figure 3.3(f) and Figure 3.4(c)). Daily summer water loss for high radiation days was remarkably similar throughout the summer season and between years. The mean was 4.0 ± 0.2 MJ m^{-2} d^{-1} (1.6 mm d^{-1}) in summer 1996 and

4.1 ± 0.2 MJ m^{-2} d^{-1} (1.7 mm d^{-1}) in summer 1997, even though the summer mean daylight VPD was significantly higher in 1996 (1.7 kPa) than in 1997 (1.3 kPa; $p>>0.05$). High rates of LE up to 10 MJ m^{-2} d^{-1} (4 mm d^{-1}) were only observed after periods of rain (Figure 3.4(c)) and were usually maintained for only one day.

Whole-ecosystem LE leveled out as VPD increased beyond ~1 kPa, suggesting that water flow may have been limited by the hydraulic capacity of the whole plant system (roots, stems, leaves). If this were the case, stomata would adjust to maintain a sustainable water flow and minimize the possibility of cavitation (Mencuccini and Grace, 1996). As a direct consequence of partial stomatal closure, the rate of CO_2 diffusion into the leaves becomes limited and assimilation is reduced. The large variations in NEE_m and relatively stable LE at our ponderosa pine site in summer were similar to the pattern of NEE and LE reported for a boreal black spruce forest by Jarvis et al. (1997).

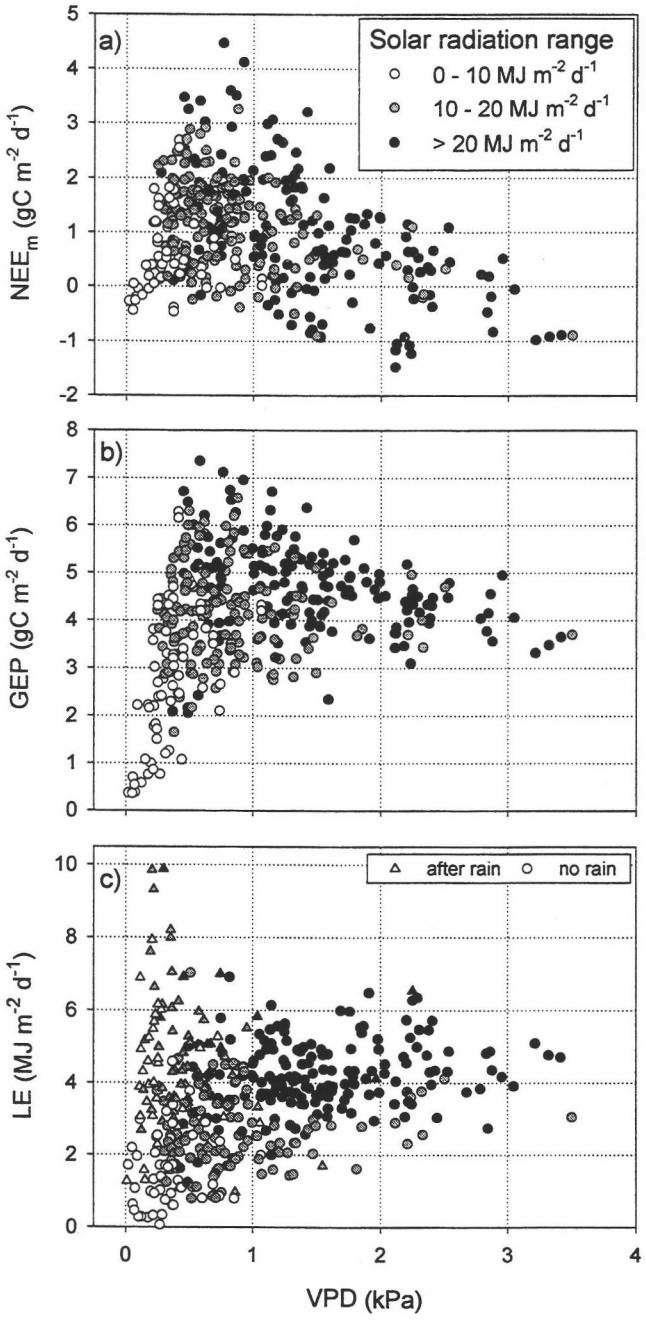

Figure 3.4 Daily total a) net ecosystem exchange (NEE_m) and b) gross ecosystem production ($GEP = NEE_m - R_e$), and c) whole ecosystem latent heat exchange versus mean daylight above-canopy vapor pressure deficit (VPD) for differing conditions of global solar radiation (symbol shading). c) Symbol form indicates days with and without rain occurrence.

3.4.4 Cumulative water vapor and net ecosystem carbon exchange

Cumulative whole ecosystem evapotranspiration, LE, and rainfall for the years 1996 and 1997 are shown in Figure 3.5. Annual whole ecosystem LE was 430 ± 70 mm in 1996 and 400 ± 60 mm in 1997, relatively constant compared to annual precipitation of 867 mm in 1996 and 488 mm in 1997.

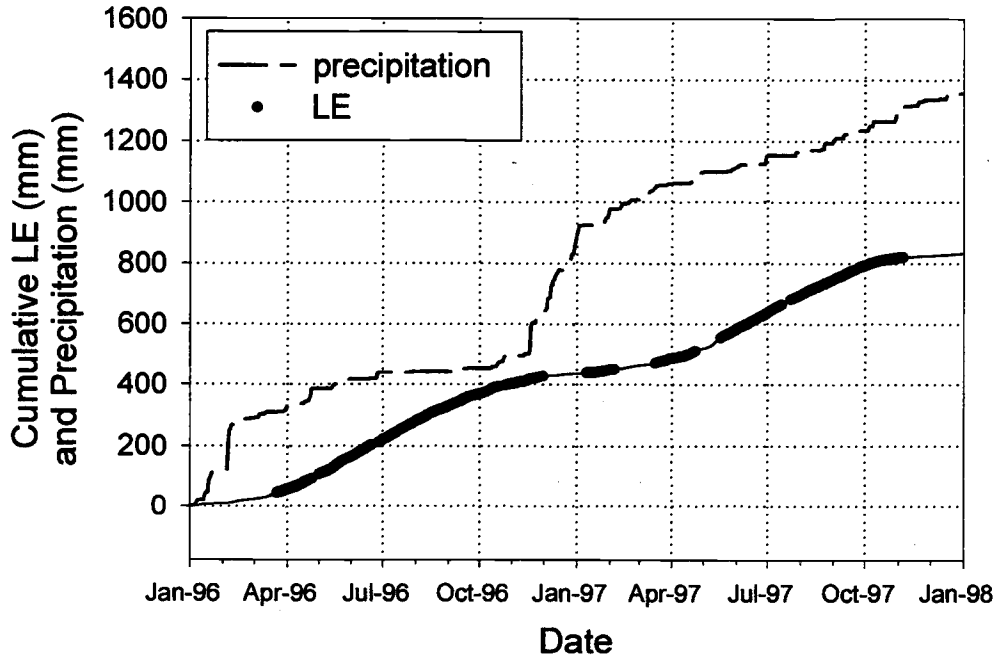

Figure 3.5 Cumulative precipitation and ecosystem water vapor exchange (LE) during 1996 and 1997. Breaks in the cumulative LE indicate periods for which data are missing; daily LE was then modeled based on the Penman-Monteith equation.

Monthly estimates of NEE, R_e and GEP for 1996 and 1997 are shown in Figure 3.6. The most striking difference between years are in summer values of R_e and NEE_m. The July-September mean daily T_a was slightly lower in 1997 than in 1996 (19.4 °C versus 18.7 °C). The soil temperature at 15 cm was also slightly lower in July-September 1997 than in 1996 (14.1°C versus 14.5°C). Interestingly, precipitation patterns were different from normal in summer 1997; precipitation was more frequent (17 days with a total of 84 mm) than in July-September 1996 (5 days with a total of 13 mm). Despite slightly cooler temperatures in 1997, the ecosystem respiration estimates for July-September were higher for 1997 (-410 gC m^{-2}) than for 1996 (-330 gC m^{-2}) (Figure 3.6). The difference was mainly due to increased soil respiration. Because of higher respiration rates in summer 1997, the NEE_m was only 10 ± 60 gC m^{-2} between July and September 1997, much less than the value of 100 ± 60 gC m^{-2} for the same time period in 1996.

Law et al. (1999a) examined the relationship of soil respiration with different environmental variables at our site in 1996, including soil moisture (0-30cm, 0-100 cm), soil temperature and soil chemistry and found only a weak correlation with soil moisture; soil temperature explained ~60% in the variation in the soil CO_2 efflux. After accounting for the temperature effect, by normalizing to a common temperature (10°C), the normalized soil respiration rates in summer 1997 (2.3 μmol m^{-2} s^{-1}) are generally higher than in summer of 1996 (1.9 μmol m^{-2} s^{-1}). The more frequent rain in summer of 1997 than in summer of 1996 might have encouraged microbial respiration, offsetting the carbon gain in 1997 more than in 1996.

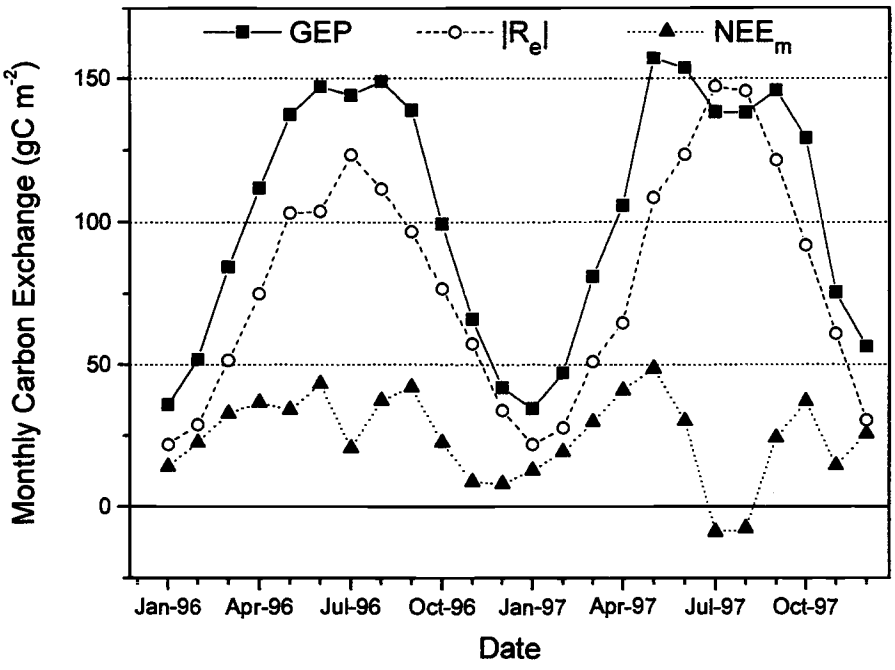

Figure 3.6 Monthly sums of net ecosystem exchange (NEE_m), ecosystem respiration (R_e; absolute value of R_e is shown) and gross ecosystem exchange (GEP = NEE_m - R_e) for 1996 and 1997.

Cumulative NEE_m for 1996 and 1997 is shown in Figure 3.7. Annual NEE_m estimated by eddy covariance was 320 ± 170 gC m^{-2} yr^{-1} in 1996 and 270 ± 180 gC m^{-2} yr^{-1} in 1997. The uncertainty in the nighttime respiration estimate based on chamber data led to uncertainties in the annual NEE_m of 80 and 90 gC m^{-2} yr^{-1} in 1996 and 1997, respectively. The uncertainty in the daytime NEE_m from the eddy covariance flux resulted in uncertainties of 90 gC m^{-2} yr^{-1} in both years. The NEE_m in the 1996 growing season (Day 125-275) was 170 ± 90 gC m^{-2}. Thus NEE_m outside the growing season in 1996 was 150 ± 80 gC m^{-2} (47% of annual NEE_m). In 1997, NEE_m was 80 ±

100 gC m^{-2} during the growing season and 180 ± 80 gC m^{-2} (67% of annual NEE_m) outside the growing season.

Annual net carbon gain by the *P. ponderosa* ecosystem is comparable to carbon gains of other temperate forests (ranging from 150 to 700 gC m-2 yr-1; Greco and Baldocchi, 1996). Compared to boreal evergreen forests at higher latitudes, the pine forest has a substantial net carbon gain outside the traditionally defined growing season. At a boreal black spruce site (Goulden et al., 1998) net carbon gain in the growing season of 1996 (~60 gC m^{-2} from May through September) was lower than at our site in 1996, but the net carbon gain of the spruce forest in the growing season of the El Niño year in 1997 (~70 gC m^{-2}) was higher than at our site during the same time period, probably because of the higher soil respiration at our site in 1997 than in 1996. From October 1996 through May 1997, our data indicate that the pine forest gained about 140 ± 80 gC m^{-2}. In contrast, the boreal spruce forest lost ~60 gC m^{-2} during the same time period (Goulden et al., 1998).

The large carbon gain of the *P. ponderosa* ecosystem outside the growing season reflects the fact that carbon assimilation continues to occur in the relatively mild winters, though at a slower rate, and ecosystem respiration is relatively low (Figure 3.6). Leaf photosynthesis measurements performed in 1996 indicated a maximum leaf level photosynthetic capacity (A_{max}) of 6-9.5 μmol m^{-2}-leaf s^{-1} in April and 16-21 μmol m^{-2}-leaf s^{-1} during July. In comparison, A_{max} at Harvard Forest was ~12 μmol m^{-2}-leaf s^{-1} in August (Williams et al., 1996), which is lower than A_{max} at our site in July. In the growing season at our site, although the photosynthetic capacity is large,

carbon assimilation is constrained by partial stomatal closure in response to high VPD, and ecosystem respiration is large because of high air and soil temperatures.

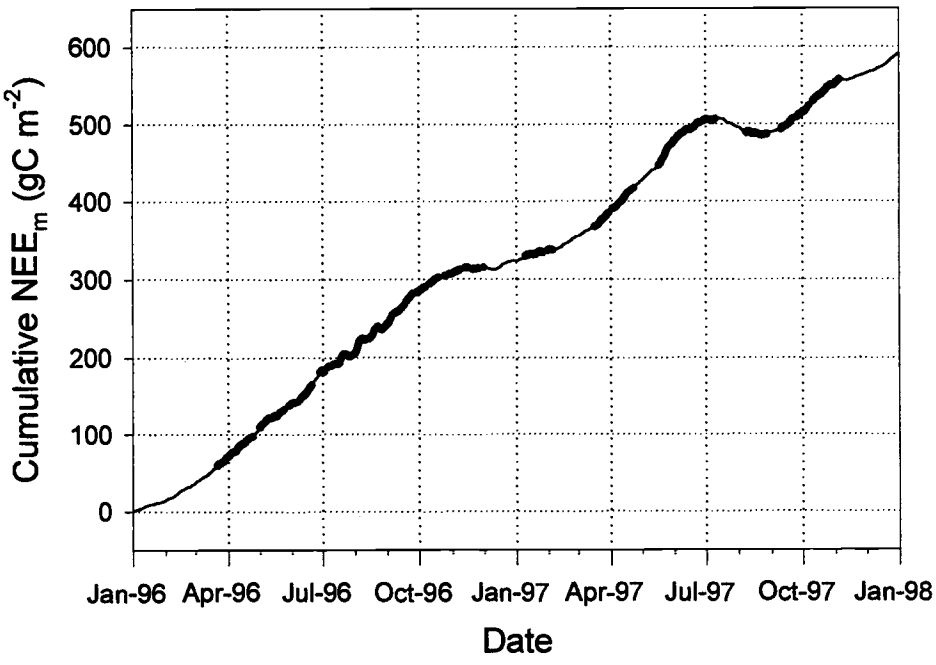

Figure 3.7 Cumulative net ecosystem exchange (NEE_m) during 1996 and 1997. Breaks in the cumulative NEE_m indicate periods for which data are missing; daily NEE_m was then modeled based on equation 3.1.

The annual estimate of NEE_p in 1996 from net primary production and heterotrophic respiration ($NEE_p = NPP + R_h$) was 130 ± 120 gC m^{-2} yr^{-1}. R_h was -280 gC m^{-2} yr^{-1} in 1996, estimated from root decomposition (-277 ± 50 gC m^{-2} yr^{-1}) and litter decomposition (-3 gC m^{-2} yr^{-1}). Total NPP was 410 ± 70 gC m^{-2} yr^{-1} (Law et al., 1999b).

The mensuration estimate of NEE_p in 1996 was lower than our micrometeorological estimate of NEE_m (320 ± 170 gC m^{-2} yr^{-1}). The disagreement could partly be due to the modeling of NEE_m of missing days with an empirical derived model (equation 3.1). About 65% of the days during the dormant season of 1996 were filled-in, if we assume that on all of the modeled days the predicted carbon assimilation was overestimated by 50% we would have to lower the annual NEE_m in 1996 by ~130 gC m^{-2}.

Our data, and results from several other groups suggest that some of discrepancy between NEE_p and NEE_m arises because soil carbon processes are poorly understood (Landsberg and Gower, 1997). Greco and Baldocchi (1996) reported an above-ground NPP at the Walker Branch deciduous forest (Oak Ridge, TN) of 192-212 gC m^{-2} yr^{-1}. Their NEE estimate from eddy covariance data was 525 ± 100 gC m^{-2} yr^{-1}. They suggested that the low NPP compared to annual NEE was either because some fraction of aboveground carbon accumulation must be supported by an accumulation of carbon in the root system, or even a small systematic error in the nocturnal carbon flux could have resulted in a large biased estimate in the annual NEE. Valentini et al. (1996) reported an annual NEE of 472 gC m^{-2} yr^{-1} and a total NPP of 802 gC m^{-2} yr^{-1} for a temperate beech forest in Italy. They suggested that there should have been a net accumulation of organic matter in the soil or in living roots in the order of 234 gC m^{-2} yr^{-1} (after taking into account annual litterfall of 107 gC m^{-2} yr^{-1} and fine root production of 457 gC m^{-2} yr^{-1}). They surmised that the high ratio of below- to aboveground productivity of the actively regrowing beech forest was due to the high investment of carbon in roots to overcome periods of water stress, which are typical

for the central-south region of Italy, as for ponderosa pine regions of the western U.S. (Law and Waring, 1994). Old-growth stands are expected to be in equilibrium in terms of carbon uptake and release. However, our mixed-age forest, which has patches of young trees, may be in a non-steady state condition and accumulating carbon belowground, offsetting some of the discrepancy between NEE_p and NEE_m. Thus, our estimate of annual NEE_p from NPP and R_h is probably low because (i) we did not include coarse root production, which can be assumed to be ~20% of above-ground wood production (Waring, pers. comm.) and (ii) we assumed steady state conditions.

3.5 Conclusions

There have been few long-term studies of carbon and energy fluxes in open-canopied semiarid ecosystems such as the ponderosa pine forest. Challenges of such systems are in understanding and modeling the interactions between water use and carbon exchange when both vegetation and the soil surface are sources of significant fluxes.

Exchange at our site is influenced by the strong seasonal variation in rainfall and temperature, and by the local topography. The complex topography appears to limit the scope for micrometeorology and simple 1-dimensional transfer models to estimate fluxes in stable conditions at night and in the early morning. Frequent low wind speeds make turbulent flux measurement difficult with current instrumentation, and drainage flows or advection limit the use of change in CO_2 storage in the canopy air

space in calculations of NEE. Measurement of horizontal gradients of CO_2 and temperature may help in quantifying advective terms. These problems are likely to be encountered increasingly often as flux studies extend to sites that are not ideal micrometeorologically, but typical of the real world. Availability of independent measurements of respired carbon fluxes from the main sources in the ecosystem allowed us to make seasonal estimates of the carbon budget in spite of the limitations in micrometeorology, and this approach should be considered in other studies at topographically complex sites.

We found that the ecosystem maintained a remarkably constant rate of water use in summer (~1.6-1.7 mm d^{-1}) despite large changes in evaporative demand. Water flow may have been limited by the hydraulic capacity of the whole plant system (roots, stems, leaves). If this were the case, stomata would adjust to maintain a sustainable water flow and minimize the possibility of cavitation. As a direct consequence of partial stomatal closure, the rate of CO_2 diffusion into the leaves becomes limited and assimilation is reduced.

Comparing carbon exchange in a typical summer (1996) and a relatively wet one (1997), we found that respiration was larger in 1997, presumably because wetter soil supported more microbial activity. Large differences in summer precipitation between years had more effect on respiration than did small differences in temperature.

Although summer growing season conditions are harsh in the ponderosa pine forest, the weather from fall through spring is mild, allowing an annual net carbon gain that is mid-range of that reported for temperate forests. Our estimate of NEE from eddy covariance was higher than an estimate of NEE from NPP and R_h. Some of

the discrepancy is probably because of errors in the estimation of belowground carbon components. Improved methods are needed for estimating heterotrophic respiration, such as a stable isotope approach (Lin et al., 1999).

The carbon balance of the ponderosa pine ecosystem is quite sensitive to climatic variability. In the short term, the ecosystem has a very dynamic response to changing weather. In the dry season, as the ecosystem stabilizes its water use, NEE can change from positive (gaining carbon from the atmosphere) to negative over a just few days (Figure 3.3). The net seasonal result depends on the frequency of cool air masses (decreasing evaporative demand) and accompanying rainfall (increasing respiration). The implication of these short-term responses is that the annual carbon budget of the ecosystem is very sensitive to weather and climate, but the water balance is not.

3.6 Acknowledgments

This study was funded by NASA (grant #NAGW-4436). We are grateful to Richard Vong, Steve Van Tuyl and Will Hutchinson for their field assistance. Steve Acker provided stem biomass equations for the site. We thank Laurel Groves for her editorial comments. Larry Mahrt and Dennis Baldocchi provided helpful comments on the eddy flux measurements and analysis. We thank Richard Waring for his continuing advice and many encouraging discussions. We gratefully acknowledge the assistance of the Sisters Ranger District of the US Forest Service in site selection, and Sarah Greene for aid in establishing the study site. The study site is located in a

Research Natural Area—areas selected to represent vegetation types in a natural condition.

3.7 Appendix

Missing carbon exchange data were estimated from an empirical relationship (equation 3.1), where model parameters were determined seasonally from valid flux data for surrounding days. Carbon assimilation (A_c) was estimated as the difference between measured CO_2 flux and an estimate of ecosystem respiration, R_e, from scaled-up chamber data. From half-hour values of A_c and measured PAR, Michaelis-Menten light-response parameters (P_{max} = maximum ecosystem photosynthetic assimilation in $\mu mol\ m^{-2}\ s^{-1}$, K_m = Michaelis-Menten constant in $\mu mol\ m^{-2}\ s^{-1}$) were determined for low-VPD conditions with a non-linear least-square (NLS) regression model. The low-VPD threshold was adjusted seasonally to have enough data for the regression analysis. Figure A.1 shows the relationship between A_c and PAR for 20 days in late summer 1996 and early spring 1997.

The light-response parameters determined for the two periods, with a VPD threshold of VPD < 1 kPa in late summer 1996 and VPD < 0.5 kPa in early spring 1997, are shown in Table A.1. Residual values of A_c from the light-response curve fitted for the low-VPD condition were calculated for high-VPD periods. The reduction in A_c due to high VPD was then estimated by linear regression of the

residual A_c versus VPD (a_0 = intercept in μmol m^{-2} s^{-1}, a_1 = slope in μmol m^{-2} s^{-1} kPa^{-1}; Figure A.2, Table A.1).

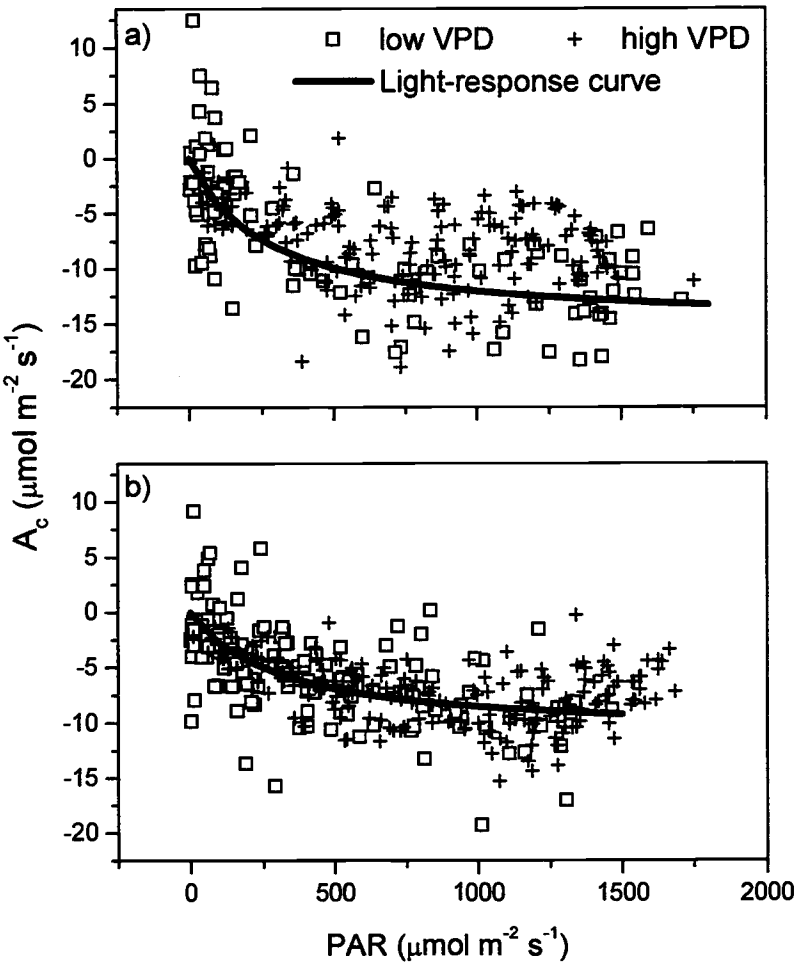

Figure A.1. Light-response curve of carbon assimilation for 20 days in a) late summer 1996 and b) early spring 1997. A_c is shown with the sign convention that a negative value indicates carbon uptake by the plant. Light-response curve was determined from periods with low VPD; a) VPD < 1 kPa, b) VPD < 0.5 kPa.

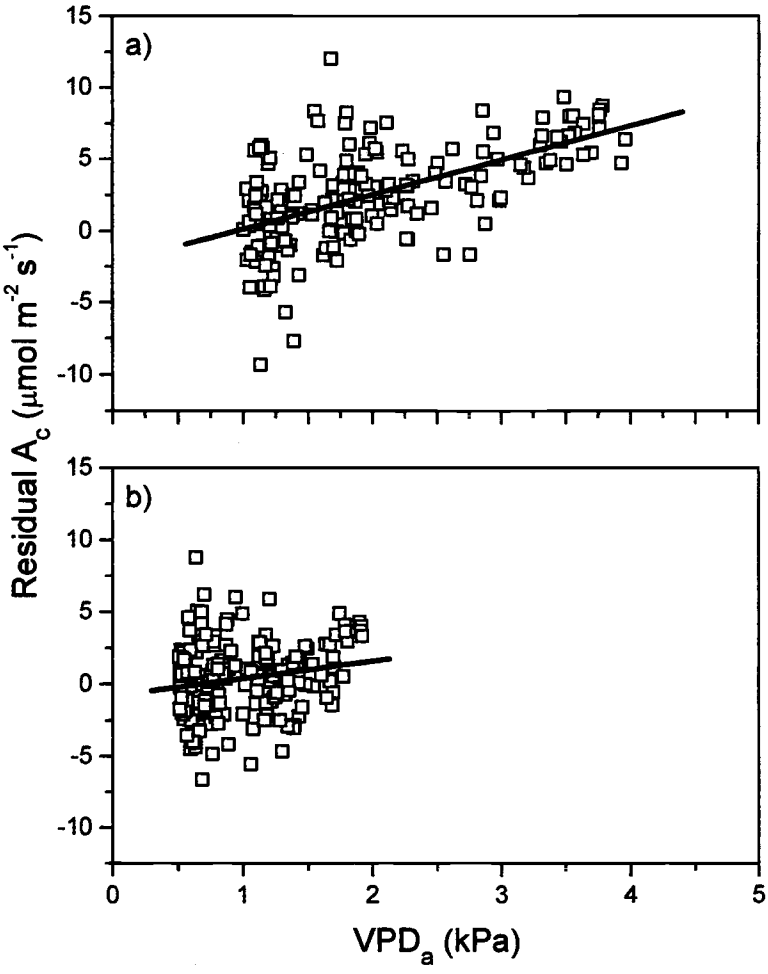

Figure A.2. Residual A_c (= A_c minus predicted carbon assimilation obtained from light-response curve; see Figure A.1) versus VPD for 20 days in a) late summer 1996 and b) early spring 1997. A positive residual A_c indicates a reduction in carbon assimilation.

Carbon assimilation (A_{cp}) was then predicted for each half hour using the determined light- (P_{max}, K_m) and VPD- (a_0, a_1) response parameters with measured PAR and VPD. Predicted net carbon exchange (F_{cp}) was calculated from predicted A_{cp} and R_e. Figure A.3 shows the predicted F_{cp} versus measured CO_2 flux for 20 days in late summer 1996 and early spring 1997.

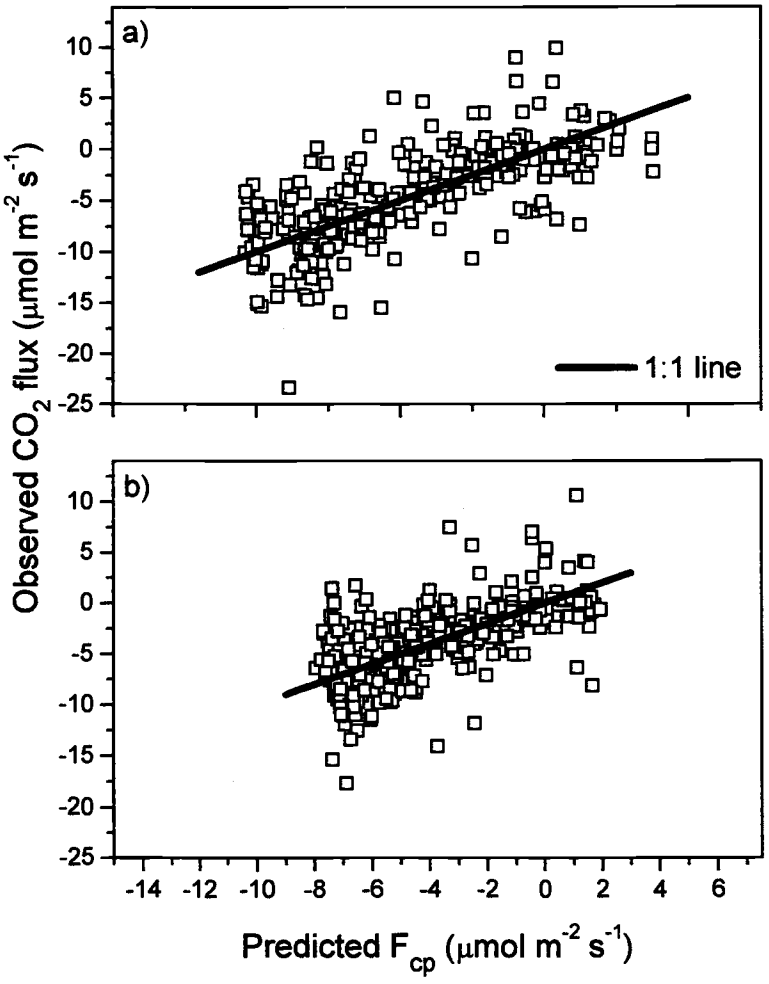

Figure A.3. Predicted (F_{cp}) versus observed CO_2 flux for 20 days in a) late summer 1996 and b) early spring 1997. F_{cp} was modeled based on equation 3.1, with the light- and VPD-response parameters determined for each period (see Table A.1).

Table A.1. Light- (P_{max} in μmol m^{-2} s^{-1}, K_m in μmol m^{-2} s^{-1}) and VPD- (a_0 in μmol m^{-2} s^{-1}, a_1 in μmol m^{-2} s^{-1} kPa^{-1}) response parameters for empirically filling in missing data during two 20 day periods (i.e. late summer 1996 and early spring 1997). (n_{MM} = number of observation for light response curve; n_{VPD} = number of observations for residual A_c to VPD regression; b = slope of predicted F_{cp} to measured CO_2 flux with forced zero intercept; r^2 = squared correlation coefficient of predicted F_{cp} to measured CO_2 flux; n = total number of observation in the period).

JD	Year	P_{max}	K_m	n_{MM}	a_0	a_1	n_{VPD}	B	r^2	n
261 – 280	1996	-15.2	263	109	-2.24	2.40	172	0.96	0.70	281
74 – 93	1997	-11.1	299	155	-0.79	1.19	188	0.97	0.74	343

3.8 References

Anthoni, P.M., Unsworth, M.H., Vong, R.J. and Law, B.E., 1998. Energy Budget of an Open-Canopied, Semi-Arid Juniper/Sagebrush Ecosystem, 23rd AMS Conference on Agricultural and Forest Meteorology.

Auble, D.L. and Meyers, T.P., 1992. An open path, fast response infrared absorption gas analyzer for H_2O and CO_2. Boundary-Layer Meteorology, 59: 243-256.

Baldocchi, D.D., Hicks, B.B. and Meyers, T.P., 1988. Measuring biosphere-atmosphere exchanges of biologically related gases with micrometeorological methods. Ecology, 69(5): 1331-1340.

Baldocchi, D.D. and Vogel, C.A., 1996. Energy and CO_2 flux densities above and below a temperate broad-leaved forest and a boreal pine forest. Tree Physiology, 16: 5-16.

Blanken, P.D., Black, T.A., Yang, P.C., Neumann, H.H., Nesic, Z., Staebler, R., den Hartog, G., Novak, M.D. and Lee, X., 1997. Energy balance and canopy conductance of a boreal aspen forest: Partitioning overstory and understory components. Journal of Geophysical Research, 102: 28915-28927.

Droppo, J.G. and Hamilton, H.L., 1973. Experimental variability in the determination of the energy balance in a deciduous forest. Journal of Applied Meteorology, 12: 781-791.

Fan, S.-M., Goulden, M.L., Munger, J.W., Daube, B.C., Bakwin, P.S., Wofsy, S.C., Amthor, J.S., Fitzjarrald, D.R., Moore, K.E. and Moore, T.R., 1995. Environmental controls on the photosynthesis and respiration of a boreal lichen woodland: a growing season of whole-ecosystem exchange measurements by eddy correlation. Oecologia, 102(4): 443-452.

Goulden, M.L., Munger, J.W., Fan, S.-M., Daube, B.C. and Wofsy, S.C., 1996. Measurements of carbon sequestration by long-term eddy covariance: methods and critical evaluation of accuracy. Global Change Biology, 2: 169-182.

Goulden, M.L., Wofsy, S.C., Harden, J.W., Trumbore, S.E., Crill, P.M., Gower, S.T., Fries, T., Daube, B.C., Fan, S.-M., Sutton, D.J., Bazzaz, A. and Munger, J.W., 1998. Sensitivity of boreal forest carbon balance to soil thaw. Science, 279: 214-217.

Grace, J., Lloyd, J., McIntyre, J., Miranda, A.C., Meir, P., Miranda, H.S., Moncrieff, J., Massheder, J., Wright, I. and Gash, J., 1995a. Fluxes of carbon dioxide and water vapour over an undisturbed tropical forest in southwest Amazonia. Global Change Biology, 1: 1-12.

Grace, J., Lloyd, J., McIntyre, J., Miranda, A.C., Meir, P., Miranda, H.S., Nobre, C., Moncrieff, J., Massheder, J., Malhi, Y., Wright, I. and Gash, J., 1995b. Carbon dioxide uptake by an undisturbed tropical rain forest in southwest Amazonia, 1992 to 1993. Science, 270: 778-780.

Grace, J., Malhi, Y., Lloyd, J., McIntyre, J., Miranda, A.C., Meir, P. and Miranda, H.S., 1996. The use of eddy covariance to infer the net carbon dioxide uptake of a Brazilian rain forest. Global Change Biology, 2: 209-217.

Greco, S. and Baldocchi, D.D., 1996. Seasonal variations of CO_2 and water vapour exchange rates over a temperate deciduous forest. Global Change Biology, 2: 183-197.

Grelle, A., 1997. Long-term water and carbon dioxide fluxes from a boreal forest. Ph.D. Thesis, Swedish University of Agricultural Sciences, Uppsala, Sweden.

Huntingford, C., Allen, S.J. and Harding, R.J., 1995. An intercomparison of single and dual-source vegetation-atmosphere transfer models applied to transpiration from Sahelian savannah. Boundary-Layer Meteorology, 74: 397-418.

Jarvis, P.G., Massheder, J.M., Hale, S.E., Moncrieff, J.B., Rayment, M. and Scott, S.L., 1997. Seasonal variation of carbon dioxide, water vapor, and energy exchanges of a boreal black spruce forest. Journal of Geophysical Research, 102(D24): 28953-28966.

Kelliher, F.M., Köstner, B.M.M., Hollinger, D.Y., Byers, J.N., Hunt, J.E., McSeveny, T.M., Mesert, R., Weir, P.L. and Schulze, E.-D., 1992. Evaporation, xylem sap

flow, and tree transpiration in a New Zealand broad-leaved forest. Agricultural and Forest Meteorology, 62: 53-73.

Landsberg, J.J. and Gower, S.T., 1997. Applications of physiological ecology to forest management. Physiological Ecology: A Series of Monographs, Texts, and Treatises. Academic Press Inc.

Laubach, J., Raschendorfer, M., Kreilein, H. and Gravenhorst, G., 1994. Determination of heat and water vapour fluxes above a spruce forest by eddy correlation. Agricultural and Forest Meteorology, 71: 373-401.

Law, B.E., Baldocchi, D.D. and Anthoni, P.M., 1999a. Below-canopy and soil CO_2 fluxes in a ponderosa pine forest. Agricultural and Forest Meteorology, in press.

Law, B.E., Ryan, M.G. and Anthoni, P.M., 1999b. Seasonal and annual respiration of a ponderosa pine ecosystem. Global Change Biology, 5(2): 169-182.

Law, B.E. and Waring, R.H., 1994. Combining remote sensing and climatic data to estimate net primary production across Oregon. Ecological Applications, 4(4): 717-728.

Law, B.E., Waring, R.H., Aber, J.D. and Anthoni, P.M., 1999c. Measurement of gross and net ecosystem productivity and water vapor exchange of a *Pinus ponderosa* ecosystem, and an evaluation of two generalized models. Global Change Biology, In review.

Lee, X., 1998. On micrometeorological observations of surface-air exchange over tall vegetation. Agricultural and Forest Meteorology, 91: 39-49.

Lee, X. and Black, T.A., 1993. Atmospheric turbulence within and above a Douglas-fir stand. Part II: Eddy fluxes of sensible heat and water vapour. Boundary-Layer Meteorology, 64: 369-389.

Lin, G., Ehleringer, J.R., Rygiewicz, P.T., Johnson, M.G. and Tingey, D.T., 1999. Elevated CO_2 and temperature impacts on different components of soil CO_2 efflux in Douglas-fir terracosms. Global Change Biology, 5(2): 157-168.

Mahrt, L., 1998. Flux sampling errors for aircraft and towers. Journal of Atmospheric and Oceanic Technology, 15: 416-429.

McCaughey, J.H., Laufleur, P.M., Joiner, D.J., Bartlett, P.A., M., C.A., Jelinski, D.E. and Ryan, M.G., 1997. Magnitudes and seasonal patterns or energy, water, and carbon exchanges at a boreal young jack pine forest in the BOREAS northern study area. Journal of Geophysical Research, 102(D24): 28997-29907.

Mencuccini, M. and Grace, J., 1996. Hydraulic conductance, light interception and needle nutrient concentration in Scots pine stands and their relations with net primary productivity. Tree Physiology, 16: 459-468.

Moncrieff, J., Malhi, Y. and Leuning, R., 1996. The propagation of errors in long-term measurements of land atmosphere fluxes of carbon and water. Global Change Biology, 2: 231-240.

Monteith, J.L. and Unsworth, M.H., 1990. Principles of Environmental Physics. Edward Arnold, Hodder Headline PLC, London.

Raich, J.W. and Nadelhoffer, K.J., 1989. Belowground carbon allocation in forest ecosystems: global trends. Ecology, 70: 1346-1354.

Runyon, J., Waring, R.H., Goward, S.N. and Welles, J.M., 1994. Environmental limits on net primary production and light-use efficiency across the Oregon transect. Ecological Applications, 4: 226-237.

Ryan, M.G., 1991a. The effects of climate change on plant respiration. Ecological Applications, 1: 157-167.

Ryan, M.G., 1991b. A simple method for estimating gross carbon budgets for vegetation in forest ecosystems. Tree Physiology, 9: 255-266.

Ryan, M.G. and Yoder, B.J., 1997. Hydraulic limits to tree height and tree growth. Bioscience, 47(4): 235-242.

Schotanus, P.H., Nieuwstadt, F.T.M. and de Bruin, H.A.R., 1983. Temperature measurements with a sonic anemometer and its application to heat and moisture fluxes. Boundary-Layer Meteorology, 26: 81-93.

Smith, E.A., Hodges, G.B., Bacrania, M., Cooper, H.J., Owens, M.A., Chappel, R. and Kincannon, W., 1997. BOREAS net radiometer engineering study, NASA-Goddard Space Flight Center, Greenbelt.

Sperry, J.S., 1995. Limitations on stem water transport and their consequences. In: B. Gardner (Editor), Plant Stems. Academic Press, San Diego, pp. 105-124.

Sun, J., Lenschow, D.H., Mahrt, L., Crawford, T.L., Davis, K.J., Oncley, S.P., MacPherson, J.I., Wang, Q., Dobosy, R.J. and Desjardins, R.L., 1997. Lake-induced atmospheric circulations during BOREAS. Journal of Geophysical Research, 102(D24): 29155-29166.

Sun, J. and Mahrt, L., 1995. Determination of surface fluxes from the surface radiative temperature. Journal of Atmospheric Science, 52: 1096-1106.

Tukey, J.W., 1977. Exploratory Data Analysis. Addison-Wesley, Reading, Massachusetts.

Valentini, R., DeAngelis, P., Matteucci, G., Monaco, R., Dore, S. and Scarascia Mugnozza, G.E., 1996. Seasonal net carbon dioxide exchange of a beech forest with the atmosphere. Global Change Biology, 2: 199-207.

Webb, E.K., Pearman, G.I. and Leuning, R., 1980. Correction of flux measurements for density effects due to heat and water vapour transfer. Quarterly Journal of the Royal Meteorological Society, 106: 85-100.

Whitney, S., 1985. Western Forests. Knopf, New York.

Williams, M., Rastetter, E.B., Fernandes, D.N., Goulden, M.L., Wofsy, S.C., Shaver, G.R., Melillo, J.M., Munger, J.W., Fan, S.-M. and Nadelhoffer, K.J., 1996. Modelling the soil-plant-atmosphere continuum in a *Quercus-Acer* stand at Harvard Forest: the regulation of stomatal conductance by light, nitrogen and soil/plant hydraulic properties. Plant, Cell and Environment, 19: 911-927.

4 Summary and Discussion

4.1 The linkage between carbon and water exchange

The annual NEE of the ponderosa pine ecosystem (~300 gC m^{-2} yr^{-1}) is in the mid-range of NEE reported for temperate forest ecosystems (Greco and Baldocchi, 1996), although, unusually, much of the annual NEE (50-70%) occurred during fall through spring. The relative mild winters at the site allowed carbon assimilation to occur at am average rate of ~1gC m^{-2} d^{-1} and ecosystem respiration was relatively low in winter (~0.5gC m^{-2} d^{-1}) because of low temperatures.

Water plays a crucial role in the net carbon exchange of the pine ecosystem, first by limiting the assimilation of carbon. Leaf photosynthesis measurements indicated a maximum leaf level photosynthetic capacity (A_{max}) of 6-9.5 μmol m^{-2}-leaf s^{-1} in April and 16-21 μmol m^{-2}-leaf s^{-1} during July. These values indicate that there is a high potential for carbon assimilation, but the high potential becomes constrained in the summer months by restrictions on water movement through the hydraulic system of the trees. In summer of 1996 (JD 190-230, Figure 3.3), on days with ample radiation exposure and high VPD (>2 kPa), net carbon uptake (0.1 gC m^{-2} d^{-1}) was lower by ~2 gC m^{-2} d^{-1} compared to days with low VPD but similar radiation exposure. On the other hand, the water loss of the ecosystem on the same summer days with plenty of radiation was remarkable similar (~1.8-1.9 mm d^{-1}) regardless of large variation in VPD. A strong linkage between carbon and water exists at the pine site. To prevent

xylem cavitation the tree stomata restrict transpiration, but as a consequence of stomatal closure carbon assimilation is reduced. Furthermore, the increased partitioning of available energy into sensible heat leads to high air temperatures and ecosystem temperatures. The high temperatures then lead to high ecosystem respiration rates, offsetting much of the already reduced carbon assimilation. Both effects combined lead to the observed reduced net carbon exchange during high VPD days. On a few days with very high VPD and ecosystem temperatures, net carbon loss was observed.

A second notable influence of water on the net carbon exchange appears to be from increased soil microbial activity following rain events in summer. Precipitation in the summer months is usually rare at the pine site, but in 1997 versus 1996 a more frequent precipitation pattern occurred. The more frequent precipitation was associated with higher soil respiration in summer of 1997 resulting in a net carbon loss from the ecosystem, where as a net carbon gain was observed in summer 1996. This influence of precipitation on soil surface respiration further emphasizes the crucial role water plays on the carbon exchange in this semi-arid ecosystem, and indicates the sensitivity of the system to climate variability.

4.2 Uncertainties in respiration estimates

Contributions from the soil to the whole ecosystem gas exchange are large in this open-canopy ecosystem compared to ecosystems with larger LAI and more uniform

canopy closure (Baldocchi and Vogel, 1996). Due to its open-canopy structure leading to good coupling of the canopy air-layer to the overlying atmosphere and the large contribution of the soil to ecosystem respiration, the pine site is well-suited for testing the applicability of the eddy covariance system for estimating nighttime respiration rates (Anthoni et al., 1999; Law et al., 1999a). From our data it seemed that the above-canopy eddy covariance system underestimated nighttime respiration by ~1-2 μmol m^{-2} s^{-1} compared to independent estimates of R_e from chamber data. At our site and several other sites the estimation of nighttime ecosystem respiration R_e from eddy flux measurements is still an unresolved issue (Lee, 1998; Baldocchi et al., 1999). Problems with estimating R_e from eddy covariance fluxes are mainly associated with the generally stable conditions that occur during the night, i.e. failure to resolve small-scale eddies, exchange dominated by short, infrequently occurring events, and advection and cold air drainage in complex terrain (Goulden et al., 1996; Sun et al., 1997; Mahrt, 1998).

Diurnally selective systematic errors could lead to a large uncertainty in the annual estimate of NEE (Greco and Baldocchi, 1996; Moncrieff et al., 1996). An underestimate in the nighttime respiration of ~1 μmol m^{-2} s^{-1} (~40% of annual mean R_e at our site) would lead to an overestimate of the annual NEE in the order of 200 gC m^{-2} yr^{-1}. Usually the eddy covariance system is thought to predict the nighttime R_e well under more turbulent conditions. Hence, for estimating daily and annual NEE, relationships between R_e and temperatures developed from eddy flux data taken under turbulent conditions are used to fill in calm periods (Goulden et al., 1996), when the eddy system has problems adequately predicting R_e. But comparison of the eddy

covariance system with data derived from chamber methods, indicated that at our site the eddy covariance might underestimate R_e even under more turbulent conditions, if the chamber estimates of R_e are assumed to be correct.

For several boreal coniferous forests, Lavigne et al. (1997) showed that under more turbulent conditions ($u_* > 0.25$ m s^{-1}) the eddy covariance estimates of nighttime NEE (calculated from above-canopy eddy CO_2 flux corrected for change in CO_2 storage, $F_c + F_{stor}$) were smaller by 6 - 42% than estimates of ecosystem respiration based on chamber methods ($R_{e.c}$). At a deciduous hardwood forest, eddy covariance estimates were 25% lower than $R_{e.c}$ (Goulden et al., 1996). At our site during more turbulent periods, $F_c + F_{stor}$ was lower than $R_{e.c}$ by 57%, but compared well with $R_{e.c}$ for calm nights (Anthoni et al., 1999; Law et al., 1999b), when CO_2 accumulated at our site. Soil R_s, contributing about 70% to whole ecosystem R_e, compared well with below-canopy CO_2 flux measured by eddy covariance system. For filling in 'bad' nighttime eddy flux data, it seems that at our site an should be used that is different from the more commonly accepted approach of modeling the calm periods based on equations derived from more turbulent periods. For our pine site, flux and storage data under calm conditions should be used to derive temperature response equations, and data during more turbulent periods need to be replaced with predicted fluxes calculated from the temperature curves.

On the basis of our experience, it seems that the suitability of a standard method for correcting for missing nighttime fluxes should be questioned. It seems likely that each site might face different problems. Efforts should be undertaken to independently estimate the magnitude of the nighttime respiration. For example,

automatic chamber systems on foliage, stems, and soil and below-canopy flux systems should be installed to determine the ecosystem respiration. The chamber measurements could be used to gather confidence in the ability of the eddy covariance system to measure nighttime respiration. More spatial measurements with a network of vertical CO_2 and wind speed profiles located around the tower should be undertaken to quantify effects of drainage flows and advection of CO_2. These efforts would help improve and derive correction terms for the eddy covariance method and ultimately lead to more confidence and less uncertainty in the derived data.

4.3 Issues of energy closure

At both the pine and juniper sites, the energy closure was not perfect. On average, 60-70% of available energy, calculated as net radiation minus soil heat flux and energy storage in the canopy layer, was accounted for by the sum of sensible and latent heat flux. On sunny days when net radiation was 600-700 Wm^{-2}, the energy imbalance amounted to 200-250 W m^{-2}. This energy imbalance is quite large compared to other research sites, where energy closure was on average ~80-100% (Kelliher et al., 1992; Lee and Black, 1993; Laubach et al., 1994; Fan et al., 1995; Goulden et al., 1996; Blanken et al., 1997; Grelle, 1997; McCaughey et al., 1997). One uncertainty in an open-canopy ecosystem is the characterization of the spatial average net radiation with a single net radiometer situated above the canopy. Modeling of the spatial variation in upwelling components of net radiation showed

that even in conditions with large differences in surface radiation properties, the variability would be below 10% of the mean net radiation, which is not enough to explain the lack of energy closure we observed.

Modeling the radiation exchange could be used to optimize radiation sampling design at heterogeneous sites and thereby reduce the number of sampling locations. At the juniper site, with radiation sensors placed 20 m above the surface, about 40 sensors would be needed to determine the average net radiation to an accuracy of 5 W m^{-2}. The number of sensors required becomes less with distance of the sensors above the ecosystem, since the microscale heterogeneity becomes smaller compared to the sampling height. To characterize the average radiation of an open-canopied ecosystem accurately one radiation sensor will not be enough unless it is placed at a height above the canopy at least 4 times the mean spacing of the trees.

The spatial variation of net radiation in tall open-canopy forest ecosystems can be quite large. Figure 4.1 shows a contour plot of the deviations of upwelling radiation R_u ($=R_{su}+R_{lu}$) from the mean R_u for surface conditions found on a cloudless summer day at the juniper site. The upwelling radiation was modeled for radiation sensors on a 5 m grid and placed 20m above the surface. The spatial variation of the upwelling radiation components was then used to generate the contour plot. Selection of measurement location could be optimized by modeling the upwelling radiation for several location and surface conditions. As can be seen from Figure 4.1, there are two distinct areas in the 100x100 m plot at the Juniper site where the placing of radiation sensors would lead to an underestimate or overestimate of the average upwelling radiation, but there are also various sections where the measured radiation would be

close to the average radiation. Ideally, the spatial variability could be modeled for various surface conditions to achieve an optimized sampling design, thereby reducing the number of samples necessary for estimating the average net radiation of the ecosystem.

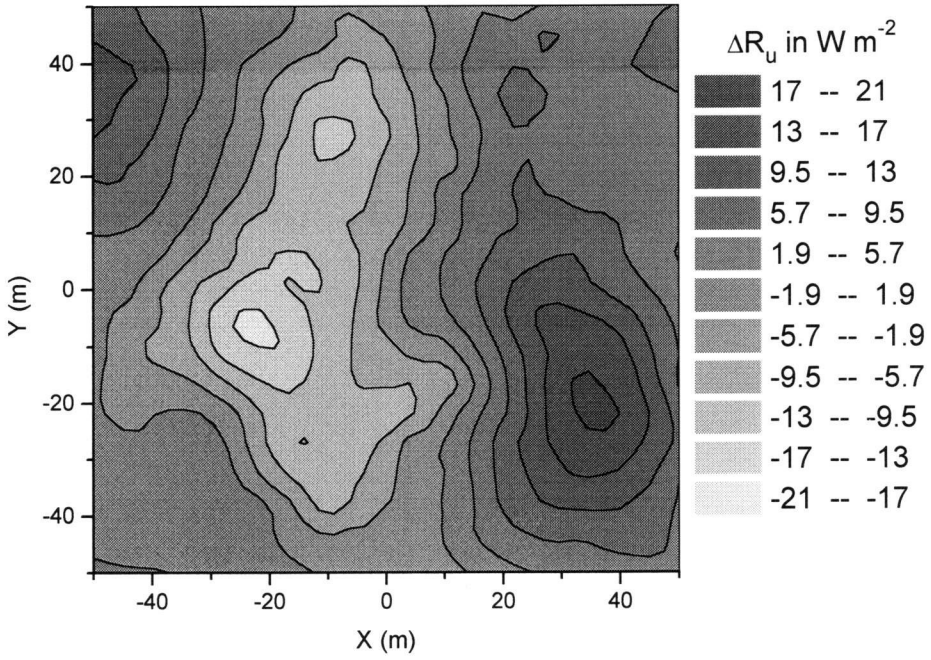

Figure 4.1 Deviations (ΔR_u) of upwelling radiation R_u ($=R_{su}+R_{lu}$) from the mean R_u in the 100 x 100 m plot for conditions of soil surface radiation temperature 56°C, vegetation radiation temperature of 29°C, soil reflection coefficient of 0.13, and vegetation reflection coefficient of 0.1.

At present the applicability of the modeling of the upwelling radiation using a ray tracing approach needs to be validated by comparing modeled versus actual measurements. This could be done by making measurements over various ecosystems, ranging from short to tall vegetation and from dense to open stands, but this approach would be quite labor and equipment intensive. An alternative would be

to make measurements above a scaled model surface for which the temperature of objects ('trees') and ground surfaces could be independently controlled. This approach has the advantages that the surface radiation properties of the objects (surface radiation temperature and albedo) could easily be varied and that several experiments could be performed by varying the size, structure, position, and number of radiation objects.

The lack of energy closure at the pine and juniper site could occur due to the neglect of advective terms. Further investigation into the problem is needed. One most likely cause of inadequate closure is vertical transport of heat due to stationary convective driven circulation, which can be particularly important in semi-arid ecosystems where surface radiation temperatures can exceed air temperatures by several degrees. Ideally, a better spatial estimation of the exchange rates would be advisable, since in highly unstable conditions the source area extent (footprint) can be of similar order of magnitude as spatial variations in canopy structure.

Footprint analysis, together with information about the spatial vegetation structure around a tower should be used to determine the minimum measurement height needed to average out microscale heterogeneities to get a representative estimate of exchange rates (Schmid and Lloyd, 1999). In general, the higher the flux measurement height the larger is the region of influence. The flux footprint extent also depends on atmospheric conditions (i.e., stability and wind speed); under neutral conditions the footprint is larger than under unstable conditions. Under highly unstable conditions the source area can shrink significantly and be very close to the tower. Because of bias in locating towers (e.g. choosing more open or drier areas) this could mean that

the measured flux might not be representativeness of the larger region. It would be best to have several eddy covariance systems, either at different heights, if fetch requirements are fulfilled, or separated horizontally, which would reduce the random uncertainties in the mean exchange. Having several systems separated horizontally would also allow advection and nighttime drainage problems to be addressed.

Unfortunately, ensuring an adequate sampling design is usually beyond funding capabilities. There is a need to develop a cost-effective way to measure the exchange rates of an ecosystem with a high enough accuracy. At present eddy covariance systems are not available on the open market and usually are custom built. The equipment cost for a single eddy covariance system currently is about $80k, which does not include costs for supporting infrastructure (tower, power supply, and site access) and site maintenance and data analysis. Clearly the reliability and the cost associated with the eddy covariance technique need to be improved. On the other hand, supplemental measurements might be able to give better confidence in the eddy covariance system (i.e. traditional mensuration methods, plant physiological measurements scaled to the canopy, respiration from ecosystem components measured with chamber method etc.).

4.4 Sensitivity to climate change

From the information gathered at our ponderosa pine site during two years with contrasting climate (1996 with a dry summer and large variations in VPD from day to

day) and 1997 with more frequent summer precipitation than in 1996 and more steady VPD), it is clear that the carbon exchange is more sensitive to global climate change than the water vapor exchange.

Water vapor exchange is coupled via feedback to the whole ecosystem energy exchange. Under drought conditions, the low water vapor exchange will result in high VPD which acts as a positive feedback on the water vapor flux (increased driving force for water diffusion), essentially stabilizing the water exchange at a rate sustainable by the soil-root-plant system. As long as the pine trees have access to water from deeper root zones the water vapor exchange will be relatively stable, even though water availability in the upper soil layer might be strongly diminished in summer dry season. Mature ponderosa pine trees can have a rooting depth of more than 2 m in porous soils and in soils with underlain rocks with deep fissures roots can reach as far down as 11 to 12m (Burns and Honkala, 1990).

The carbon exchange strongly depends on the stomatal response to VPD limiting the diffusion of CO_2 into the leave. This could have a substantial effect on the carbon cycle at the ponderosa pine site in an altered climate. NCAR's Climate System Model (CSM), a coupled ocean/atmosphere general circulation model, predicts a temperature increase in the next 100 years for Central Oregon of ~2.6°C in Summer (July-September) and ~1.4°C for Fall through Spring for a "business-as-usual" CO_2 emissions scenario with a doubling of atmospheric CO_2 by the year 2100 (www.cgd.ucar.edu/cas/ACACIA/csmresults.html; Boville and Gent, 1998). The increased temperature would result in increased respiration rates and larger VPD, leading to higher constraints on carbon assimilation. Under this scenario the

ecosystem would be a smaller carbon sink, or even a carbon source, more often in the summer, but during fall through spring the slight increase in temperature would lead to better conditions for carbon uptake, possibly compensating for the reduced carbon gain in summer. How exactly the ecosystem would respond to a different climate is difficult to quantify, since phenological and physiological adjustment would be likely to occur to the altered climate in the 100-year time span. For example, the optimal zone for ponderosa pine ecosystem could move northward and current pine region might become more suitable for juniper woodlands. To address such questions of ecosystem change and climate it will be necessary to continue to make progress in the measurements of vegetation atmosphere exchange, the physiological analysis of ecosystem components, and the further development of mechanistic models of ecosystem dynamics. This project has benefited from such multidisciplinary integration, and has indicated a number of specific areas for further research.

Bibliography

Anthoni, P.M., Law, B.E. and Unsworth, M.H., 1999. Carbon and water vapor exchange of an open-canopied ponderosa pine ecosystem. Agricultural and Forest Meteorology, 95(3): 151-168.

Anthoni, P.M., Unsworth, M.H., Vong, R.J. and Law, B.E., 1998. Energy Budget of an Open-Canopied, Semi-Arid Juniper/Sagebrush Ecosystem, 23rd AMS Conference on Agricultural and Forest Meteorology.

Auble, D.L. and Meyers, T.P., 1992. An open path, fast response infrared absorption gas analyzer for H_2O and CO_2. Boundary-Layer Meteorology, 59: 243-256.

Baldocchi, D.D., Hicks, B.B. and Meyers, T.P., 1988. Measuring biosphere-atmosphere exchanges of biologically related gases with micrometeorological methods. Ecology, 69(5): 1331-1340.

Baldocchi, D.D., Valentino, R., Running, S., Oechel, W. and Dahlman, R., 1996. Strategies for measuring and modelling carbon dioxide and water vapour fluxes over terrrestrial ecosystems. Global Change Biology, 2: 101-110.

Baldocchi, D.D. and Vogel, C.A., 1996. Energy and CO_2 flux densities above and below a temperate broad-leaved forest and a boreal pine forest. Tree Physiology, 16: 5-16.

Baldocchi, D.D., Wilson, K. and Paw U, K.T., 1999. On measuring net ecosystem carbon exchange in complex terrain over tall vegetation. Boundary-Layer Meteorology, submitted.

Blanken, P.D., Black, T.A., Yang, P.C., Neumann, H.H., Nesic, Z., Staebler, R., den Hartog, G., Novak, M.D. and Lee, X., 1997. Energy balance and canopy conductance of a boreal aspen forest: Partitioning overstory and understory components. Journal of Geophysical Research, 102: 28915-28927.

Blyth, E.M. and Harding, R.J., 1995. Application of aggregation models to surface heat flux from the Sahelian tiger bush. Agricultural and Forest Meteorology, 72: 213-235.

Boville, B.A. and Gent, P.R., 1998. The NCAR Climate System Model, Version One. Journal of Climate, 11(6): 1115-1130.

Burns, R.M. and Honkala, B.H., 1990. Silvics of North America. Agriculture Handbook, 654. Forest Service, U.S. Dept. of Agriculture, Washington, D.C.

Denning, A.S., Fung, I.Y. and Randall, D., 1995. Latitudinal gradient of atmospheric CO_2 due to seasonal exchange with land biota. Nature, 376: 240-243.

Dirmhirn, I. and Belt, G.H., 1971. Variation of albedo of selected sagebrush range in the intermountain region. Agricultural Meteorology, 9: 51-61.

Dolman, A.J., 1993. A multiple-source land surface energy balance model for use in general circulation models. Agricultural and Forest Meteorology, 65: 21-45.

Droppo, J.G. and Hamilton, H.L., 1973. Experimental variability in the determination of the energy balance in a deciduous forest. Journal of Applied Meteorology, 12: 781-791.

Fan, S.-M., Gloor, M., Mahlman, J., Pacala, S., Sarmiento, J., Takahashi, T. and Tans, P., 1998. A large terrestrial carbon sink in North America implied by atmospheric and oceanic carbon dioxide data and models. Science, 282: 442-446.

Fan, S.-M., Goulden, M.L., Munger, J.W., Daube, B.C., Bakwin, P.S., Wofsy, S.C., Amthor, J.S., Fitzjarrald, D.R., Moore, K.E. and Moore, T.R., 1995. Environmental controls on the photosynthesis and respiration of a boreal lichen woodland: a growing season of whole-ecosystem exchange measurements by eddy correlation. Oecologia, 102(4): 443-452.

Garratt, J.R., 1978. Transfer characteristics for a heterogeneous surface of large aerodynamic roughness. Quarterly Journal of the Royal Meteorological Society, 104: 491-502.

Goulden, M.L., Munger, J.W., Fan, S.-M., Daube, B.C. and Wofsy, S.C., 1996. Measurements of carbon sequestration by long-term eddy covariance: methods and critical evaluation of accuracy. Global Change Biology, 2: 169-182.

Goulden, M.L., Wofsy, S.C., Harden, J.W., Trumbore, S.E., Crill, P.M., Gower, S.T., Fries, T., Daube, B.C., Fan, S.-M., Sutton, D.J., Bazzaz, A. and Munger, J.W., 1998. Sensitivity of boreal forest carbon balance to soil thaw. Science, 279: 214-217.

Grace, J., Lloyd, J., McIntyre, J., Miranda, A.C., Meir, P., Miranda, H.S., Moncrieff, J., Massheder, J., Wright, I. and Gash, J., 1995a. Fluxes of carbon dioxide and water vapour over an undisturbed tropical forest in southwest Amazonia. Global Change Biology, 1: 1-12.

Grace, J., Lloyd, J., McIntyre, J., Miranda, A.C., Meir, P., Miranda, H.S., Nobre, C., Moncrieff, J., Massheder, J., Malhi, Y., Wright, I. and Gash, J., 1995b. Carbon dioxide uptake by an undisturbed tropical rain forest in southwest Amazonia, 1992 to 1993. Science, 270: 778-780.

Grace, J., Malhi, Y., Lloyd, J., McIntyre, J., Miranda, A.C., Meir, P. and Miranda, H.S., 1996. The use of eddy covariance to infer the net carbon dioxide uptake of a Brazilian rain forest. Global Change Biology, 2: 209-217.

Greco, S. and Baldocchi, D.D., 1996. Seasonal variations of CO_2 and water vapour exchange rates over a temperate deciduous forest. Global Change Biology, 2: 183-197.

Grelle, A., 1997. Long-term water and carbon dioxide fluxes from a boreal forest. Ph.D. Thesis, Swedish University of Agricultural Sciences, Uppsala, Sweden.

Gritz, L. and Hahn, J.K., 1996. BMRT: A global illumination implementation of the RenderMan standard. Journal of Graphic Tools, 1(3): 29-47.

Hipps, L.E., 1989. The infrared emissivities of soil and *Artemisia tridentata* and subsequent temperature corrections in a shrub-steppe ecosystem. Remote Sensing of Environment, 27: 337-342.

Holland, E.A. and Brown, S., 1999. North American Carbon Sink. Science, 283: 1815a.

Houghton, J.T., Filho, L.G.M., Callander, B.A., Harris, N., Kattenberg, A. and Maskell, K. (Editors), 1996. Climate Change 1995: The Science of Climate Change. Intergovernmental Panel on Climate Change, Cambridge University Press, Cambridge.

Huband, N.D.S. and Monteith, J.L., 1986. Radiative surface temperature and energy balance of a wheat canopy. Boundary-Layer Meteorology, 36: 1-17.

Humes, K.S., Kustas, W.P., Moran, M.S., Nichols, W.D. and Weltz, M.A., 1994. Variability of emissivity and surface temperature over a sparsely vegetated surface. Water resources research, 30(5): 1299-1310.

Huntingford, C., Allen, S.J. and Harding, R.J., 1995. An intercomparison of single and dual-source vegetation-atmosphere transfer models applied to transpiration from Sahelian savannah. Boundary-Layer Meteorology, 74: 397-418.

Jarvis, P.G., Massheder, J.M., Hale, S.E., Moncrieff, J.B., Rayment, M. and Scott, S.L., 1997. Seasonal variation of carbon dioxide, water vapor, and energy exchanges of a boreal black spruce forest. Journal of Geophysical Research, 102(D24): 28953-28966.

Jones, H.G., 1992. Plants and microclimate: a quantitative approach to environmental plant physiology. Cambridge University Press, Great Britain.

Keeling, C.D., Piper, S.C. and Heiman, M., 1989. A three dimensional model of atmospheric CO2 transport based on observed winds: 4. Mean annual gradients

and interannual variations. In: Peterson, D.H. (Editor), Aspects of climate variability in the Pacific and the western Americas. American Geophysical Union, Washington, DC, pp. 305-363.

Kelliher, F.M., Köstner, B.M.M., Hollinger, D.Y., Byers, J.N., Hunt, J.E., McSeveny, T.M., Mesert, R., Weir, P.L. and Schulze, E.-D., 1992. Evaporation, xylem sap flow, and tree transpiration in a New Zealand broad-leaved forest. Agricultural and Forest Meteorology, 62: 53-73.

Landsberg, J.J. and Gower, S.T., 1997. Applications of physiological ecology to forest management. Physiological Ecology: A Series of Monographs, Texts, and Treatises. Academic Press Inc.

Laubach, J., Raschendorfer, M., Kreilein, H. and Gravenhorst, G., 1994. Determination of heat and water vapour fluxes above a spruce forest by eddy correlation. Agricultural and Forest Meteorology, 71: 373-401.

Lavigne, M.B., Ryan, M.G., Anderson, D.E., Baldocchi, D.D., Crill, P.M., Fitzjarrald, D.R., Goulden, M.L., Gower, S.T., Massheder, J.M., McCaughey, J.H., Rayment, M. and Striegl, R.G., 1997. Comparing nocturnal eddy covariance measurements to estimates of ecosystem respiration by scaling chamber measurements at six coniferous boreal sites. Journal of Geophysical Research, 102(D24): 28977-28986.

Law, B.E., Baldocchi, D.D. and Anthoni, P.M., 1999a. Below-canopy and soil CO_2 fluxes in a ponderosa pine forest. Agricultural and Forest Meteorology, 94(3-4): 13-30.

Law, B.E., Ryan, M.G. and Anthoni, P.M., 1999b. Seasonal and annual respiration of a ponderosa pine ecosystem. Global Change Biology, 5(2): 169-182.

Law, B.E. and Waring, R.H., 1994. Combining remote sensing and climatic data to estimate net primary production across Oregon. Ecological Applications, 4(4): 717-728.

Law, B.E., Waring, R.H., Aber, J.D. and Anthoni, P.M., 1999c. Measurement of gross and net ecosystem productivity and water vapor exchange of a *Pinus ponderosa* ecosystem, and an evaluation of two generalized models. Global Change Biology, In review.

Lee, X., 1998. On micrometeorological observations of surface-air exchange over tall vegetation. Agricultural and Forest Meteorology, 91: 39-49.

Lee, X. and Black, T.A., 1993. Atmospheric turbulence within and above a Douglas-fir stand. Part II: Eddy fluxes of sensible heat and water vapour. Boundary-Layer Meteorology, 64: 369-389.

Lin, G., Ehleringer, J.R., Rygiewicz, P.T., Johnson, M.G. and Tingey, D.T., 1999. Elevated CO_2 and temperature impacts on different components of soil CO_2 efflux in Douglas-fir terracosms. Global Change Biology, 5(2): 157-168.

Mahrt, L., 1998. Flux sampling errors for aircraft and towers. Journal of Atmospheric and Oceanic Technology, 15: 416-429.

McCaughey, J.H., Laufleur, P.M., Joiner, D.J., Bartlett, P.A., M., C.A., Jelinski, D.E. and Ryan, M.G., 1997. Magnitudes and seasonal patterns or energy, water, and carbon exchanges at a boreal young jack pine forest in the BOREAS northern study area. Journal of Geophysical Research, 102(D24): 28997-29907.

Mencuccini, M. and Grace, J., 1996. Hydraulic conductance, light interception and needle nutrient concentration in Scots pine stands and their relations with net primary productivity. Tree Physiology, 16: 459-468.

Moncrieff, J., Malhi, Y. and Leuning, R., 1996. The propagation of errors in long-term measurements of land atmosphere fluxes of carbon and water. Global Change Biology, 2: 231-240.

Monteith, J.L. and Unsworth, M.H., 1990. Principles of Environmental Physics. Edward Arnold, Hodder Headline PLC, London.

Norman, J.M., Kustas, W.P. and Humes, K.S., 1995. Source approach for estimating soil and vegetation energy fluxes in observations of directional radiometric surface temperature. Agricultural and Forest Meteorology, 77: 263-293.

Paw U, K.T., 1992. Development of models for thermal infrared radiation above and within plant canopies. ISPRS. Journal of Photogrammetry and Remote Sensing, 47: 189-203.

Potter, C.S. and Klooster, S.A., 1999. North American Carbon Sink. Science, 283: 1815a.

Raich, J.W. and Nadelhoffer, K.J., 1989. Belowground carbon allocation in forest ecosystems: global trends. Ecology, 70: 1346-1354.

Runyon, J., Waring, R.H., Goward, S.N. and Welles, J.M., 1994. Environmental limits on net primary production and light-use efficiency across the Oregon transect. Ecological Applications, 4: 226-237.

Ryan, M.G., 1991a. The effects of climate change on plant respiration. Ecological Applications, 1: 157-167.

Ryan, M.G., 1991b. A simple method for estimating gross carbon budgets for vegetation in forest ecosystems. Tree Physiology, 9: 255-266.

Ryan, M.G. and Yoder, B.J., 1997. Hydraulic limits to tree height and tree growth. Bioscience, 47(4): 235-242.

Schmid, H.P., 1997. Experimental design for flux measurements: matching scales of observations and fluxes. Agricultural and Forest Meteorology, 87: 179-200.

Schmid, H.P. and Lloyd, C.R., 1999. Spatial representativeness and the location bias of flux footprints over inhomogeneous areas. Agricultural and Forest Meteorology, 93: 195-209.

Schotanus, P.H., Nieuwstadt, F.T.M. and de Bruin, H.A.R., 1983. Temperature measurements with a sonic anemometer and its application to heat and moisture fluxes. Boundary-Layer Meteorology, 26: 81-93.

Schwerdtfeger, P., 1976. Physical principles of micro-meteorological measurements. Development in atmospheric science. Elsevier Scientific Publishing Company, Amsterdam.

Shuttleworth, W.J. and Wallace, J.S., 1985. Evaporation from sparse crops - an energy combination theory. Quarterly Journal of the Royal Meteorological Society, 111: 839-855.

Smith, E.A., Hodges, G.B., Bacrania, M., Cooper, H.J., Owens, M.A., Chappel, R. and Kincannon, W., 1997. BOREAS net radiometer engineering study. NASA Contractor Report (NASA Grant NAG5-2447), NASA-Goddard Space Flight Center, Greenbelt.

Sperry, J.S., 1995. Limitations on stem water transport and their consequences. In: Gardner, B. (Editor), Plant Stems. Academic Press, San Diego, pp. 105-124.

Stull, R.B., 1988. An Introduction to Boundary Layer Meteorology. Kluwer Academic, Dordrecht, The Netherlands.

Sun, J., Lenschow, D.H., Mahrt, L., Crawford, T.L., Davis, K.J., Oncley, S.P., MacPherson, J.I., Wang, Q., Dobosy, R.J. and Desjardins, R.L., 1997. Lake-induced atmospheric circulations during BOREAS. Journal of Geophysical Research, 102(D24): 29155-29166.

Sun, J. and Mahrt, L., 1995. Determination of surface fluxes from the surface radiative temperature. Journal of Atmospheric Science, 52: 1096-1106.

Tans, P.P., Fung, I.Y. and Takahashi, T., 1990. Observational constraints on the global atmospheric CO_2 budget. Science, 247: 1431-1438.

Tukey, J.W., 1977. Exploratory Data Analysis. Addison-Wesley, Reading, Massachusetts.

Unsworth, M.H. and Monteith, J.L., 1975. Geometry of long-wave radiation at the ground. I. Angular distribution of incoming radiation. Quarterly Journal of the Royal Meteorological Society, 101: 13-24.

Valentini, R., DeAngelis, P., Matteucci, G., Monaco, R., Dore, S. and Scarascia Mugnozza, G.E., 1996. Seasonal net carbon dioxide exchange of a beech forest with the atmosphere. Global Change Biology, 2: 199-207.

Vitousek, P.M., 1994. Beyond global warming: Ecology and global change. Ecology, 75(7): 1861-1876.

Webb, E.K., Pearman, G.I. and Leuning, R., 1980. Correction of flux measurements for density effects due to heat and water vapour transfer. Quarterly Journal of the Royal Meteorological Society, 106: 85-100.

Whitney, S., 1985. Western Forests. Knopf, New York.

Williams, M., Rastetter, E.B., Fernandes, D.N., Goulden, M.L., Wofsy, S.C., Shaver, G.R., Melillo, J.M., Munger, J.W., Fan, S.-M. and Nadelhoffer, K.J., 1996. Modelling the soil-plant-atmosphere continuum in a *Quercus-Acer* stand at Harvard Forest: the regulation of stomatal conductance by light, nitrogen and soil/plant hydraulic properties. Plant, Cell and Environment, 19: 911-927.

Appendices

Appendix A Site description

A.1 Ponderosa pine site

Eddy covariance measurements of carbon dioxide and water vapor exchange were made above a ponderosa pine (*Pinus ponderosa* Dougl. ex P. & C. Laws.) forest located in a USDA Forest Service Research Natural Area (RNA) in the Metolius River basin in a semi-arid environment in central Oregon (44° 29' 56" N, 121° 37' 25" W, elevation 941 m). Micrometeorological measurements were recorded above and below the canopy of the old-growth ponderosa pine forest (summarized in Table A.1). Data were processed on half-hour basis from data sampled at 10Hz; power consuming sensors (CS615 soil water content sensors and HMP35C air temperature and relative humidity probe) were sampled on a longer time interval (every 5 minutes).

In a young stand soil temperature was measured with thermocouples (Type T) at 3 locations at two depth (5 and 15 cm; 15 and 30cm before Day 280, in 1996). Sapwood temperature was measured with thermocouples (Type K) at breast height (1.5m) on the North and South side of two trees at a depth of 2 cm into the sapwood. Soil water content was measured in the 0-30 cm soil layer with CS615 sensors (CSI, Logan, Utah; two sensors were setup from June 1996 until May 1997, when one sensor was moved to the juniper/sagebrush site). Transmitted photosynthetically active radiation (PAR) was measured at 1.5 m height with a LI-190 sensor (Licor, Lincoln, Nebraska).

In a mixed stand soil temperature was measured with thermocouples (Type T) at 3 locations at two depth (5 and 15 cm; 15 and 30cm prior to Day 280, in 1996). Sapwood temperature was measured with thermocouples (Type K) at breast height on the North and South side of two trees at a depth of 2 cm into the sapwood. Precipitation reaching the ground was recorded with two tipping bucket rain gauges (model TM525, Texas, ; starting Day 255, 1996). Transmitted PAR was measured at 1.5 m height with a LI-190 sensor (Licor, Lincoln, Nebraska).

In an old stand (Figure A.1), close to the flux tower, soil temperature was measured with thermocouples (Type T) at 3 locations at two depth (5 and 15 cm; 15 and 30cm prior to Day 280, in 1996) and at two locations at six depth (2, 4, 8, 16, 32, and 64 cm). Sapwood temperature was measured with thermocouples (Type K) at breast height on the North and South side of two trees at a depth of 2 cm into the sapwood. Soil water content was measured in the 0-30 cm soil layer with CS615 sensors (CSI, Logan, Utah; two sensors were setup from May 1996 until April 1997, when one sensor was moved to the juniper/sagebrush site). Transmitted PAR and solar radiation were measured at 1.5 m height with a LI-190 and LI-200 sensor (LI-COR Inc, Lincoln, NE). Air temperature and relative humidity was measured at 1 m height with a Vaisala HMP35C probe (Vaisala, Helsinki, Finland).

Figure A.1 Meteorological station in an old stand.

At the base of the flux tower the CO_2 profile was measured within and above the canopy (1 and 8 m starting Day 146, 1996, after Day 172, 1996 extended to 1, 8, 31, and 45 m), using a LI-6262 gas analyzer (LI-COR Inc, Lincoln, NE) and a solenoid switching system controlled by a 21X datalogger (CSI, Logan, Utah) (Figure . Gas analyzer zero and span calibrations were performed daily with calibration gases, which were compared to a NIST traceable calibration standard. Air temperature and relative humidity was measured at 8 m height with a Vaisala HMP35C probe (Vaisala, Helsinki, Finland).

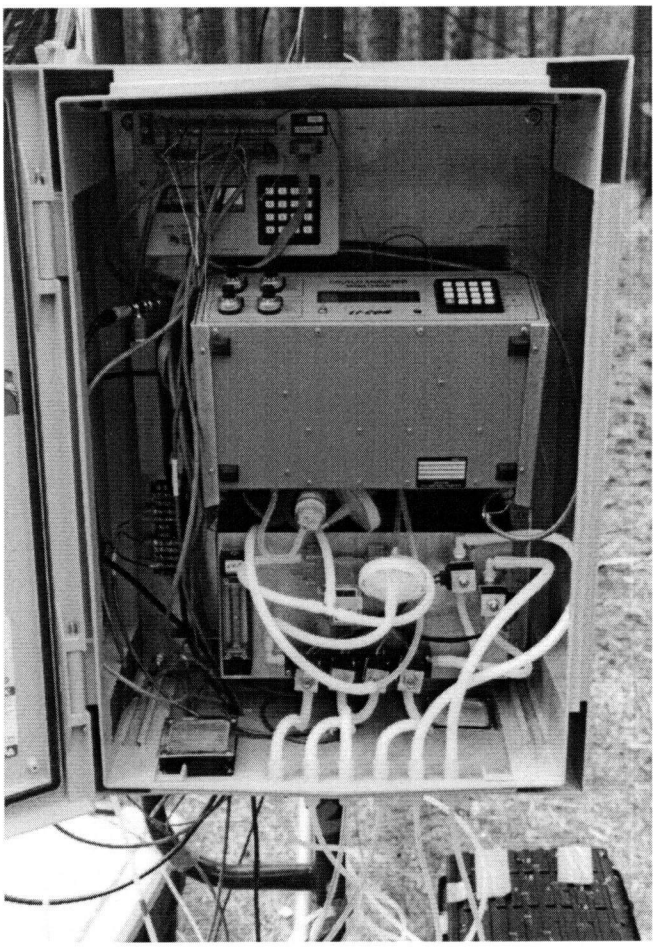

Figure A.2 CO_2 profile sampling system at base of tower.

At the top of the flux tower (Figure A.3) a micrometeorological station was setup with a CR10X datalogger (CSI, Logan, UT). Above-canopy net radiation (R_n) was measured with a net radiometer (model Q7, REBS, Seattle, WA), deployed from the south side of the tower. Downward global solar (S_r) and PAR were measured with radiation sensors (model LI-200SZ and LI-190SZ, respectively, LI-COR Inc, Lincoln, NE). Air temperature (T_a) and relative humidity (RH) were measured with a thermistor and capacitive RH sensor probe (model HMP35C, Vaisala, Helsinki,

Finland). Wind speed and direction were monitored with a Wind Sentry set (model 03001, RM Young, Traverse City, MI).

a)

b)

Figure A.3 a) Side view of the flux tower, and b) aerial view of the ponderosa pine site. Flux tower is located in the center of the picture.

Table A.1 Summary of micrometeorological, physiological and phenological measurements at the Metolius/RNA site in 1996 and 1997: Meteorological stations are located in old stand (O), young stand (Y), mixed stand (M), and top of tower (TOT).

Variable	Frequency	Notes
Flux Data:		
CO_2 (F_c), latent (LE) and sensible heat (H), momentum (uw)	1/2 hourly	TOT (JD 82-present), Eddy Jr. (July 1996; March, May August, 1997)
CO_2 profile (ppm)	1/2 hourly	1m, 8m JD 146-178; 1m, 8m, 31m, 47m; JD 179 – end of 1997
Automated Weather and Soils Data:		
wind speed (m s^{-1}), wind direction (°)	1/2 hourly	TOT, O
Precipitation (mm)	1/2 hourly	TOT, M, O
air temperature (°C), RH (%)	½ hourly	TOT (1m, 8m, 45m)
net radiation (W m^{-2})	½ hourly	TOT, O, tram periodically
diffuse and direct PAR (µmol m^{-2} s^{-1})	½ hourly	TOT
diffuse and direct solar radiation (W m^{-2})	½ hourly	TOT, O (direct only)
transmitted PAR (µmol m^{-2} s^{-1})	½ hourly	O, Y, M stands, tram
sapwood temperature (°C)	½ hourly	O, Y, M stands;3 old & 3 young trees/station 2cm depth into sapwood, N and S side of tree)
soil heat flux (W m^{-2})	½ hourly	2 at Y, 2 at O (2cm depth)
soil moisture content (m^3 m^{-3})	½ hourly	O, Y stands; 0-30cm depth
soil temperature profile (°C)	½ hourly	O stand; 2cm, 4cm, 8cm, 16cm,32cm, 64cm
spatial variation in soil temperature (°C)	½ hourly	O, Y, M stands; 15cm, 30cm @ 3 per station 30cm placed at 5 cm depth in September, 1997
Tree Physiology, Stand Structure:		
pre-dawn water potential (MPa)	monthly	old and young trees
mid-day water potential (MPa)	monthly	old and young trees
relative water content of sapwood	monthly	old and young trees
foliage N, C, chlorophyll concentration	3x	lower, mid, upper canopy
above ground biomass and growth of foliage, branches, stems (g m^{-2})	1x	45 plots on 4 transects centered on tower (2000mx800m area)
tree and crown height (m)	1x	45 plots, all trees 7cm dbh
intercepted PAR (µmol m^{-2} s^{-1}), leaf area index (LAI; projected m^2 leaf m^{-2} ground)	1x, mid-summer	45 mensuration plots (n=225) 100x100m area at 121 points on 10 m grid
foliage respiration (µmol m^{-2} s^{-1})	3x	old and young trees
photosynthesis, leaf conductance	2x	lower and mid-canopy young trees
stem respiration (µmol m^{-2} s^{-1})	4x	old and young trees
Soils:		
soil respiration; co-located soil temperature, soil moisture (µmol m^{-2} s^{-1})	monthly	3 locations at 5 O, 5 Y, 5 M stands; soil temp @ 15 cm; soil moisture @ 30 cm, 60 cm (TDR)
litterfall (g m^{-2})	monthly	O,Y,M; 3 traps @ each of 15 respiration plots
soil,litter,humus chemistry (N,C)	1x	O,Y,M stands
soil texture (%sand,silt,clay)	1x	O,Y,M stands
Misc.Site Characteristics:		
phenology overstory and understory	bi-weekly to monthly	includes budbreak and needle elongation data for PIPO, leaf fall
understory % cover	1x	area centered on Eddy Jr.

A.2 Juniper/sagebrush site

Eddy covariance measurements of carbon dioxide and water vapor exchange were made above a juniper/sagebrush ecosystem in a semi-arid environment about 15 km east of Sisters, Oregon (44°15′54′′ N, 121°23′3′′ W, elevation 945 m). Micrometeorological measurements were recorded above the canopy with instruments setup on a 20 m tall tri-angular aluminum tower (summarized in Table A.2). Eddy flux data were processed on half-hour basis from data sampled at ~8 Hz.

At the top of the tower (20m above ground level) air temperature and relative humidity were measured with a Vaisala HMP35C probe (Vaisala, Helsinki, Finland). Above-canopy net radiation (R_n) was measured with a net radiometer (model Q7, REBS, Seattle, WA), deployed from the south side of the tower. Downward PAR was measured with a LI-190SZ quantum sensor (LI-COR Inc, Lincoln, NE). Wind speed and direction were monitored with a Wind Sentry set (model 03001, RM Young, Traverse City, MI).

At the ground level soil temperature were measured with thermocouples (Type T) at 2 locations at three depth (2, 8, and 16 cm) at the North and south side of a tree. Soil heat flux was measured next to the soil temperature probes with heat flux plates (HFP-3, REBS, Seattle, WA) at 2 and 10 cm depth. Sapwood temperature was measured with thermocouples (Type T) at 1.5m height on the North and South side of a juniper tree at 2 cm into the sapwood. Soil water content was measured in the 0-30 cm soil layer with CS615 sensors (CSI, Logan, Utah). Precipitation was recorded with a tipping bucket rain gauge (model TM525, Texas).

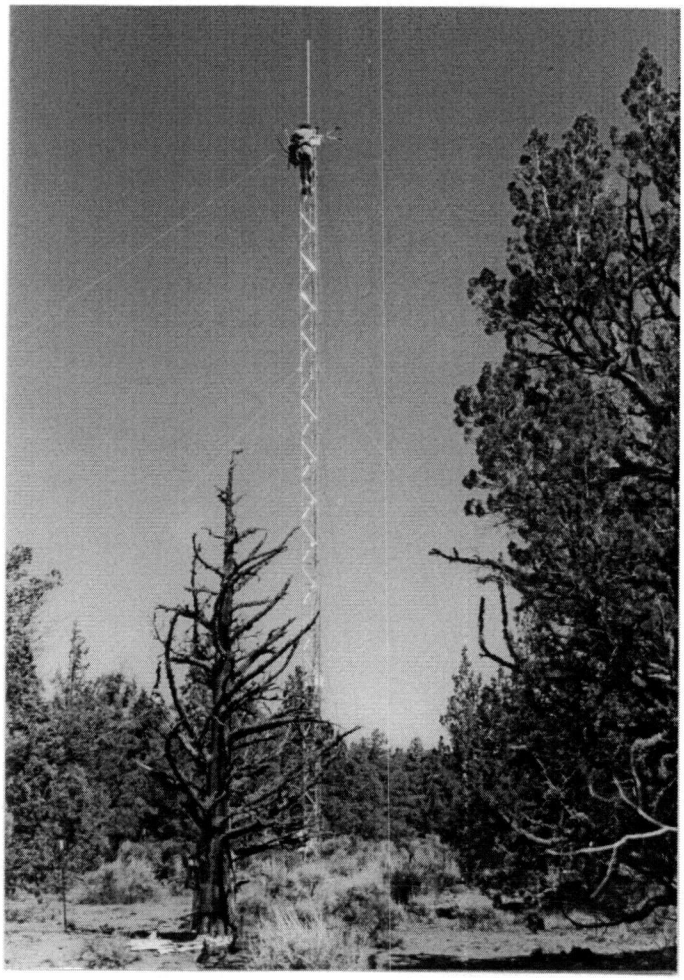

Figure A.4 Flux tower at the juniper/sagebrush site

A CO_2 profile was measured at three heights (1, 8, and 20 m), using a LI-6262 gas analyzer (LI-COR Inc, Lincoln, NE) and a solenoid switching system controlled by a CR10X datalogger (CSI, Logan, Utah). Gas analyzer zero and span calibrations were performed periodically with calibration gases, which were compared to a NIST traceable calibration standard.

Table A.2 Summary of micrometeorological, physiological and phenological measurements at the juniper/sagebrush site: Meteorological stations are located at the ground (G) and top of tower (TOT).

Variable	Frequency	Notes
Flux Data:		
CO2, water vapor, sensible heat, and momentum	1/2 hourly	51 days in Spring and Summer 1997
CO2 profile	1/2 hourly	1m, 5m and 20m
Automated Weather and Soils Data:		
wind speed (m s-1) and wind direction	1/2 hourly	above canopy
precipitation (mm)	1/2 hourly	setup in clearing
air temperature (C), RH (%)	1/2 hourly	above canopy
net radiation (W m-2)	1/2 hourly	above canopy
direct PAR (umol m-2 s-1)	1/2 hourly	above canopy
sapwood temperature (deg. C)	1/2 hourly	2cm depth into sapwood, N and S side of tree
soil heat flux (W m-2)	1/2 hourly	heat flux plates 2 locations (N and S of tree) at depth of 2cm and 10 cm
soil moisture content (m3 m-3)	1/2 hourly	CS615 sensors: 2 locations, N and S of tree TDR: 10 locations along 100m transect
soil temperature profile (deg. C)	1/2 hourly	2cm, 16cm and 32cm, N and S of tree
Tree Physiology, Stand Structure:		
pre-dawn water potential (MPa)	monthly	Juniper trees
foliage N, C, chlorophyll concentration	1x	Juniper trees
above ground biomass and growth of foliage, branches, stems (g m-2)	1x	45 plots on 4 transects centered on tower (2000mx800m area)
tree and crown height (m)	1x	100x100 m area, all trees > 7cm dbh
intercepted PAR, LAI	1x, mid-summer	transmitted PAR at 121 points within 100x100 m area
foliage respiration, night and day (umol m-2s-1)	2x	Juniper trees
photosynthesis, stomatal conductance (umol m-2s-1)	2x (spring, summer)	Juniper trees
Soils:		
soil respiration; co-located soil temperature, soil moisture (umol m-2s-1)	monthly	10 locations along 100 m transect; soil moisture @ 10 cm, 20 and 40 cm with TDR
litterfall (g m-2)	monthly	10 traps along 100 m transect

Appendix B Methods

B.1 Theoretical background

Conservation equation for a constituent (C) in the atmosphere is given by (Stull, 1988)

$$\frac{\partial \overline{C}}{\partial t} = -\overline{u_i}\frac{\partial \overline{C}}{\partial x_i} - \frac{\partial \overline{u_i' C'}}{\partial x_i} + D + S \qquad \text{(B.1)}$$

where u_i is the i^{th} wind speed component (x-component u_1 = u , y-component u_2 = v, z-component u_3 = w), D is a molecular diffusion term, and S is a sink/source term. Primed quantities denote deviations from the mean (i.e., C' = C – $\overline{C}$)

Molecular diffusion in the atmosphere is several order of magnitudes smaller than turbulent transport and is usually neglected; it becomes important only very close to the surface. Horizontal advection effects are usually minimized by selection of a site with enough fetch in the most common wind direction. Assuming a zero vertical wind component, this leads to

$$\frac{\partial \overline{C}}{\partial t} = -\frac{\partial \overline{w' C'}}{\partial z} + S \qquad \text{(B.2)}$$

Integration from the ground to the measurement height h and rearranging terms gives

$$\int_0^h S\,dz + \overline{w'C'}_0 = \int_0^h \frac{\partial \overline{C}}{\partial t} dz + \overline{w'C'}_h \qquad \text{(B.3)}$$

where the left-hand side is the net flux density of material in and out of the underlying soil and the integration of all sources/sinks in the air-layer from 0 to h, i.e. in case for CO_2 the net ecosystem exchange (NEE).

Lee (1998) suggested that in complex terrain over tall vegetation a vertical mass-flow, arising from horizontal flux convergence/divergence or a non-zero vertical wind component, can become important and should not be neglected. With the inclusion of the mass flow term the conservation equation becomes

$$\int_0^h S\,dz + \overline{w'C'}_0 = \int_0^h \frac{\partial \overline{C}}{\partial t} dz + \overline{w'C'}_h + \overline{w}_h\left(\overline{C}_h - \left\langle \overline{C} \right\rangle\right) \qquad \text{(B.4)}$$

where subscript h denotes a quantity at the measurement height h and $\left\langle \overline{C} \right\rangle$ is the averaged concentration between the surface and the height h. The right hand side consists of a 1) change of C storage in the air-layer, 2) eddy flux and 3) vertical mass flow term across the boundary at height h.

B.2 Storage term and massflow correction

The rate of change in carbon dioxide ($F_{stor} = \int_0^h \frac{\partial \overline{C}}{\partial t} dz$) stored in the canopy air-layer was estimated from CO_2 concentration measurements at four heights (1, 8, 31, and 46 m). The trend in the CO_2 concentration at each height over time was computed with a smoothing algorithm using running medians. The value of F_{stor} below the eddy covariance system was then calculated by interpolating the CO_2 concentration trends in 1-m intervals and summing the change with time over all layers. During periods when the CO_2 profile system was not operational, the rate of change of the CO_2 signal of the eddy covariance IRGA, located above the canopy, was used to estimate F_{stor}. Similarly the rate of change in water vapor and air temperature was calculated from temperature and relative humidity measurements made at three heights (1, 8, and 46 m).

Rates of energy storage (S) within the canopy was estimated by

$$S = S_a + S_v + S_c \qquad \text{(B.5)}$$

where S_a is energy storage in air, S_v is energy storage in water vapor, and S_c is the energy stored in the canopy biomass of tree sapwood, branch, bark and foliage (Jarvis et al., 1976). Sa and S_v were calculated from half-hour changes of the air temperatures and water vapor concentrations measured at 1 m and 8 m in the canopy and at 45 m above the canopy. Storage of energy in tree sapwood was estimated for young and old

trees separately from the change in measured sapwood temperature at breast height, calculation of mean sapwood volume for each tree class and sapwood heat capacity corrected for its relative water content. Sapwood volume was calculated from measured mensuration data, using tapper equations for P. pine (Walters et al., 1985) and measured sapwood to hardwood ratios. Energy storage in the hardwood of the trees was assumed to be negligible, since temperature changes of the hardwood are most likely small. Storage of energy in branch, bark and foliage was calculated from mensuration estimates of branch, bark and foliage mass and assuming their temperature follows closely the air temperature in the canopy layer.

The influence of a mass flow component on nighttime CO_2 fluxes arising from horizontal flow divergence/convergence, resulting in a non-zero mean vertical velocity at the height of the flux observation was assessed following methods presented by Lee (1998). The non-zero mean vertical velocity ($\overline{w}_r$) at the eddy covariance measurement height was calculated from the difference between measured vertical velocity in the sonic coordinate system and the vertical velocity induced due to the instrument orientation with respect to local terrain. The influence of the local terrain on the vertical velocity was determined by linear regression using

$$\hat{w} = \overline{w} + a(\phi) + b(\phi)\hat{u} \qquad \text{(B.6)}$$

where $\hat{w}$ and $\hat{u}$ are the measured mean vertical and horizontal velocities in the instrument coordinates, $\overline{w}$ is a true mean vertical velocity assumed to behave in a

random fashion, and a and b are wind direction (ϕ) dependent coefficients. Values of a and b were determined for 1° increments using all measurements that fall within ±10°. Then for each half-hour a mean vertical velocity was calculated as the difference between measured and terrain influenced vertical velocity ($\overline{w}_r = \hat{w} - a(\phi) + b(\phi)\hat{u}$) using the wind direction dependent coefficients (a and b) and the measured mean horizontal velocity of that half-hour. An advection correction (F_{av}) to the carbon dioxide flux was then calculated by

$$F_{av} = \overline{w}_r \left(C_r - \langle C \rangle\right) \tag{B.7}$$

where C_r is the CO_2 concentration at the eddy covariance measurement height and $\langle C \rangle$ is the spatial mean CO_2 concentration below the measurement height, estimated by linear interpolation between the CO_2 profile heights. The advection correction was then added to the carbon dioxide flux, which was rotated to be normal to the plane that is defined by the horizontal velocity vector and the predicted terrain-influenced vertical velocity for that half hour ($a(\phi) + b(\phi)\hat{u}$). The mass-flow term was then added to the measured carbon dioxide eddy flux, which was rotated to be normal to the plane defined by the horizontal velocity vector and the predicted mean vertical velocity.

B.3 Eddy flux

Measurement of the eddy flux is based on measurement of turbulent wind variations and associated fluctuations of scalars, such as temperature, water vapor content, or gas concentrations. The measured turbulence consists of eddies (swirls of air motion superimposed on the mean wind) with various sizes, directions and time scales. The transport of a scalar quantity by those eddies is the so called "eddy flux" or "turbulent flux". The eddy flux $\overline{w'C'}$ in the vertical wind direction (w) of a scalar (C) can be calculated from rapidly sampled data as

$$\overline{w'C'} \equiv \frac{1}{N} \sum (w - \bar{w})(C - \bar{C}) \qquad \text{(B.8)}$$

where w' or C' are deviations of individual samples w or C from the mean value $\bar{w}$ or $\bar{C}$ (overbars denote a time average) in the sampled time period consisting of N data points. Thus the eddy flux of a scalar is given by the covariance with the wind speed in the direction of interest, hence the name eddy covariance technique.

For example, in the case of an idealized eddy mixing process in an unstable environment (hot summer day over land where temperature decreases with height z), upward moving eddies transport air that is warmer than average (T'>0, w'>0) and downward moving eddies transport colder air down (T'<0, w'<0) (see Figure B.1). The net eddy flux $\overline{w'T'}$ is positive, since in both cases the product w'T' is positive (adopting the sign convention that fluxes away from the surface are positive), corresponding to a net upward heat flux.

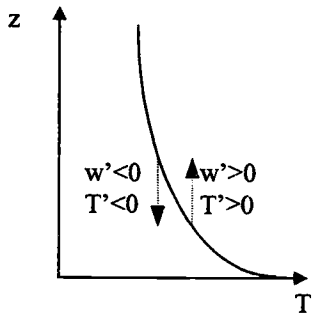

Figure B.1 Idealized mixing process

B.4 Data Preprocessing

Fast response data time series generally are "cleaned" before computing covariances. The time series often are processed by despiking, detrending with high-pass filtering and rotation into a different coordinate system (Baldocchi et al., 1988; McMillen, 1988; Stull, 1988). Despiking removes anomalously large or small values (Spikes) caused by non-meteorological events. Detrending with high-pass filtering eliminates non stationary trends within the averaging time period. Rotation allows the interpretation of a flux oriented normal to the mean streamwise wind.

The sonic anemometer data were despiked according to procedure by Hojstrup (1993), which identifies anomalous data spikes caused by electronic measurement errors, blocked path between the transducers, or accumulated water or rime frost on the transducer surface. The spike removal algorithm determines an unusual measurement by calculating a prediction variance based on the difference between the measured value and a predicted value, which itself is based on the serial correlation in

the data series. The prediction variance for a data point is compared to a pooled variance for a "memory" consisting of the (10^2 to 10^3) most recently acquired data points from the same variable. When the prediction variance exceeds the memory-based variance by more than 6 times its magnitude, the data point is identified as spike. A detected spike is replaced by its predicted value and the data point is flagged as a spike. If the number of spikes in the data series used for a flux calculation exceeds one percent, the calculated covariance flux is not used for further analysis.

The detrending procedure uses an approximation to a running mean as a high-pass filter that removes trends with wavelengths longer than about one-third to one-fifth of the time series length and retain enough complete cycles of shorter wavelength for significant statistical averaging (Stull, 1988). The trend in the time series data was calculated with a running-mean high-pass filter following McMillen (1988), which is given by

$$y_i = \alpha y_{i-1} + (1-\alpha)x_i \qquad \text{(B.9)}$$

where x_i is a sample taken at time t_i, y_i is the trend of the data series at t_i, and α is a filter parameter defined by

$$\alpha = e^{\frac{1}{f\tau}} \qquad \text{(B.10)}$$

where f is the sample frequency, τ is the time constant of the filter. A 400 second time constant was used in the detrending procedure, which had previously been found to be adequate for flux sampling studies (Baldocchi and Vogel, 1996). Deviations (x_i') from the running mean (y_i) are then calculated with

$$x_i' = x_i - y_i \tag{B.11}$$

Due to imperfect sensor alignment and non-homogenous terrain, coordinate rotations are often necessary to determine the surface flux normal to the streamlines (Baldocchi et al., 1988). The rotation scheme transforms the three measured mean wind components from an orientation aligned with the instrument axes to a new orientation, where the x-component $\bar{u}$ is aligned into the mean wind, and consequently the rotated mean vertical $\bar{w}$ and horizontal crosswind $\bar{v}$ are zero over the flux time period. The azimuthal (η) and vertical (θ) rotation angles are calculated from the three orthogonal mean wind components $\bar{u}_{unrot}$, $\bar{v}_{unrot}$, and $\bar{w}_{unrot}$ (means over the flux time period calculated before rotation) according to

$$\eta = \tan^{-1} \frac{\bar{v}_{unrot}}{\bar{u}_{unrot}} \tag{B.12}$$

$$\theta = \tan^{-1} \frac{\bar{w}_{unrot}}{(\bar{u}_{unrot}^2 + \bar{v}_{unrot}^2)^{0.5}} \tag{B.13}$$

and the magnitudes of the instantaneous, rotated wind components (u_{rot}, v_{rot}, w_{rot}) are given by transformation of the unrotated data samples u_{unrot}, v_{unrot}, w_{unrot} according to

$$u_{rot} = u_{unrot} \cos(\eta) \cos(\theta) + v_{unrot} \sin(\eta) \cos(\theta) + w_{unrot} \sin(\theta) \quad \text{(B.14)}$$

$$v_{rot} = -u_{unrot} \sin(\eta) + v_{unrot} \cos(\eta) \quad \text{(B.15)}$$

$$w_{rot} = -u_{unrot} \cos(\eta) \sin(\theta) - v_{unrot} \sin(\eta) \sin(\theta) + w_{unrot} \cos(\theta) \quad \text{(B.16)}$$

B.5 Data Analysis

The eddy flux computations for latent (LE) and sensible (H) heat flux, and carbon dioxide flux (F_c) were calculated for 30 minute intervals. For each eddy flux calculation the despiked sonic anemometer wind speed components were rotated into a coordinate system aligned with the streamlines ($\overline{w}_{rot} = 0$ and $\overline{v}_{rot} = 0$), where the rotation angles were determined from the mean wind velocities over the flux averaging period (Baldocchi et al., 1988; McMillen, 1988). After rotation the scalar and wind speed signals were detrended with an exponential running mean filter (high-pass filter with time constant $\tau = 400$ s), and the covariance eddy flux was computed from the detrended sample data, as in equation B.2 .

B.5.1 Friction velocity u_*

The friction velocity u_*, used as a measure of the strength of the turbulence, was calculated from measured momentum flux $\overline{u'w'}$ according to

$$u_* = (-\overline{u'w'})^{1/2} \tag{B.17}$$

B.5.2 Sensible and latent heat flux

The sensible heat flux (H) was calculated from measured temperature flux ($\overline{w'T_s'}$) according to

$$H = c_p \rho \overline{w'T_s'} + \delta H \tag{B.18}$$

where ρ is the mean air density, c_p is the specific heat of air at constant pressure (= 1010 J kg^{-1} K^{-1}), and δH is a correction term to remove lateral momentum flux perturbations (Schotanus et al., 1983) and moisture influences on T_s.

The Schotanus (1983) correction is given by

$$\delta H_{Schotanus} = c_p \rho \frac{2 \cdot T \cdot \bar{u} \cdot \overline{u'w'}}{c^2} \tag{B.19}$$

where T is the mean air temperature in K, $\bar{u}$ is mean wind speed, $\overline{u'w'}$ is the momentum flux, and c is the speed of sound. Using representative values of T = 293 K, ρ = 1.1 kg m^{-3}, $\bar{u}$ = 2 m s^{-1}, $\overline{u'w'}$ = -0.3 m^2 s^{-2} and c = 344 m s^{-1}, $\delta H_{Schotanus}$ = –3.3 W m^{-2}, about 1% of a typical daytime H of 250 W m^{-2}.

The moisture correction is given by

$$\delta H_v = -0.51\, c_p\, \rho \frac{T\ \overline{w'\rho_v'}}{\rho} \qquad \text{(B.20)}$$

where $\overline{w'\rho_v'}$ is the measured moisture flux , T is the mean air temperature, ρ is the mean air density. With representative values of T = 293 K, air pressure of 900 hPa, and $\overline{w'\rho_v'}$ of 60 mg m^{-2} s^{-1} the correction term is 9 W m^{-2}, about 4% of a typical daytime H of 250 W m^{-2}.

Latent heat flux (LE) is calculated from measured moisture flux as

$$LE = \lambda\ \overline{w'\rho_v'} + \delta LE \qquad \text{(B.21)}$$

where λ is the temperature dependent latent heat of evaporation (= 3.149x10^6 J kg^{-1} - 2370 J kg^{-1} K^{-1} · T_a), $\overline{w'\rho_v'}$ is the moisture flux normal to the streamlines, and δLE is a correction term.

Corrections to LE_{raw} (=$\lambda\ \overline{w'\rho_v'}$) arise from density fluctuations in the sampled air introduced by temperature fluctuations that are associated with a sensible heat flux

(Webb et al., 1980). For open-path instruments the corrections have a significant effect and can not be neglected. Webb et al. (Webb et al., 1980) obtained the following expression for the LE flux correction term for an open-path analyzer system

$$\delta LE_{,Webb} = \mu\sigma \cdot \left(LE_{raw} + \lambda \frac{\rho_v}{\rho} \frac{H}{c_p T} \right) \qquad \text{(B.22)}$$

where $\mu = M_a/M_v$ (=0.622) is the ratio of the molecular weights of dry air and water, ρ is the total mean air density, σ is the ratio of water vapor (ρ_v) to dry air density (ρ_a), T is the mean air temperature in K, c_p is the specific heat of air at constant pressure (= 1010 J kg^{-1} K^{-1}), LE_{raw} (=$\lambda\ \overline{w'\rho_v'}$) is the uncorrected latent heat exchange, and H is the sensible heat flux. With representative values of T = 293 K, air pressure of 900 mb, and a relative humidity of 40%, (i.e. σ = 0.0065), the correction term is

$$\delta LE_{,Webb} = 0.004 \cdot LE_{raw} + 0.053 \cdot H \qquad \text{(B.23)}$$

For typical summer time conditions with H of 250 W m^{-2} and LE_{raw} of 150 W m^{-2} the correction $\delta LE_{,Webb}$ is 15 W m^{-2}, about 10% of measured LE_{raw}.

B.5.3 Carbon Dioxide Flux

The net carbon dioxide eddy flux was calculated from the covariance of the IRGA CO_2 output and the sonic wind speed component normal to the streamline. The carbon dioxide signal was sampled at the same rate (10 Hz) as the sonic anemometer. Analyzer specific calibration coefficients were determined in the lab from calibrations with four CO_2 span gases. Carbon dioxide flux (F_c in $\mu mol\ m^{-2}\ s^{-1}$) was calculated as

$$F_c = \frac{\overline{w'C'_{CO2}}}{M_{CO2}} + \delta F_c \qquad \text{(B.24)}$$

where M_{CO2} is the molecular weight of carbon dioxide, $\overline{w'C'_{CO2}} = F_{c.raw}$ is the uncorrected CO_2 flux in $mg\text{-}CO_2\ m^{-2}\ s^{-1}$ and δF_c is a correction term.

Correction to $F_{c.raw}$ arise mainly from density fluctuations in the sampled air (Webb et al., 1980). Account has to be taken for density fluctuations in the carbon dioxide concentration introduced by fluxes of heat and water vapor. For open-path instruments the corrections have a significant effect. The major part of the correction is caused by the temperature fluctuations that are associated with a sensible heat flux. Webb et al. (Webb et al., 1980) obtained the following expression for the CO_2 flux correction term for an open-path analyzer system

$$\delta F_{c.Webb} = \frac{\rho_c}{\rho_a} \cdot \frac{\mu}{1+\mu\sigma} \cdot \frac{LE}{\lambda} + \frac{\rho_c}{\rho} \frac{H}{c_p T} \qquad \text{(B.25)}$$

with symbols as defined earlier.

With representative values of T = 293 K, air pressure of 900 hPa, a relative humidity of 40%, (i.e. $\sigma = 0.0065$), and atmospheric CO_2 concentration of 355 ppm, the correction term computes to

$$\delta F_{c.Webb} = 0.0033 \frac{\mu mol\ m^{-2}\ s^{-1}}{W\ m^{-2}} \cdot LE + 0.044 \frac{\mu mol\ m^{-2}\ s^{-1}}{W\ m^{-2}} \cdot H \qquad (B.26)$$

For typical summer time conditions with LE of 150 W m^{-2} and H of 250 W m^{-2} the corrections are +0.5 and +11.0 μmol m^{-2} s^{-1} respectively, about 80% of uncorrected $F_{c.raw}$ of -14.5 μmol m^{-2} s^{-1}.

B.6 Energy balance

The first law of thermodynamics states that energy is conserved in any system when heat is taken into account. A state of energy balance for the atmosphere-surface system occurs when the energy input equals the sum of the energy lost out of the system and the change in stored energy over a specified time frame. The major source of energy for the atmosphere-surface layer is solar radiation, where the net input of radiation-energy is determined by the difference in downwelling and upwelling short and long wave radiation:

$$R_n = (R_{sd} - R_{su}) + (R_{ld} - R_{lu}) \qquad (B.27)$$

where R_n denotes net radiation, R_{sd} and R_{ld} are downwelling and R_{su} and R_{lu} are upwelling short and long wave radiation.

During the day, the net radiation absorbed by the surface is to a large extent, returned to the atmosphere via conduction and turbulent exchange of sensible and latent heat, with a small portion typically stored as internal energy (temperature raise of ecosystem components, i.e. biomass) or biochemical energy (photosynthesis of plants). During daytime heat is usually transported from the warmer surface by conduction and evaporation into the lowest atmosphere layer, where turbulent transport dominates. A loss of energy for the system results due to sensible and latent heat fluxes directed away from the surface. Some part of the heat is conducted into the ground, which results in a ground heat flux. At nighttime, energy exchange in the atmosphere-surface system is generally smaller than by day, since the major energy contributor, solar radiation (R_{su}) is zero.

Atmospheric conditions, such as the difference in air-surface temperature, cloud cover, and any evaporation or condensation of water, control the magnitude and direction of net radiation, sensible and latent heat exchange and ground heat flux, and changes in energy storage.

The overall energy balance for the surface can be written as (neglecting advection effects)

$$R_n - G - S = H + LE \qquad \text{(B.28)}$$

where R_n is incoming net radiation, G is ground heat flux, S is energy storage, (R_n – G – S is often termed available energy), H is sensible heat flux, and LE is latent heat flux. The common sign convention for net radiation is positive for energy directed towards the surface. Heat fluxes are by convention positive if they are directed away from the surface. An increase of stored energy in the system mass is treated as positive, and release is negative.

At the ponderosa pine site, G and S were estimated with the following methods. The soil heat flux (G) was derived from the average of four soil heat flux plate measurements in the old and young stand, equally weighted assuming that the whole forest is a homogeneous mix of old and young stands.

Rates of energy storage below the measurement level was estimated by

$$S = S_a + S_v + S_c \tag{B.29}$$

where S_a is energy storage in air, S_v is energy storage in water vapor, and S_c is the energy stored in the canopy biomass of tree sapwood, branch, bark and foliage (Jarvis et al., 1976). S_a and S_v were calculated from half-hour changes of the air temperatures and water vapor concentrations measured at 1 m and 8 m in the canopy and at 45 m above the canopy. Storage of energy in tree sapwood was estimated for young and old trees separately from the change in measured sapwood temperature at breast height, calculation of mean sapwood volume for each tree class and sapwood heat capacity corrected for its relative water content. Sapwood volume was calculated from measured mensuration data, using site specific tapper equations for ponderosa pine

trees provided by Steve Acker (pers. comm.) and measured sapwood to hardwood ratios. Energy storage in the hardwood of the trees was assumed to be negligible, since temperature changes of the hardwood are most likely small. Storage of energy in branch, bark and foliage was calculated from mensuration estimates of branch, bark and foliage mass and assuming their temperature follows closely the air temperature in the canopy layer.

Appendix C Related references

Anthoni, P.M., Law, B.E., Unsworth, M.H. and Vong, R.J., 1999. Variation of net radiation over heterogeneous surfaces: measurements and simulation in a juniper-sagebrush ecosystem. Agricultural and Forest Meteorology, In review.

Anthoni, P.M., Law, B.E. and Unsworth, M.H., 1999. Carbon and water vapor exchange of an open-canopied ponderosa pine ecosystem. Agricultural and Forest Meteorology, 95(3): 151-168.

Anthoni, P.M., Unsworth, M.H., Vong, R.J. and Law, B.E., 1998. Energy Budget of an Open-Canopied, Semi-Arid Juniper/Sagebrush Ecosystem, 23rd AMS Conference on Agricultural and Forest Meteorology.

Baldocchi, DD, Law BE, Anthoni PM (1999) On measuring and modeling energy fluxes above the floor of a homogeneous and heterogeneous conifer forest. Agricultural and Forest Meteorology, (submitted).

Law, B.E., Anthoni, P.M., Baldocchi, D.D. and Unsworth, M.H., 1998. Below-Canopy and Nocturnal CO2 Fluxes in a Ponderosa Pine Forest, 23rd AMS Conference on Agricultural and Forest Meteorology.

Law, B.E., Baldocchi, D.D. and Anthoni, P.M., 1999. Below-canopy and soil CO2 fluxes in a ponderosa pine forest. Agricultural and Forest Meteorology, 94(3-4): 13-30.

Law, B.E., Ryan, M.G. and Anthoni, P.M., 1999. Seasonal and annual respiration of a ponderosa pine ecosystem. Global Change Biology, 5(2): 169-182.

Law, B.E., Waring, R.H., Aber, J.D. and Anthoni, P.M., 1999. Measurement of gross and net ecosystem productivity and water vapor exchange of a Pinus ponderosa ecosystem, and an evaluation of two generalized models. Global Change Biology, In review.

Law, B.E., Goldstein, A., Williams, M., Anthoni, P.M., Panek, J., Bauer, M.R., Fracheboud, J.-M. and Unsworth, M.H., 1999. A comparison of CO2 and water vapor exchange by young and old ponderosa pine ecosystems during a drought year. For submission to Tree Physiology (special issue from the Ponderosa Pine Workshop).

Law BE, Ryan MG, Anthoni PM (1999) Seasonal and annual respiration of a ponderosa pine ecosystem. Global Change Biology 5:169-182.

Law BE, Waring RH, Aber JD, Anthoni PM (1999) Measurement of gross and net ecosystem productivity and water vapor exchange of a Pinus ponderosa ecosystem, and an evaluation of two generalized models. Global Change Biology (in press).

Law BE, Williams M, Anthoni PM, Baldocchi DD, Unsworth MH (1999) Measuring and modeling seasonal variation of carbon dioxide and water vapor exchange of a Pinus ponderosa forest subject to soil water deficit. Global Change Biology (in review).